TECHNISCHE UNIVERSITÄT DRESDEN

Fractionalized Fermionic Quantum criticality in Kitaev spin-orbital models

Master-Arbeit
zur Erlangung des Hochschulgrades
Master of Science
im Master-Studiengang Physik

vorgelegt von

Max Fornoville
geboren am 19.10.1998 in Berlin

Institut für Theoretische Physik
Fakultät Physik
Bereich Mathematik und Naturwissenschaften
Technische Universität Dresden
2023

Eingereicht am 23. Dezember 2023

1. Gutachter: Prof. Dr. Matthias Vojta
2. Gutachter: Dr. Lukas Janssen

Abstract

We investigate topological quantum phase transitions with concomitant symmetry breaking in Kugel-Khomskii type models with bond-dependent interactions in the orbital degrees of freedom. These models support Kitaev spin-orbital liquid ground states, featuring gapless Majorana fermions in the presence of a static Z_2 gauge field. We present a class of spin-only interactions that do not perturb the gauge field, such that the low-energy physics are described by a theory of interacting Majorana fermions, which supports various symmetry-breaking channels, depending on the nature of the perturbation. An approximate phase diagram for two of those models is derived from Majorana mean-field theory. The resulting quantum critical points describe new fractionalized fermionic universality classes, whose critical behavior we estimate using the ε-expansion to leading order.

First, we consider the Kitaev-XY spin orbital model, featuring U(1) spin-rotational symmetry. The model is shown to undergo a phase transition into a partially ordered phase with a spontaneously broken U(1) symmetry. The quantum critical point is governed by the Gross-Neveu-SO(2)* universality class. Furthermore, we consider the anisotropic Kitaev spin-orbital, which features two independent parameters, describing spin-only Ising and XY interactions. The model exhibits $U(1) \times Z_2$ symmetry, featuring multiple symmetry-breaking channels. In the easy-plane regime, the system supports a line of U(1) symmetry-breaking transition, whose critical behavior is shown to be governed by the GN-SO(2)* universality class. In the easy-axis regime, we uncover a Z_2 symmetry-breaking transition governed by the GN-Ising* universality universality class. We show that the endpoint connecting the two transitions, where both orders compete, describes a bicritical point governed by the bicritical fractionalized universality class GN-(SO(2)+I)*, which is characterized by two relevant eigenvalues and features an emergent SO(3) symmetry. Additionally, we present evidence for the appearance of a symmetry-enhanced first-order transition between the partially symmetry-broken phases.

Kurzzusammenfassung

Wir untersuchen topologische Quantenphasenübergänge mit simultaner Symmetriebrechung in Kugel-Khomskii-Modellen mit richtungsabhängigen Austauschwechselwirkungen in den orbitalen Freiheitsgraden. Diese Modelle beschreiben Kitaev-Spin-Orbital-Flüssigkeiten mit masselosen Majorana-Fermionen in Gegenwart eines statischen Z_2-Eichfeldes. Wir stellen eine Klasse von Spin-Wechselwirkungen vor, die das Eichfeld unberührt lassen, so dass die Niederenergiephysik durch eine Theorie wechselwirkender Majorana-Fermionen beschrieben wird, die je nach Art der Wechselwirkung verschiedene symmetriebrechende Kanäle unterstützt. Ein genähertes Phasendiagramm für zwei dieser Modelle wird aus der Majorana-Mean-Field-Theorie abgeleitet. Die sich daraus ergebenden quantenkritischen Punkte beschreiben neue fraktionialisierte fermionische Universalitätsklassen, deren kritisches Verhalten wir mit Hilfe der ε-Entwicklung in führender Ordnung abschätzen.
Zunächst betrachten wir das Kitaev-XY-Spin-Orbital-Modell mit U(1)-Symmetrie under Spin-Rotationen. Es wird gezeigt, dass das Modell einen Phasenübergang in eine teilweise geordnete Phase mit einer spontan gebrochenen U(1)-Symmetrie aufweist. Der quantenkritische Punkt wird von der Gross-Neveu-SO(2)*-Universalitätsklasse beschrieben. Darüber hinaus betrachten wir das anisotrope Kitaev-Spin-Orbital, das zwei unabhängige Parameter aufweist, die jeweils Ising- und XY-Wechselwirkungen beschreiben. Das Modell weist eine $\mathrm{U}(1)\times\mathsf{Z}_2$-Symmetrie auf und besitzt mehrere symmetriebrechende Kanäle. Im easy-plane Regime weist das System eine Linie von Übergängen mit U(1)-Symmetriebrechung auf, deren kritisches Verhalten durch die GN-SO(2)* Universalitätsklasse bestimmt wird. Analog entdecken wir im easy-axis Regime Übergänge mit spontan gebrochener Z_2-Symmetrie, die von der GN-Ising*-Universalitätsklasse bestimmt werden. Wir zeigen, dass der Endpunkt beider Übergänge, wo beide Ordnungen miteinander konkurrieren, einen bikritischen Punkt beschreibt, der von der bikritischen fraktionalisierten Universalitätsklasse GN-(SO(2)+I)* bestimmt wird, die durch zwei relevante Eigenwerte charakterisiert ist und eine emergente SO(3)-Symmetrie aufweist. Zusätzlich präsentieren wir Hinweise für das Auftreten eines symmetrieverstärkten Übergangs erster Ordnung zwischen den teilweise symmetriebrechenden Phasen.

Contents

1 Introduction

Quantum spin liquids (QSLs) present one of the most active and exciting fields of research in contemporary condensed matter physics. The defining feature of a QSL is that, even though it appears to be a featureless paramagnet, strong quantum fluctuations inhibit the formation of a magnetically ordered state down to vanishing temperature [1]. A key observation that distinguishes QSLs from classical paramagnets is their appearance as an inherent quantum phase. In contrast to conventional magnetic phases, QSL states cannot be derived from a semiclassical expansion about a classical reference state due to the extensive ground-state degeneracy of the underlying classical spin models [2]. Consequently, quantum tunneling leads to hybridization of the classical ground-state manifold, resulting in a macroscopically entangled ground-state, describing a unique superposition of all classical ground-state configurations featuring topological degeneracy [3]. Thus, center stage for the emergence of QSL ground states is given to the field of frustrated magnets, where competing interactions naturally lead to the required ground-state degeneracy in the classical limit. Although no material has been unequivocally confirmed to exhibit a spin-liquid ground state, a few promising candidate materials have been proposed, the most prominent being *Herbertsmithie* [4, 5], which realizes a spin $S = \frac{1}{2}$ Heisenberg model on the Kagome lattice and has been confirmed to stay paramagnetic to very low temperatures by NMR measurements. Another, historically important example is Anderson's resonating valence-bond (RVB) state for the Heisenberg model on the triangular lattice [6], which is generally seen as the first theoretical example of a QSL state, featuring a highly entangled ground state and a gapped excitation spectrum.

From a modern perspective, quantum spin liquids are characterized by the appearance of fractionalized low-energy excitations, so-called *spinons*, which are coupled by an emergent gauge field [1]. The nature of these excitations is non-local and can realize anyonic statistics, emphasizing the topological character of QSL phases [7]. Most importantly, the spinons are deconfined in the QSL phase, thus allowing them to propagate independently, which can in principle be measured in appropriate transport experiments [1]. Within this paradigm, a large variety of qualitatively different QSL phases, which are usually categorized by their gauge symmetry as well as the nature of their low-energy excitations. In particular, it allows for gapless QSL phases because the spinons usually do not carry charge. The paradigmatic example of a gapless QSL is given by the celebrated *Kitaev honeycomb model*, first introduced by Kitaev in his seminal work in 2006 [8]. Even though the model is highly frustrated, im-

plementing Ising interactions with bond-dependent quantization axes between spins $S = \frac{1}{2}$, it can be exactly solved, featuring gapless itinerant Majorana fermion excitations coupled to a static Z_2 gauge field with localized, gapped flux excitations. Additionally, the model features various gapped QSL phases if we also allow for bond-dependend exchange couplings. It was initially introduced as toy model to demonstrate the feasibility of topological quantum computing due to its ability to support non-abelian anyons [8]. However, the model quickly caught interest in the condensed matter community after Jackeli and Khalluin [9] discovered that the highly anisotropic Kitaev interaction, which seems quite artificial at the first glance, could be engineered in certain Mott insulators with strong spin-orbit coupling. The most prominent example of such materials is -$RuCl_3$, which has been argued to be in the proximity of a QSL phase based on measurements of a half-quantized thermal Hall conductivity [10, 11], which can be explained by the appearance of deconfined fractionalized quasiparticles [12, 13]. However, the debate on the interpretation of these results is still ongoing.

From a theoretical point of view, the Kitaev honeycomb model is particularly interesting due to its exact solution, which can be used as a starting point for a more general class of model, featuring a rich phase diagram with various magnetic phases [14]. However, the introduction of arbitrary interactions does not only spoil the exact solvability of the model, but also generically introduces gauge dynamics, which makes a detailed analysis of the quantum phase transitions in such a model difficult. Fortunately, the strategy of Kitaev's exact solution is not restricted to spin $S = \frac{1}{2}$ and has been extended to several models with more internal degrees of freedom. Previously studied models include spin $S = \frac{3}{2}$ Hamiltonians [15] as well as spin $S = \frac{1}{2}$ models with two spins per site of a honeycomb lattice [16] or, similarly, on a decorated honeycomb lattice [17], the latter two producing effective spin-orbital descriptions of the Kugel-Khomskii type [18]. A more detailed exposure on the physical relevance of such models is given in Ref. [19]. All of these models arise from a more general family of exactly solvable models [20] and can be exactly solved by a Majorana representation, displaying so-called *Kitaev spin-orbital liquid* (Kitaev SOL) ground states with static Z_2 gauge fields and gapless itinerant Majorana fermions, fully analogous to the Kitaev honeycomb model. In contrast to the $S = \frac{1}{2}$ model, starting from exactly solvable models in the spin-orbital formulation allows for numerous interactions that will leave the Z_2 gauge field static, such that the corresponding low-energy description can be purely formulated in terms of interacting Majorana fermions. Interestingly, this also includes the $S = \frac{3}{2}$ Kitaev honeycomb model, which can be rewritten in a pseudo spin-orbital formulation [21, 22]. Another example has been presented in Ref. [23], which studies the critical behavior of a spin-orbital with full SU(2) symmetry in the spin sector [24] in the presence of a spin-only Heisenberg interaction. While the ground state of the exactly solvable model, characterized by three flavors of gapless Majorana fermions, is stable against small perturbations, it transitions into a topologically different SOL phase at strong couplings, gapping out two of the three itinerant Majorana fermions. At the transition, the SU(2) spin

symmetry of the model is spontaneously broken, thus describing a continuous phase transition, giving rise to a quantum critical point whose behavior is governed by the coupling of the order parameter to gapless fractionalized fermionic degrees of freedom. This gives rise to a previously unknown universality class *Gross-Neveu-SO(3)**, the up to now first and only known example of a *fractionalized fermionic quantum critical point*. In contrast to their bosonic counterparts, which are known to describe transitions between trivial and topologically ordered phases [25] or deconfined quantum critical points [26], these critical points have well-defined order parameters and can thus be studied within the framework of continuous phase transitions.

Motivated by these developments, the aim of this thesis is to study similar Kitaev spin-orbital models and uncover related universality classes and their associated critical behavior for different symmetry-breaking patterns by means of Majorana mean-field theory and the momentum-shell Renormalization Group in the ε-expansion. It turns out that spin-only interactions generically decouple from the Z_2 gauge field, such that the model in Ref. [23] is straightforwardly generalized to models of lower symmetry, which will be the starting point of the analysis carried out in this thesis.

This work is outlined as follows: Following a brief review of the basic concepts of continuous phase transitions and the Renormalization Group in Ch. 2, we start the main part of this thesis by investigating the properties of various types of exactly solvable Kitaev spin-orbital models and suitable perturbations in Ch. 3. In Ch. 4 we discuss the phase diagram and the critical behavior of a spin-orbital model with U(1) spin-rotation symmetry, which is spontaneously broken at strong couplings, giving rise to a new fractionalized universality class. In Ch. 5, we then expand on the previous findings by introducing anisotropy, giving a model with two inequivalent symmetry-breaking channels and thus two order parameters, featuring a bicritcal point with two relevant parameters. We summarize our results and give an outlook on possible future directions of research in Ch. 6.

2 Phase transitions and the Renormalization group

One of the key insights of statistical mechanics is that the equilibrium properties of a system can be described by a few macroscopic quantities. When external parameters such as temperature, pressure or an external magnetic field are varied, it may happen that the qualitative behavior of these quantities changes abruptly, marking the onset of a phase transition[27]. Formally, all macroscopic properties of the system are encoded in in its free energy, or appropriate thermodynamic potential. Thus, phase transitions may be defined as points in the space of possible control parameters where the free energy exhibits non-analytic behavior. A small but remarkable subset of phase transitions are continuous phase transitions, where the first derivatives of the free energy behave continuously between the two adjacent phases. They are usually described by an order parameter, which acquires a finite expectation value in the ordered phase and thus spontaneously breaks a symmetry of the underlying Hamiltonian. In the symmetric phase, the order parameter vanishes. Continuous phase transitions have a remarkable property known as *critical phenomena*. In the vicinity of the critical point, many of the equilibrium properties of the system obey power laws as they approach the transition. Remarkably, the critical exponents are insensitive to the microscopic details of the system at hand and depend only on global properties of the system, such as dimensionality or symmetry. Most importantly, the critical exponents agree for many systems with seemingly no physical connection, a phenomenon known as *universality*. Continuous phase transitions can thus be organized into *universality classes*, which are characterized by the same set of critical exponents.

This chapter introduces the basic concepts necessary to understand and characterize critical phenomena. In Sec. 2.1, we introduce the most common critical exponents and the relations between them. Sec. 2.2 briefly introduces the concept of a quantum phase transition. In Sec. 2.3, we introduce the concept of the Renormalization Group, providing both an explanation for critical phenomena and a calculational tool to characterize various universality classes.

2.1 Critical exponents and scaling laws

For magnetic transitions, which we consider in this work, the magnetization takes the role of the order parameter and the most common power laws are [28]

Specific heat:	$C(t) \propto \lvert t\rvert^{-\alpha}$;	(2.1)
Magnetization:	$m(t) \propto (-t)^{\beta}$; $t \leq 0$;	(2.2)
Susceptibility:	$\chi(t) \propto \lvert t\rvert^{-\gamma}$	(2.3)
Critical isotherm:	$m(h) \propto \lvert h\rvert^{\delta} \operatorname{sgn}(h)$; $t = 0$; ;	(2.4)

where h denotes a magnetic field variable and t is some measure for the distance of the system from the critical point. Commonly, and for the following discussion, t denotes the reduced temperature

$$t = \frac{T - T_C}{T_C}; \tag{2.5}$$

where T_C denotes the critical temperature of the phase transition, but it is straightforward to generalize Eqs. (2.1)–(2.4) to any non-thermal control parameter and other order parameters. The powers ; ; and are called *critical exponents*. Two more exponents, which are not connected to thermodynamic quantities but to local fluctuations of the magnetization can be defined via the correlation function of the local magnetization density, whose asymptotic behavior away from the critical point

$$G(r) \propto e^{-\frac{r}{\xi}} \qquad (r \qquad); \tag{2.6}$$

defines the *correlation length* . Loosely speaking, the correlation length describes the typical linear size of magnetic fluctuations, or, more formally, a typical length scale. Approaching the transition the correlation length obeys a power law

$$\propto \lvert t\rvert^{-\nu} ; \tag{2.7}$$

where we have introduced the correlation length exponent . Close to the critical point, the correlation length is large and presents the only relevant length scale in the system. At the critical point, the correlation length diverges and the system becomes *scale invariant* and fluctuations at all length scales become important. The scale dependence of the correlation function (2.6) disappears and the correlation function becomes

$$G(r) \propto \frac{1}{r^{D-2+\eta}}; \tag{2.8}$$

where D denotes the dimensionality of space. The critical exponent is usually called *anomalous dimension*, since it provides an apparent correction to the space dimension D if we compare

Eq. (2.8) to the form of the correlation function obtained from naive scaling [27]. The importance of scaling to the understanding of critical phenomena was first realized by Widom [29]. If we assume the singular part of the free energy density to satisfy a generalized homogeneity relation

$$f(t;h) = b^{-D} f(tb^{y_t}; hb^{y_h}); \tag{2.9}$$

where y_t and y_h are two critical exponents and $b > 1$ refers to an arbitrary scaling parameter, the power laws (2.1)–(2.4) can be derived from Eq. (2.9) for a suitable choice of scaling parameter [28]. Additionally, the scaling form reveals that only two of the four macroscopic exponents are independent, giving rise to two *scaling relations*

$$2 - \quad = 2 \quad + \quad ; \tag{2.10}$$

$$2 - \quad = \quad (\quad + 1): \tag{2.11}$$

A similar scaling assumption for the correlation function derives the power laws (2.7) and (2.8) and introduces hyperscaling relations

$$2 - \quad = D \ ; \tag{2.12}$$

$$= (2 - \ ) \ ; \tag{2.13}$$

as well as the relation

$$= \frac{1}{y_t}: \tag{2.14}$$

This allows us to express all thermodynamic critical exponents in terms of the correlation length exponents, which will turn out to be accessible for practical calculations. A microscopic derivation of the scaling assumptions as well as a framework for the calculation of the critical exponents in Eq. (2.9) is given by the *Renormalization Group*, which will be introduced with more detail in Sec. 2.3. Note that the hyperscaling relations fail above the *upper critical dimension*, describing the dimension below which fluctuations become important to the critical behavior. This is due to the appearance of a dangerously irrelevant scaling variable in the RG sense, see e. g. Ref. [30].

2.2 Quantum phase transitions

This chapter briefly reviews the basic aspects of quantum phase transitions and how their critical behavior differs from the thermal transitions discussed in the previous section. A thorough introduction to the field by be found in Refs. [31, 32]. A quantum phase transition is a phase transition that takes place at $T = 0$ and is thus facilitated by a non-analyticity of the ground-state energy at some critical value for a non-thermal control parameter r, denoting the distance from the quantum critical point. This can be external parameters, such as a magnetic

field or pressure, but also parameters intrinsic to the system, such as coupling constants. In the absence of thermal fluctuations, the transition is solely driven by quantum effects.

It is convenient to describe the properties of systems near the quantum critical point in the imaginary time functional integral formulation [33], providing a unified description of finite and zero temperature phenomena. Near the transition, the important degrees of freedom are long-wavelength order-parameter fluctuations . Thus, they can be appropriately described by an effective field theory

$$Z = \int D \; e^{-S[\,]}; \tag{2.15}$$

$$S = \int_0 d \int d^D r L[\,]; \tag{2.16}$$

where d is the space dimension, $= \frac{1}{T}$ is the inverse temperature and the functional integral assumes periodic boundary conditions $(= 0) = (=)$ because is bosonic. The order parameter fluctuations are slowly varying functions of space and imaginary time [3]. $S[\,]$ is the *Euclidean e ective action*, such that $L[\,]$ denotes the effective Lagrangian. Formally, the Lagrangian is given by including fluctuations in imaginary time

$$L[\,] = @ \quad + H[\,]; \tag{2.17}$$

where $H[\,]$ is the low-energy effective Hamiltonian of the microscopic theory. Calculating Eq. (2.17) from first principles can be challenging because the the order parameter typically describes coarse-grained collective behavior of the microscopic degrees of freedom. In Sec. 4.2 we show how to obtain the effective action for the order parameter using a suitable Hubbard-Stratonovich transformation, which often requires an educated guess or pre-existing knowledge about the phase transition. Close to a continuous phase transition, a phenomenological approach in the spirit of Landau is also viable. Since the order parameter is small close to the transition, the action (2.16) can be expanded in powers of , generating only symmetry-allowed terms. This approach is used in Sec. 5.2.

For finite temperatures, all but the $(!_n = 0)$ Matsubara mode are gapped and do not contribute to the singular part of the free energy [30], which consequently is independent of imaginary time, resulting in the homogeneity relation (2.9). Thus, finite temperature transition are dominated by classical thermal fluctuations. At $T = 0$, the integral over imaginary time acts as an extra space dimension and the Matsubara frequencies become gapless. Both fluctuations in space and imaginary time contribute to the singular part of the ground-state energy, such that the transition is described by an Euclidean quantum field theory, with a suitable microscopic cutoff. This introduces a new characteristic scale, the *correlation time*

$$_c \; / \; ^z; \tag{2.18}$$

with the *dynamical critical exponent* z, which is finite at $T = 0$ and diverges at the quantum critical point. Consequently, the homogeneity relation for the singular part of the free energy density is modified, giving

$$f(r;h) = b^{-(D+z)} f(rb^{y_t}; hb^{y_h}); \tag{2.19}$$

such that the quantum system in D space dimensions behaves like a a classical system in $D + z$ dimensions. This is the celebrated quantum-classical correspondence [32]. However, the situation changes in the presence of fermions that couple to the order parameter, which are naturally present in many electronic systems. If the fermions are gapped, they can be integrated out in the functional integral, only contributing to the regular part of the free energy. Integration over gapless fermions leads to divergencies which fundamentally change the critical behavior, giving rise to fermionic universality classes with different critical exponents. Of particular interest are systems featuring fermions with a linear-low energy spectrum. Since such systems have $z = 1$, they show an emergent Lorentz symmetry near criticality and are described by relativistic quantum field theories. Examples include graphene, producing a zoo of universality classes in the presence of interactions between the fermions [34], but also the Kitaev spin-orbitals considered in this work, whose gapless Majorana excitations have a linear dispersion in the low-energy limit, facilitating the appearance of fractionalized fermionic universality classes.

2.3 Renormalization Group

2.3.1 Wilsonian Renormalization Group

Due to the relevance of order parameter fluctuations at all scales at the phase transition, any approximation scheme that does not systematically include these fluctuations will ultimately fail in the proximity of the critical point. The appropriate tool to study the effects of fluctuations on all scales is the *Renormalization Group* (RG), which provides a radically different approach to the systematic study of critical behavior. The idea goes back to the work of Kadanoff [35], who proposed that the scaling form of the parameters in the scaling hypothesis (2.9) could in principle be derived by successively averaging over small-distance degrees of freedom and appropriate rescaling. This idea was then formalized by Wilson in form of the *momentum-shell* RG. Wilson's key insight was that Kadanoff's iterative coarse-graining can be effectively carried out in momentum space [36, 37], allowing us to calculate the critical exponents explicitly, to a certain degree of approximation. This is particularly attractive in the context of the field theories discussed in the previous section, where the coarse-graining step is naturally implemented by integrating over modes with large momenta, called fast modes, in the functional integral. Starting from the the initial effective action (2.16) with the microscopic cutoff , the RG procedure is based on the assumption that the coarse-grained action for the

remaining low-momentum modes, called slow modes, can be transformed into its initial form, but with couplings that have been renormalized by interactions between fast and slow modes. This can be achieved by appropriate rescaling of momenta and fields, which only enter the the partition function (2.15) as integration variables. The resulting renormalized action describes the same physics as the initial action. Following Ref. [38], the detailed implementation of the RG step is described as follows:

1. Integration over fast modes. This is also known as momentum-shell integration. The first step is to explicitly integrate over fast modes in the partition function. This amounts to integrating over fields within the spherical momentum shell

$$=b < p < \quad ; \tag{2.20}$$

   where p denotes the absolute value of the momenta and $b > 1$ is an arbitrary scale parameter that can be identified with the scale parameter in the homogeneity relations (2.9) and (2.19), as we will demonstrate shortly. The coarse-grained action has momentum cutoff .

2. Rescale momenta $bp \; ! \; p$. In the second step, we rescale all momenta in the coarse-grained action from step 1 to bring back the cutoff to its initial value . This step is necessary to make the RG procedure independent of scale.

3. Renormalize fields. This step is usually chosen to make the momentum-dependent contributions in the effective action contributions invariant under RG transformations, which is necessary to compare correlation functions at different scales.

Following this procedure, we obtain the renormalized effective action S^0, which takes the same form as the initial action with renormalized coupling constants. Denoting the set of coupling constants describing the action (2.16) with $[K]$, the RG procedure thus produces a map in the space of coupling constants

$$[K^0] = R_b[K]; \tag{2.21}$$

which expresses how the couplings of the theory change defining the RG recursion relation. Since the recursion relation does not explicitly depend on the inital scale, fluctuations can now be integrated out systematically by successive application of the RG transformation to obtain an effective theory which includes fluctuation effects up to the correlation length [39].

2.3.2 Fixed points and critical behavior

Since the partition function remains invariant under the RG transformation by construction, the recursion relation (2.21) enables us to connect physical quantities of the theory at different

scales [40]. This also explains the significance of *fixed points* of the RG transformation, which satisfy

$$[K_*] = R_b[K_*]: \tag{2.22}$$

Fixed point define scale-invariant theories in the space of coupling constants. Since the fixed point maps onto itself under RG transformations, all dimensionful observables either diverge or vanish, in particular the correlation length. Fixed points with diverging correlation length are associated with critical points of continuous phase transitions. Remarkably, all theories that flow into the critical fixed point, the so-called basin of attraction, also have infinite correlation length and thus describe critical points. This feature is responsible for the phenomenon of universality. At infinite correlation length, all fluctuations have to be taken into account, corresponding to infinite iterations of the RG recursion relations, after which all theories in the basin of attraction flow into the fixed point, which it therefore also called *IR*.
Since the scale parameter b in the momentum-shell RG is continuous, the recursion relations (2.21) are conveniently studied in differential form [41]

$$\frac{\mathrm{d}}{\mathrm{d}\ln b} K_i = \beta_i([K]); \tag{2.23}$$

where K_i denotes a single coupling from the set $[K]$, defining a set of differential equations governing the *Renormalization Group flow*. Fixed points of the RG flow are then given by the zeros of the functions β_i, which can be obtained by performing the integral over fast modes. The scaling behavior in the vicinity of the continuous phase transition is connected to the RG flow close to the associated fixed point. For small deviations from the fixed point, the RG flow equations (2.23) can be linearized, giving

$$\frac{\mathrm{d}}{\mathrm{d}\ln b} \delta K_i = \sum_j \left.\frac{\partial \beta_i}{\partial K_j}\right|_* \delta K_j; \tag{2.24}$$

where δK_i denotes the deviation from the fixed point value K_{i*}. The RG flow in the vicinity of the fixed point is characterized by the eigenvectors $\delta\kappa_i$ of the stability matrix

$$M_{ij} = \left.\frac{\partial \beta_i}{\partial K_j}\right|_*; \tag{2.25}$$

given by the Jacobian of the flow equations (2.23), evaluated at the fixed point. In the eigenbasis, the linearized flow reads

$$\frac{\mathrm{d}}{\mathrm{d}\ln b} \delta\kappa_i = y_i \delta\kappa_i: \tag{2.26}$$

Consequently, the stability of the fixed point depends on the sign of the eigenvalues y_i. For positive y_i, deviations in the direction of the corresponding eigenvector $\delta\kappa_i$ grow under RG

transformations, rendering the fixed point unstable in this direction. This is called a *relevant* direction in RG terminology. For negative y_i, deviations flow into the fixed point, marking stable directions, which are called *irrelevant*. Directions with $y_i = 0$ do not change under RG transformations and are called *marginal*. The identification of a fixed point with a continuous phase transition is straightforward. Fully stable fixed points usually represent stble thermodynamic phases. In the usual setup, with a single control parameter t, tuning to critcality corresponds to fixing a single relevant direction, such that the critical fixed point has one positive eigenvalue. The RG scaling of the control parameter is then governed by the RG flow of the single relevant direction of the critical fixed point. Upon solving the corresponding differential equation in Eq. (2.26) and identifying the control parameter with the relevant direction at the fixed point, we get

$$t' = tb^{y_t}; \tag{2.27}$$

where y_t denotes the relevant eigenvalue of the critical fixed point, which precisely takes the form required in the homogeneity relation (2.9). Consequently, we can identify the relevant eigenvalue of the critical fixed point with y_t in Eq. (2.14), providing a microscopic explanation for the appearance of scaling laws and universal critical exponents close to continuous phase transitions. Irrelevant eigenvalue turn out to produce leading corrections to the scaling. However, this will not be discussed in this work and we refer to the references in this section for a detailed exposure. A specific implementation of the Renormalization Group well suited for the application to quantum field theories will be introduced in detail in Ch. 4. For systems with more than one control parameter, interesting phenomena like multicriticality arise [41]. An example of a multicritical point will be studied in Ch. 5.

3 Kitaev spin-orbital models

This chapter aims to introduce a variety of exactly solvable spin-orbital models, which support gapless itinerant Majorana excitation and static Z_2 gauge fields. In Sec. 3.1, we introduce the celebrated Kitaev honeycomb model and its exact solution [8] to some detail, obtaining the low-energy spectrum and the phase diagram. In Sec. 3.2, we generalize the exact solution to various spin-orbital models via Ref. [20] and present a class of perturbations that leave the gauge field static, such that the low-energy description only involves the fermionic degrees of freedom. The resulting models will prove to be candidates for the appearance of new fractionalized fermionic quantum critical points.

3.1 Kitaev honeycomb model

3.1.1 Hamiltonian

The Kitaev honeycomb model describes a system of quantum spin $S = \frac{1}{2}$ degrees of freedom on the two-dimensional honeycomb lattice, with spins interacting via nearest-neighbor interactions, featuring Ising type interactions with bond-dependent quantization axis [8]. The Hamiltonian reads

$$H = -\sum_{\langle ij\rangle_\alpha} K_\alpha \sigma_i^\alpha \sigma_j^\alpha; \tag{3.1}$$

where the sum is over all nearest-neighbor bonds $\langle ij\rangle_\alpha$ and α refers to the bond type on the honeycomb lattice, as shown in Fig. 3.1a. The exchange couplings $K_\alpha \geq 0$ are in general considered bond-dependent and ferromagnetic, but can also take antiferromagnetic values without changing the physics, as discussed shortly. While the lattice itself exhibits no geometrical frustration, the nature of the interaction does not allow a single spin to minimize the energy along all neighboring bonds, giving rise to so-called exchange frustration [42]. This leads to suppression of long-range magnetic order and a residual ground-state entropy (i. e. an extensive ground-state degeneracy) [13], making the problem generically difficult to solve. Surprisingly, the Hamiltonian (3.1) features an extensive amount of conserved quantities. In fact, a plaquette operator associated with closed loops on the underlying lattice can be constructed as follows [8],

$$W_p = \prod_{j\in p} \sigma_j^{\alpha_j} \sigma_{j+1}^{\alpha_{j+1}}. \tag{3.2}$$

It is easy to show that the plaquette operators defined in Eq. (3.2) are Hermitian and unitary and have eigenvalues ± 1, corresponding to a Z_2 flux through the plaquettes. Additionally, they commute with Hamiltonian and with each other, describing intergrals of motion of the system. This allows partitioning the Hilbert space into orthogonal sectors of conserved flux. The local flux conservation already predicts several of the defining properties of QSLs. As local spin flips create flux excitations on neighboring plaquettes, they project any state onto an orthogonal flux sector. Consequently, spin expectation values vanish on all lattice sites. Additionally, these fluxes have no dynamics and hence cannot propagate through the lattice, leading to extremely short-ranged spatial spin-spin correlations [43, 44]. The ground state may be identified following a theorem by Lieb which states that the energy of the Hamiltonian (3.1) is minimized by the flux-free field configuration [45]. This corresponds to choosing $W_p = 1$ for every plaquette.

3.1.2 Majorana representation

Following the remarks of the previous section, the ground state can be found by diagonalizing the remaining degrees of freedom in the flux-free Hilbert space sector. By expressing the spin operators in terms of 4 flavors of Majorana fermions, the Hamiltonian (3.1) can be exactly solved [8]. Physically, Majorana fermions are neutral fermions that simultaneously describe particle and anti-particle. Following Ref. [8], they are formally described by so-called Majorana operators, which are Hermitian, square to unity and are mutually anti-commuting

$$\{c_\alpha, c_\beta\} = 2\delta_{\alpha\beta}, \tag{3.3}$$

where c_α and c_β denote distinct Majorana operators if $\alpha \neq \beta$. They can be constructed from linear combinations of fermionic creation and annihilation operators, mimicking imaginary and real part of the corresponding bosonic operators. Accordingly, a single complex fermion mode gives rise to two Majorana modes [46]. For the model at hand, 4 Majorana operators b_j^x, b_j^y, b_j^z, c_j can now be defined on each lattice site j to represent the local spins as

$$\sigma_j^\alpha \rightarrow i b_j^\alpha c_j. \tag{3.4}$$

Inspection of the dimensionality of the internal Hilbert space on each site reveals that the 4 Majorana operators act on a 4-dimensional fermionic Fock space, while the local Hilbert space of the spin carries dimension 2 [8]. This means that the Hilbert space of the Majorana representation is enlarged in comparison to the physical Hilbert space and generic states in the Majorana representation contain unphysical components. A local constraint that restricts extended states to the physical subspace may be formulated in terms of the operator

$$D_j = \sigma_j^x \sigma_j^y \sigma_j^z \rightarrow b_j^x b_j^y b_j^z c_j, \tag{3.5}$$

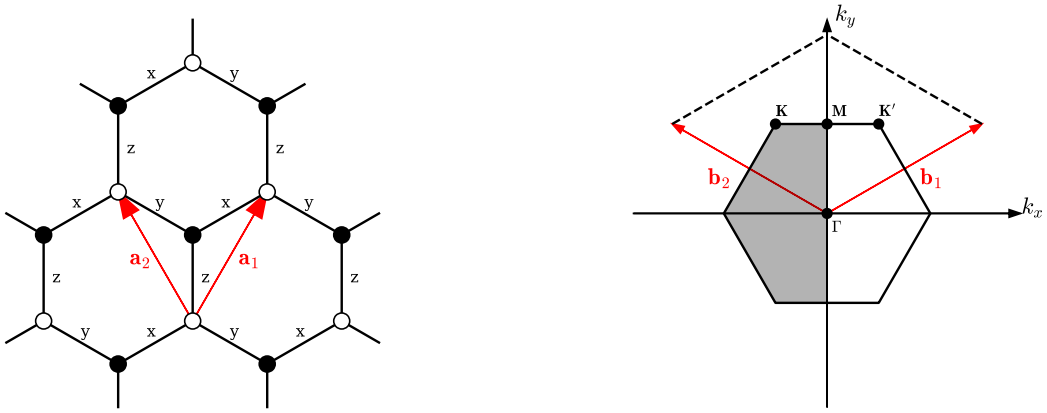

(a) (b)

Figure 3.1: (a) Schematic picture of the honeycomb lattice. The bond type is given by the letters $x; y$ and z and denotes the quantization axis for the bond-dependent Ising interactions. The red arrows denote the unit vectors, which in our convention are defined to be of unit length, giving $\mathbf{a}_1 = \frac{1}{2}(1; \sqrt{3})$ and $\mathbf{a}_2 = \frac{1}{2}(-1; \sqrt{3})$. (b) Brillouin zone (BZ) of the honeycomb lattice. The red arrows denote the reciprocal vectors $\mathbf{b}_1 = \frac{2}{3}(3; \sqrt{3})$ and $\mathbf{b}_2 = \frac{2}{3}(-3; \sqrt{3})$ and the special points $\mathbf{K} = -\mathbf{K}'$ are given by $\mathbf{K} = \frac{2}{3}(-1; \sqrt{3})$. In the Kitaev honeycomb model, we consider only half of the first BZ, given by the grey shaded area, only containing one of the two special points.

where the second expression follows trivially from insertion of the representation given in Eq. (3.4). The operator D_j is Hermitian and unitary and thus has eigenvalues ± 1. It turns out that the SU(2) spin algebra is faithfully repoduced only for the subspace with eigenvalue $D_j = +1$, which corresponds to the identity $\sigma^x_j \sigma^y_j \sigma^z_j = i$. The physical states of the system may then be recovered by a Gutzwiller projection

$$P_G = \prod_j \left(\frac{1 + D_j}{2} \right); \tag{3.6}$$

which projects states in the extended space onto the local physical Hilbert space given by the subspace with $D_j = +1$ on each lattice site [42]. Formally, the operator D_j acts as a local Z_2 gauge transformation. In this language, the Gutzwiller projection P_G corresponds to a symmetrization over all gauge configurations [8].

Application of the spin representation in Eq. (3.4) to the Hamiltonian (3.1) maps it onto a Hamiltonian of interacting Majorana fermions

$$H = \sum_{\langle ij \rangle_\alpha} K_\alpha \left(i b_i b_j \right) i c_i c_j; \tag{3.7}$$

consisting of quartic terms in the Majorana operators. Defining bond operators $u_{ij} = ib_i b_j$ on each bond, where corresponds to the bond type, the Hamiltonian (3.7) takes the form

$$H = \sum_{\langle ij \rangle_\alpha} K_\alpha u_{ij} i c_i c_j . \tag{3.8}$$

Similar to the plaquette operators defined in Eq. (3.2), the u_{ij} are Hermitian and unitary and commute with themselves and the Hamiltonian. Thus, they can equally be replaced by their eigenvalues ± 1. This reduces the Hamiltonian (3.8) to a quadratic form of a single flavor of non-interacting Majorana fermions, rendering it exactly solvable. Note that the bond operators are not gauge invariant and hence do not represent physical quantities. More precisely, applying a local gauge transformation on site j flips the sign of all adjacent bond operators. On the other hand, a gauge-invariant loop operators may be constructed from the bond operators

$$W_p = \prod_{j \in p} u_{j,j+1} . \tag{3.9}$$

Note that $u_{ij} = -u_{ji}$ due to the anti-commutativity of the Majorana operators. To avoid confusion, we will use a notation where site i (j) belongs to sublattice A (B) on the honeycomb lattice. Application of the gauge transformation on a single site flips the sign of two bond operators on each adjacent loops and hence leaves their total sign unchanged [42]. Projection onto the physical subspace then recovers the definition of the plaquette operators formulated in Eq. (3.2).

One may think of the u_{ij} as an emergent $\mathbb{Z}_2$ gauge field that determines the hopping amplitude of the remaining Majorana flavor and the plaquette operators as the corresponding gauge-invariant $\mathbb{Z}_2$ flux [43, 46]. Importantly, the Hamiltonian (3.8) does not contain hopping terms for the bond operators, which describe gauge field dynamics. As such, the problem may be viewed as hopping of a single Majorana fermion flavor in the background of a static $\mathbb{Z}_2$ gauge field. Following these considerations, the model supports two kinds of fractionalized excitations: localized $\mathbb{Z}_2$ flux excitations, also called visons, and itinerant Majorana fermions, the spinons [43]. While the localized flux excitations are gapped for any finite exchange coupling, the nature of the fermionic spectrum depends on these couplings and may either be gapped or gapless.

3.1.3 Spectrum and phase diagram

The low-energy spectrum of the Hamiltonian (3.1) can now be obtained by diagonalizing the Majorana hopping problem in the ground-state flux sector, corresponding to a particular choice of the $\mathbb{Z}_2$ gauge variables. Due to the gauge redundancy, a given flux configuration may be realized by multiple configurations of the underlying gauge field and the choice of a

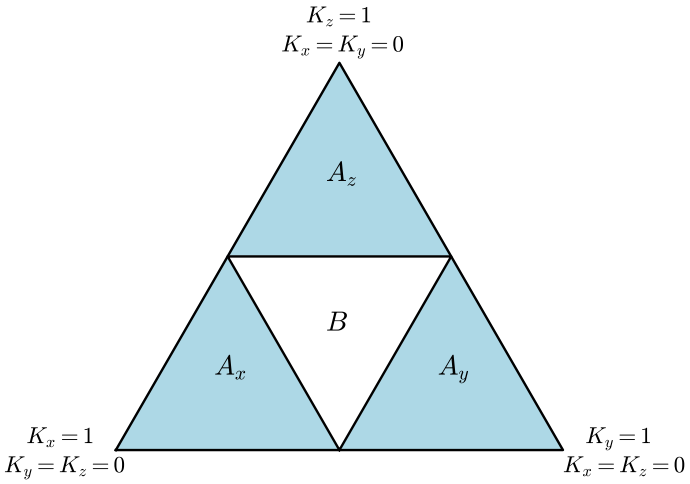

Figure 3.2: Cutout of the phase diagram of the Kitaev honeycomb model. The triangle represents the plane $K_x + K_y + K_z = 1$ in the positive octant of parameter space. The light blue shaded areas with $A_x; A_y$ and A_z denoted gapped spin-liquid phases, whereas the B phase near the isotropic point is gapless.

suitable configuration should therefore be considered as fixing a particular gauge [42]. This redundancy has important consequences. Firstly, while we assumed the exchange couplings to be ferromagnetic, exchanging their signs may be compensated by a sign change of the associated bond variables. For instance, replacing K_x with $-K_x$ is equivalent to a sign change of the u_{ij} on all x-bonds. This corresponds to a local gauge transformation , so that the ground-state energy and the spectrum of the Kitaev honeycomb model do not depend on the sign of the exchange couplings [8]. Secondly, although the ground-state sector in the physical Hilbert space is uniquely defined by the zero-flux configuration due to Lieb's theorem, the gauge redundancy of the Majorana description introduces additional gauge copies to any eigenstate spanning the extended space. These states have the same energy eigenvalues and may be obtained by a suitable local gauge transformation [44].

Now, there is a multitude of gauge configurations that recover the zero-flux sector. The most convenient choice for further calculations would be setting the bond variables to be equal on all bonds, e. g. $u_{ij} = +1$. The inverse convention may be recovered by a global gauge transformation on all lattice sites and is thus physically equivalent. The Hamiltonian in the ground-state flux sector then reads

$$H = \sum_{\langle ij\rangle} K \, ic_i c_j : \tag{3.10}$$

This gauge choice preserves the translational symmetry of the underlying honeycomb lattice and allows us to employ periodic boundary conditions to diagonalize the Hamiltonian (3.10)

by means of a Fourier transform of the Majorana operators on site j [8]

$$c_{j;s} = \sqrt{\frac{2}{N}} \sum_{\mathbf{k} 2 BZ} c_{\mathbf{k};s} e^{i\mathbf{k}\cdot\mathbf{r}_j}; \tag{3.11}$$

where s and N refer to the sublattice index and the number of sites, respectively, $\mathbf{r}_j$ denotes the unit cell vector and $\mathbf{k}$ denotes a momentum vector in the first Brillouin zone, which is depicted in Fig. 3.1b. Note that the operators $c_{\mathbf{k};s}$ defined in Eq. (3.11) are not Hermitian and thus do not describe Majorana operators. They satisfy anti-commutation relations $fc_{\mathbf{k};s}; c_{-\mathbf{k};l}g = {}_{sl}$ and the conjugate operator reads $c^{y}_{\mathbf{k};s} = c_{-\mathbf{k};s}$. Thus, Fourier-transformed Majorana operators at opposite momenta form a single complex fermion. Summation over the Brillouin zone then counts every mode twice and introduces a two-fold redundancy in the spectrum. Since the eigenvalues of quadratic forms of Majorana operators always appear in pairs $\pm"$ [8], there are two ways to deal with this redundancy. In Ref. [8], it is taken into account by only considering positive eigenvalues of the energy spectrum. For vanishing eigenvalues, two Majorana zero modes at opposite momenta are obtained. In this work, we will deal with the redundancy by considering only half of the Brillouin zone instead [17]. Here, the modes with finite energy are described by a single symmetric particle-hole spectrum and the Majorana zero modes are combined into a single fermionic mode with vanishing energy. Using this convention, the Fourier-transformed Hamiltonian reads

$$H = \sum_{\mathbf{k} 2 BZ=2} \begin{pmatrix} c^{y}_{\mathbf{k};A}; & c^{y}_{\mathbf{k};B} \end{pmatrix} \begin{pmatrix} 0 & if(\mathbf{k}) \\ -if^{*}(\mathbf{k}) & 0 \end{pmatrix} \begin{pmatrix} c_{\mathbf{k};A} \\ c_{\mathbf{k};B} \end{pmatrix}; \tag{3.12}$$

with

$$f(\mathbf{k}) = 2\left[K_x e^{-i\mathbf{k}\cdot\mathbf{a}_1} + K_y e^{-i\mathbf{k}\cdot\mathbf{a}_2} + K_z\right]; \tag{3.13}$$

where A and B again refer to sublattice indices and $\mathbf{a}_1$ and $\mathbf{a}_2$ are the unit vectors of the honeycomb lattice as defined in Fig. 3.1a. The single-particle energy levels are then given by the eigenvalues of the Bloch matrix in Eq. (3.12) and read

$$"(\mathbf{k}) = \pm jf(\mathbf{k})j: \tag{3.14}$$

A cutout of the phase diagram is shown in Fig. 3.2. At the isotropic point, the spectrum resembles the graphene dispersion with two Dirac cones centered at the highly symmetric points $\mathbf{K}$ and $\mathbf{K}^{0}$ (see Fig. 3.1b). As only half the Brillouin zone is considered here, these points coincide, leaving a low-energy description of just a single Dirac cone. The absence of an energy gap for the fermionic excitations stabilizes a gapless spin liquid phase, which is stable for small perturbations away from the isotropic point if the exchange couplings satisfy triangle

inequalities [8]

$$|K_x| \leq |K_y| + |K_z|; \quad |K_y| \leq |K_z| + |K_x|; \quad |K_z| \leq |K_x| + |K_y|: \tag{3.15}$$

For higher anisotropies, the dispersion acquires a gap, signaling a topological phase transition to a gapped spin liquid phase.

Note that, similar to the gauge field, the fermionic operators are not gauge-invariant, such that single fermions cannot form physical excitations. In fact, arbitrarily representing the four Majorana operators at each site by two fermions, one can show that the gauge transformation (3.5) measures the fermion parity at each site [20]. Thus, only states with even amount of fermions survive the Gutzwiller projection (3.6). Since two of the Majorana operators on each lattice site represent gauge excitations, itinerant Majorana fermions can thus only appear by exciting two gauge fluxes simultaneously, as we have already discussed earlier. This is a hallmark feature of fractionalization in condensed matter systems. Even though the elementary excitations feature fractional quantum numbers, physical states still have to obey the initial quantum numbers of the constituents, thus only allowing suitable composite states. For the specific case of the Kitaev honeycomb model, this is for instance expressed in the fact that the spin response features a flux-induced gap, even in the gapless phase [46, 24].

3.2 Kitaev spin-orbital models

3.2.1 Exactly solvable models

As we have already pointed out in the introduction, the an exact solution in terms of Majorana operators may be generalized to higher-dimensional local Hilbert spaces in various ways. A direct generalization to the Kitaev honeycomb model is given by the SU(2)-symmetric Kitaev spin-orbital model [17, 24]. It is defined on the honeycomb lattice by the Hamiltonian

$$H = -K \sum_{\langle ij \rangle_\gamma} \tau^\gamma_i \tau^\gamma_j \sigma^\gamma_i \sigma^\gamma_j \qquad (\gamma = x, y, z): \tag{3.16}$$

The notation carries over from Eq. (3.1), so that $\langle ij \rangle_\gamma$ refers to nearest-neighbor bonds and denotes the bond type. The local Hilbert space of the model results from a tensor product of a spin $S = \frac{1}{2}$ and a two-fold degenerate orbital degree of freedom. The Pauli matrices σ^γ_i and τ^γ_i act on spin and orbital degrees of freedom, respectively. While the coupling is of Kitaev type in the orbital sector, the operator acting on the spin sector corresponds to a Heisenberg term, so that the model possesses full SU(2) spin-rotation symmetry. The model corresponds to the $N_M = 3$ case of a more general class of exactly solvable models that can be constructed from the generators Γ^γ of higher-dimensional representations of the Clifford algebra [20], which reduces to the Hamiltonian (3.16) for a suitable choice of the Γ^γ matrices in terms of Pauli

matrices [23],

$$= - \quad ^{y} \quad ; \qquad ^{4} = \quad ^{x} \quad 1; \qquad ^{5} = - \quad ^{z} \quad 1: \tag{3.17}$$

The model shares many of the same features as the Kitaev honeycomb model and the exact solution can be derived in similar fashion. Accordingly, the model possesses an extensive amount of mutually commuting plaquette operators

$$W_p = 1 \quad \begin{matrix} x & y & z & x & y & z \\ i & j & k & l & m & n \end{matrix}; \tag{3.18}$$

which only affect the orbital degrees of freedom and act trivially in the spin sector. As before, they commute with the Hamiltonian and partition the Hilbert space into subspaces of conserved flux [23, 24]. Following Refs. [20] and [23], the Hamiltonian (3.16) may be diagonalized by a Majorana representation of the spin-orbital operators. In the 4-dimensional representation, the five matrices are mapped onto 6 Majorana operators

$$^{y} \qquad = -ib \; c^{y}; \qquad ^{x} \quad 1 = ic^{z}c^{y}; \qquad ^{z} \quad 1 = -ic^{x}c^{y}; \tag{3.19}$$

satisfying canonical anti-commutation relations given in Eq. (3.3). In analogy to the Kitaev honeycomb model, the Majorana operators can be combined into 3 complex fermions spanning an 8-dimensional Fock space, which is twice as large as the spin-orbital Hilbert space. The physical subspace may again be recovered by fixing the on-site fermion parity. This may be achieved by imposing a local constraint

$$D_j = \begin{matrix} x & y & z \\ j & j & j \end{matrix} \qquad \begin{matrix} x & y & z \\ j & j & j \end{matrix} \stackrel{!}{=} -1; \tag{3.20}$$

which reproduces the SU(2) algebra faithfully in spin and orbital sectors. In the Majorana description, the Hamiltonian (3.16) reduces to

$$H = K \sum_{\langle ij \rangle_{\alpha}} u_{ij} \sum \quad ic_i \, c_j \qquad (\quad = x; y; z); \tag{3.21}$$

where the bond variables $u_{ij} = ib_i b_j$ again define a static Z_2 gauge field connected to the conserved flux given by the plaquette operators (). Lieb's theorem is applicable here as well, so that the ground stat may be found in the flux-free sector, with the eigenvalues of the plaquette operators being equal to $+1$. By the same arguments as in Sec. 3.1.3, a zero-flux configuration may be achieved by choosing $u_{ij} = +1$ on all bonds. In the background of this gauge configuration, the Hamiltonian (3.21) reduces to

$$H = K \sum_{\langle ij \rangle_{\alpha}} \sum \quad ic_i \, c_j \qquad (\quad = x; y; z); \tag{3.22}$$

describing 3 decoupled flavors of non-interacting itinerant Majorana fermions. Interestingly,

the vison gap, which energetically separates the zero-flux sector from subspaces with non-zero flux, is thrice as large as in the spin $S = \frac{1}{2}$ model due to the additional Majorana degrees of freedom [24]. To obtain the energy spectrum of the Hamiltonian, we extend the Fourier transform defined in Eq. (3.10) to all 3 flavors of Majorana operators

$$c_{j;s} = \sqrt{\frac{2}{N}} \sum_{\mathbf{k} \in BZ} c_{\mathbf{k};s} e^{i\mathbf{k}\cdot\mathbf{r}_j} = \sqrt{\frac{2}{N}} \sum_{\mathbf{k} \in BZ=2} \left[c_{\mathbf{k};s} e^{i\mathbf{k}\cdot\mathbf{r}_j} + (c_{\mathbf{k};s})^y e^{-i\mathbf{k}\cdot\mathbf{r}_j} \right]; \tag{3.23}$$

where $= x; y; z$ denotes the additional flavor degree of freedom and the second equality is due to the $c_{j;s}$ being Hermitian as before. Insertion into the Hamiltonian (3.22) gives

$$H = \sum_{\mathbf{k} \in BZ=2} \begin{pmatrix} c^y_{\mathbf{k};A}, & c^y_{\mathbf{k};B} \end{pmatrix} \begin{pmatrix} 0 & iKf(\mathbf{k}) \\ -iKf^*(\mathbf{k}) & 0 \end{pmatrix} \otimes 1_3 \begin{pmatrix} c_{\mathbf{k};A} \\ c_{\mathbf{k};B} \end{pmatrix}; \tag{3.24}$$

where the $c_{\mathbf{k};s} = \left(c^x_{\mathbf{k};s}, c^y_{\mathbf{k};s}, c^z_{\mathbf{k};s} \right)^|$ denote 3-component spinors on sublattice $s = A; B$, describing the 3 flavors of Majorana fermions and the summation is over half of the Brillouin zone, again. With the function $f(\mathbf{k}) = 1 + e^{-i\mathbf{k}\cdot\mathbf{a}_1} + e^{-i\mathbf{k}\cdot\mathbf{a}_2}$, where, just as in Eq. (3.12), $\mathbf{a}_1$ and $\mathbf{a}_2$ refer to the primitive vectors of the honeycomb lattice, the spectrum of the Hamiltonian (3.24) is given by

$$\varepsilon(\mathbf{k}) = \pm K|f(\mathbf{k})|. \tag{3.25}$$

Thus, the Hamiltonian (3.24) describes 3 decoupled copies of the isotropic spin $S = \frac{1}{2}$ Kitaev honeycomb model, featuring 3 degenerate complex Dirac cones located at the symmetric $\mathbf{K}$ point, one for each flavor of Majorana fermions, realizing a so-called *spin-orbital liquid* (SOL). The corresponding normalized spectrum is shown in Fig. 3.3a.

The model construction described above is not restricted to Heisenberg interactions in the spin sector. More precisely, as long as the interaction in the orbital sector is of Kitaev type, an exact solution may be derived in the same spirit as the above discussion. This conclusion becomes clear when revisiting the specific form of the plaquette operator given in Eq. (3.18). The plaquette operators constitute conserved quantities due to their commutativity with the Hamiltonian. As the plaquette operator acts as unity in the spin sector and thus trivially commutes with arbitrary spin interaction terms, flux conservation is guaranteed in models featuring these interactions. The exact solvability then follows from the fact that interactions containing Kitaev exchange in the orbital sector will always allow for separation of the Majorana operators into bond variables u_{ij} and quadratic forms of the remaining c-flavor Majoranas. Although this insight in principle allows the construction of more exotic spin interactions, we will focus on more straightforward adaptions of the Hamiltonian (3.16) for now, namely by introducing anisotropies in the Heisenberg spin interaction. This will leave the Majorana fermions decoupled, whereas off-diagonal spin interaction of the type $_i \ _j$ with $\neq$ would introduce hybridization between the flavors. The corresponding spin-orbital

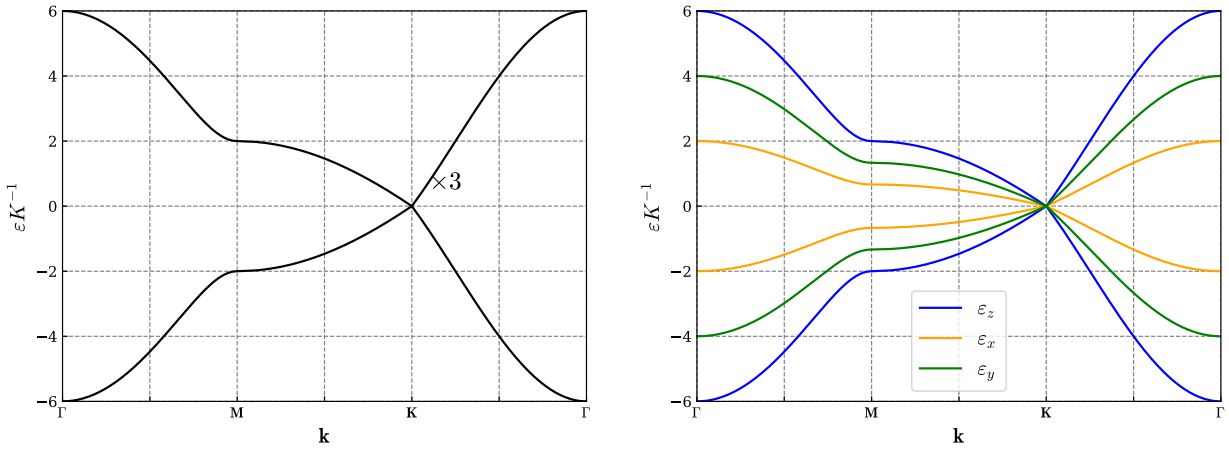

(a) (b)

Figure 3.3: (a) Normalized spectrum of the SU(2)-symmetric spin-orbital model, featuring three fully degenerate bands. (b) The introduction of spin-space anisotropies in Eq. () lifts the degeneracy of the three bands, while retaining their gapless nature. Here, we have used anisotropy factors $\Delta_x = \frac{1}{3}$ and $\Delta_y = \frac{2}{3}$. Both spectra have particle-hole symmetry, which is typical for quadratic Majorana Hamiltonians [8].

Hamiltonian reads

$$H = -K \sum_{\langle ij \rangle_i} \left({}_x {}^x_i {}^x_j + {}_y {}^y_i {}^y_j + {}^z_i {}^z_j \right) \quad {}_i \, {}_j ; \tag{3.26}$$

where $_x$ and $_y$ denote the degree of anisotropy in the respective spin direction. The introduction of coordinate-dependent anisotropies explicitly breaks the SU(2) symmetry of the isotropic Hamiltonian (3.16), corresponding to $_x = {}_y = 1$, to a global $\mathbb{Z}_2 \times \mathbb{Z}_2 \times \mathbb{Z}_2$ symmetry. Diagonalization of the momentum space Hamiltonian reveals that the introduction of anisotropies generically lifts the degeneracy of the Dirac cones associated with the 3 Majorana flavors. The dispersion relations for the three bands read

$$"_x(\mathbf{k}) = \pm \; {}_x K |f(\mathbf{k})|; \qquad "_y(\mathbf{k}) = \pm \; {}_y K |f(\mathbf{k})|; \qquad "_z(\mathbf{k}) = \pm K |f(\mathbf{k})|; \tag{3.27}$$

resulting in flavor-dependent Fermi velocities that scale with the respective degree of anisotropy. We have shown the lift of degeneracy for an exemplary configuration in Fig. 3.3b.

Two limits shall be discussed here in more detail. First, the limit $_x = 0; \; {}_y = 1$ (or vice versa, corresponding to a rotation by $\frac{}{2}$ in the x-y plane followed by a $\mathbb{Z}_2$ transformation in the y-coordinate) describes a spin-orbital model with XY-type interaction in the spin sector, given by

$$H = -K \sum_{\langle ij \rangle_i} \left({}^y_i {}^y_j + {}^z_i {}^z_j \right) \quad {}_i \, {}_j ; \tag{3.28}$$

which displays a global U(1) symmetry under rotations in the y-z plane. The vanishing Fermi velocity of the c^x band describes localized Majorana zero modes on every lattice site. Similarly, in the limit $_x = _y = 0$, two of the 3 Fermi velocities vanish, describing two flat bands and a single remaining Dirac cone. This is realized by an Ising-type interaction in the spin-orbital language. The corresponding model reads

$$H = -K \sum_{\langle ij \rangle_i} {}^z_i \, {}^z_j \quad _i \, _j ; \tag{3.29}$$

and possesses a global Z_2 spin-flip symmetry. An overview of the exactly solvable spin-orbital models presented in this section and their corresponding zero-flux Majorana Hamiltonians may be found in Table (3.1).

3.2.2 Perturbations

A key difference of spin-orbital realizations of the model in Ref. [20] compared to the spin $S = \frac{1}{2}$ Kitaev honeycomb model is that it allows for perturbations which, although spoiling the exact solvability of the model, do not introduce any gauge field dynamics into the system. In fact, any perturbation that commutes with the plaquette operators in Eq. (3.18) will keep the gauge field static and the local flux conserved. This is generically true for interactions that act trivially in the orbital degrees of freedom, i. e. pure spin interactions. To express interactions of this type in the Majorana representation, it is necessary to reformulate the spin operators, given by the SU(2) generators in spin space, in terms of Majorana operators. From Eq. (3.19) and the SU(2) algebra, we obtain

$$1_2 \; ! \; \frac{1}{2} c^{\dagger} L \; c; \tag{3.30}$$

where $(L \;)\quad = -i\quad$ are SO(3) generators acting on the three-dimensional Majorana flavor space represented by $c = (c^x; c^y; c^z)^{\dagger}$. Thus, spin rotations in the spin-orbital formulation map to SO(3) flavor rotations in the Majorana language and an SU(2) spin rotation symmetry induces a symmetry under global SO(3) flavor rotations[23].

Here, we will focus on perturbations corresponding to spin-only antiferromagnetic nearest-neighbor interactions. Due to the bipartite nature of the honeycomb lattice, such interactions will naturally manifest antiferromagnetic long-range order in the strong-coupling limit, thus making them prime candidates to facilitate symmetry-breaking phase transitions in the models presented in the previous chapter. For this purpose, we consider the Hamiltonian (3.16) augmented by the aforementioned interactions. One example of such a perturbation is given

	Kitaev spin-orbital Hamiltonian	Majorana Hamiltonian (flux-free)	spin symmetry
(a)	$-\sum_{\langle ij\rangle_\gamma} \tau^\gamma_i \tau^\gamma_j$	$\sum_{\langle ij\rangle_\gamma} i c_i c_j$	SU(2)
(b)	$-\sum_{\langle ij\rangle_\gamma} (\tau^x_i \tau^x_j + \tau^y_i \tau^y_j + \tau^z_i \tau^z_j)$	$\sum_{\langle ij\rangle_\gamma} (i \tau^x_i \tau^x_j c^x_i c^x_j + i \tau^y_i \tau^y_j c^y_i c^y_j + i c^z_i c^z_j)$	$\mathbb{Z}_2 \times \mathbb{Z}_2 \times \mathbb{Z}_2$
(c)	$-\sum_{\langle ij\rangle_\gamma} (\tau^x_i \tau^x_j + \tau^y_i \tau^y_j)$	$\sum_{\langle ij\rangle_\gamma} (i c^x_i c^x_j + i c^y_i c^y_j)$	U(1)
(d)	$-\sum_{\langle ij\rangle_\gamma} \tau^z_i \tau^z_j$	$\sum_{\langle ij\rangle_\gamma} i c^z_i c^z_j$	$\mathbb{Z}_2$

Table 3.1: Exactly solvable Kitaev spin-orbital Hamiltonians and their Majorana counterparts in the flux-free regime, as well as their respective spin and flavor symmetries. The exchange coupling has been normalized ($K = 1$).

by a spin-only SU(2)-symmetric Heisenberg interaction

$$H_J^{\mathrm{SU(2)}} = J \sum_{\langle ij\rangle_\gamma} \tau^\gamma_i \tau^\gamma_j \, \mathbb{1}_i \mathbb{1}_j \qquad (\gamma = x, y, z), \tag{3.31}$$

corresponding to (a) in Table 3.2, where $J > 0$ is the antiferromagnetic exchange coupling. With Eq. (3.16), the full Hamiltonian $H_K^{\mathrm{SU(2)}} = H_K + H_J^{\mathrm{SU(2)}}$ reads

$$H_K^{\mathrm{SU(2)}} = -K \sum_{\langle ij\rangle_\gamma} \tau^\gamma_i \tau^\gamma_j + J \sum_{\langle ij\rangle_\gamma} \tau^\gamma_i \tau^\gamma_j \, \mathbb{1}_i \mathbb{1}_j \qquad (\gamma = x, y, z). \tag{3.32}$$

This model has been studied extensively in Refs. [23] and [47]. Both the exactly solvable model H_K and the perturbation $H_J^{\mathrm{SU(2)}}$ exhibit SU(2) spin rotation symmetry, which is inherited by the full Hamiltonian (3.32). The model is shown to support a continuous phase transition to an antiferromagnetic phase in which the SU(2) symmetry is spontaneously broken. Although Lieb's theorem does not explicitly hold when such interactions are switched on, numerical results in Ref. [23] suggest that the vison gap remains finite for any value of the antiferromagnetic coupling J. Thus, the ground state may still be found in the zero-flux sector. Insertion of Eq. (3.30) into the interaction (3.31) then yields the corresponding SO(3)-invariant Majorana Hamiltonian

$$H_K^{\mathrm{SU(2)}} \overset{\hat{u}^{\gamma\gamma}_{ij}=-1}{=} K \sum_{\langle ij\rangle_\gamma} i c_i c_j + J \sum_{\langle ij\rangle_\gamma} \left(\tfrac{1}{2} c_i^\dagger L^\gamma c_i\right)\left(\tfrac{1}{2} c_j^\dagger L^\gamma c_j\right) \qquad (\gamma = x, y, z). \tag{3.33}$$

Unlike the Kitaev term, the antiferromagnetic interaction is quartic in the Majorana operators, describing a system of interacting fermionic degrees of freedom. Due to the absence of gauge

	Spin-orbital perturbation	Majorana expression	spin symmetry
(a)	$J \sum_{\langle ij\rangle_i} \mathbf{S}_i \mathbf{S}_j \mathbb{1}_i \mathbb{1}_j$	$J \sum_{\langle ij\rangle_i} \sum_{\alpha=x,y,z} (\frac{1}{2} c_i^\dagger L^\alpha c_i)(\frac{1}{2} c_j^\dagger L^\alpha c_j)$	SU(2)
(b)	$J \sum_{\langle ij\rangle_i} (S_i^x S_j^x + S_i^y S_j^y) \mathbb{1}_i \mathbb{1}_j$	$J \sum_{\langle ij\rangle_i} \sum_{\alpha=x,y} (\frac{1}{2} c_i^\dagger L^\alpha c_i)(\frac{1}{2} c_j^\dagger L^\alpha c_j)$	U(1)
(c)	$J \sum_{\langle ij\rangle_i} S_i^z S_j^z \mathbb{1}_i \mathbb{1}_j$	$J \sum_{\langle ij\rangle_i} (\frac{1}{2} c_i^\dagger L^z c_i)(\frac{1}{2} c_j^\dagger L^z c_j)$	$\mathbb{Z}_2$
(d)	$J_{xy} \sum_{\langle ij\rangle_i} (S_i^x S_j^x + S_i^y S_j^y) \mathbb{1}_i \mathbb{1}_j$ $+ J_z \sum_{\langle ij\rangle_i} S_i^z S_j^z \mathbb{1}_i \mathbb{1}_j$	$J_{xy} \sum_{\langle ij\rangle_i} \sum_{\alpha=x,y} (\frac{1}{2} c_i^\dagger L^\alpha c_i)(\frac{1}{2} c_j^\dagger L^\alpha c_j)$ $+ J_z \sum_{\langle ij\rangle_i} (\frac{1}{2} c_i^\dagger L^z c_i)(\frac{1}{2} c_j^\dagger L^z c_j)$	U(1) $\times \mathbb{Z}_2$

Table 3.2: Overview of the spin-orbital perturbations presented in this section, their corresponding Majorana representations and their symmetry in spin-orbital and Majorana flavor space. All perturbations leave the gauge field static and thus present candidate perturbations for inducing continuous phase transitions in the exactly solvable models from Table. 3.1.

dynamics, the universality class of the discovered transition is fully governed by the quartic interaction between the Majorana fermions. In our pursuit for related universality classes, it seems reasonable to consider the effect of similar perturbations on the ground state of the Hamiltonian (3.16). Under the assumption that the ground state remains flux-free when these interactions are turned on, two models will be the subject of further investigation. First, H_K may also be perturbed by an XY interaction in the spin sector, see (b) in Table 3.2, which gives the full Hamiltonian of the *Kitaev-XY spin-orbital model*

$$H_K^{\mathrm{U}(1)} = -K \sum_{\langle ij\rangle_i} \hat{u}_{ij} \hat{u}_{ij} + J \sum_{\langle ij\rangle_i} (S_i^x S_j^x + S_i^y S_j^y) \mathbb{1}_i \mathbb{1}_j \qquad (\alpha = x,y,z); \tag{3.34}$$

whose critical behavior we investigate in Ch.4. In contrast to Eq. (3.31), the XY perturbation does not exhibit full SU(2) symmetry in the spin degrees of freedom, instead displaying a U(1) symmetry under rotations around the z-axis. Thus, the SU(2) symmetry of the unperturbed Hamiltonian is explicitly broken down to U(1). The corresponding Majorana Hamiltonian may be read off from Table 3.2.

It may be reasoned that real materials will never exactly realize the interactions covered in the above discussion, e. g. due to the introduction of anisotropies by crystal field effects or spin-orbit coupling [9, 14]. Thus, it is instructive to consider a model wich allows for said anisotropies, away from the highly symmetrical limits given by the Heisenberg and XY interactions. A suitable interaction reads

$$H_{J_{xy};J_z} = J_{xy} \sum_{\langle ij\rangle_i} (S_i^x S_j^x + S_i^y S_j^y) \mathbb{1}_i \mathbb{1}_j + J_z \sum_{\langle ij\rangle_i} S_i^z S_j^z \mathbb{1}_i \mathbb{1}_j. \tag{3.35}$$

This interaction contains two antiferromagnetic exchange couplings, J_{xy} and J_z, which can in principle be tuned independently, describing easy-axis anisotropy for $J_z > J_{xy}$ and easy-plane anisotropy for $J_{xy} > J_z$. It is symmetric under U(1) spin rotations in the $x-y$ plane and Z_2 transformations in the z-direction, adding up to a $\mathrm{U}(1)\times\mathsf{Z}_2$ spin symmetry. The special cases $J_{xy} = J_z$ and $J_z = 0$ recover the Heisenberg and XY interactions, respectively. Additionally, $J_{xy} = 0$ reduces to a Z_2-symmetric Ising interaction, see (c) in Table 3.2. Adding Eq. (3.35) to the unperturbed Hamiltonian (3.16) gives the *anisotropic Kitaev spin-orbital model*

$$H_K^{\text{ani}} = -K \sum_{\langle ij\rangle_\gamma} \sum_{\gamma=x,y,z} \tau_i^\gamma \tau_j^\gamma + J_{xy} \sum_{\langle ij\rangle_\gamma} \sum_{\gamma=x,y} \tau_i^\gamma \tau_j^\gamma \mathbb{1}_i \mathbb{1}_j + J_z \sum_{\langle ij\rangle_\gamma} \tau_i^z \tau_j^z \mathbb{1}_i \mathbb{1}_j; \quad (3.36)$$

which will be studied in more detail in Ch. 5. As before, the SU(2) symmetry of the unperturbed Hamiltonian is explicitly broken by the lower-symmetric perturbation, so that the full Hamiltonian retains the symmetry of the perturbation, namely $\mathrm{U}(1)\times\mathsf{Z}_2$. The Majorana representation of the Hamiltonian (3.36) can again be read off from Table 3.2.

4 Kitaev-XY spin-orbital model

The first model we are going to discuss in more detail is the Kitaev-XY spin-orbital model introduced in Sec. 3.2.2. The model features a U(1) spin-rotation symmetry in the $x-y$ plane and will be shown to support a symmetry-breaking phase transition governed by the gapless fermion excitations. Under the assumption the the ground-state is in the flux-free sector, the remaining low-energy degrees of freedom describe fractionalized Majorana fermions with an interaction featuring an SO(2) symmetry in flavor space.

This chapter introduces the tools needed to study quantum phase transitions of strongly correlated systems step-by-step. In Sec. 4.1, we employ a mean-field expansion of the Majorana Hamiltonian to obtain an approximate phase diagram of the Kitaev spin-orbital model. In Sec. 4.2, we derive an effective field theory for the order parameter and repeat the mean-field analysis in the functional integral formulation. In Sec. 4.3 the ε-expansion and Feynman diagrams are introduced as a tool to calculate leading corrections to the renormalized coupling constants introduced in Eq. (2.21) and the fixed points of the RG flow are analyzed.

4.1 Majorana mean-field theory

4.1.1 Mean-field Hamiltonian

In the Majorana representation, the Hamiltonian of the Kitaev-XY spin-orbital model in the flux-free sector $u_{ij} = +1$ reads

$$H_K^{\mathrm{U}(1)} = K \sum_{\langle ij\rangle_i} i c_i^{\dagger} c_j + J \sum_{\langle ij\rangle_i} \sum_{\gamma=x,y} \left(\frac{1}{2} c_i^{\dagger} L^{\gamma} c_i\right)\left(\frac{1}{2} c_j^{\dagger} L^{\gamma} c_j\right). \tag{4.1}$$

By Eq. (3.30), the U(1) symmetry of the spin-orbital model maps onto an SO(2) symmetry in Majorana flavor space. To see this, consider the explicit form of the SO(2) transformation. It is generated by L^z, acting on flavor space, and reads

$$c_i \;\mapsto\; \exp(-i\,\alpha\, L^z) c_i, \tag{4.2}$$

where $\alpha \in [0, 2\pi]$ denotes the angular parameter of the transformation. Whereas the invariance of the Kitaev term in Eq. (4.1) under the transformation (4.2) is trivial, it is not immediately

clear for the interaction term. To this end, we consider the vector

$$ _i = \frac{1}{2} \begin{pmatrix} c_i^\dagger L^x c_i \\ c_i^\dagger L^y c_i \end{pmatrix}; \tag{4.3} $$

corresponding to the spin vector operator in the spin-orbital formulation, thus giving an expression for the microscopic magnetization. An infinitesimal transformation of the vector components

$$ \frac{1}{2} c_i^\dagger L \; c_i \; ! \; c_i^\dagger O^\dagger L \; O c_i; \qquad O = 1 - i \; L^z + O(\; ^2); \tag{4.4} $$

reveals that the vector $ _i$ as defined in Eq. (4.3) transforms as a vector under SO(2), and the interaction is written in a manifestly SO(2)-invariant form.. Thus, the Hamiltonian (4.1) is invariant under SO(2) and the vector $ _i$ may act as an order parameter for the transition we are looking for, since it breaks the symmetry when acquiring an expectation value.

At weak antiferromagnetic couplings J, we expect a perturbative analysis to provide an adequate picture. However, to probe the physics of the Hamiltonian (4.1) beyond the region of applicability of perturbation theory, other methods are necessary. A simple but powerful tool to study interacting theories is the mean-field expansion. The aim is to replace the microscopic interactions by a static *mean field*, whose ground-state value may then be obtained by variational means. The structure of the mean-field Hamiltonian can be deduced from the expectation value of the Hamiltonian (4.1), which can be resolved by Wick's theorem [48], giving

$$ hH_K^{U(1)} i = K \sum_{hij i} hic_i^\dagger c_j i + J \sum_{=x;y} \left[\frac{1}{2} c_i^\dagger L \; c_i \; \frac{1}{2} c_j^\dagger L \; c_j \; - hc_i \, c_j \, ihc_i^z c_j^z i + hc_i^z c_j \, ihc_i \, c_j^z i \right]; \tag{4.5} $$

where the negative sign in the second line is due to the anti-commutativity of the Majorana operators. Thus, we have to perform the mean-field decoupling in three channels. Accordingly, our mean-field ansatz reads

$$ \begin{aligned} H_{\text{mf}} = K \sum_{hij i} ic_i^\dagger c_j + J \sum_{hij i} \Bigg[& \sum_{=x;y} \left(\frac{1}{2} c_i^\dagger \; _j L \; c_i + \frac{1}{2} c_j^\dagger \; _i L \; c_j \; \right) - ic_i^\dagger (\; _{ij} - \; _{ij}) c_j \\ & - \underbrace{\sum_{|=x;y} \left(\; _i \; _j - \; _{ij}^z \; _{ij} + \; _{ij}^z \; _{ij}^z \right)}_{C(\; ; \; ;} \Bigg]; \end{aligned} \tag{4.6} $$

where we have introduced mean-field parameters

$$ _i = \frac{1}{2} c_i^\dagger L \; c_i \; ; \qquad _{ij} = hic_i \, c_j \, i; \qquad _{ij} = hic_i \, c_j \, i; \tag{4.7} $$

as well as matrices

$$ {}_{ij} = \begin{pmatrix} {}^{z}_{ij} & 0 & 0 \\ 0 & {}^{z}_{ij} & 0 \\ 0 & 0 & {}^{x}_{ij} + {}^{y}_{ij} \end{pmatrix}; \qquad {}_{ij} = \begin{pmatrix} 0 & 0 & {}^{zx}_{ij} \\ 0 & 0 & {}^{zy}_{ij} \\ {}^{xz}_{ij} & {}^{yz}_{ij} & 0 \end{pmatrix}; \tag{4.8} $$

where $i(j)$ denotes lattice sites on sublattice $A(B)$. In the mean-field expansion, fluctuations of the mean-field parameters are assumed to vanish. In accordance with the earlier discussion, the on-site parameters denote the magnetization and will act as an order parameter for the transition. The parameters $_{ij}$ and $_{ij}$ refer to the diagonal and off-diagonal components of the tensor-valued bond variable $c_i c_j$, describing hopping of Majorana fermions between lattice sites. The last term only depends on the mean-field parameters and thus takes a constant value. The symmetries of the spin-orbital system should also hold for H_{mf}, greatly reducing the amount of allowed mean-field parameters. First, we expect the mean-field solution to exhibit the same translational invariance as the honeycomb lattice, such that $_{ij} =$, $_{ij} =$ and $_{i;j} = {}_{A;B}$. Under this assumption, we can Fourier transform the mean-field Hamiltonian using Eq. (3.23), giving

$$ H_{\text{mf}} = \sum_{\mathbf{k}\in BZ/2} \begin{pmatrix} c^{y}_{\mathbf{k};A}, & c^{y}_{\mathbf{k};B} \end{pmatrix} \begin{pmatrix} 0 & i[K - J(\ - \ )]f(\mathbf{k}) \\ -i[K - J(\ - \ )]f^{*}(\mathbf{k}) & 0 \end{pmatrix} \otimes 1_3 + \sum_{=x,y} \begin{pmatrix} 6J_{\ B} & 0 \\ 0 & 6J_{\ A} \end{pmatrix} \begin{pmatrix} c_{\mathbf{k};A} \\ c_{\mathbf{k};B} \end{pmatrix} + C(\ ;\ ;\ ); \tag{4.9} $$

where $f(\mathbf{k})$ is defined as usual and $C(\ ;\ ;\ )$ denotes the constant contribution to the mean-field Hamiltonian. Now, we enforce the SO(2) symmetry in flavor space. With Eq. (4.4), the second term takes the form of a scalar product of two SO(2) vectors and is naturally SO(2) invariant. The first term takes the form of a scalar, such that SO(2) invariance follows if it commutes with the generator L^z, thus requiring

$$ [L^z;\ ] \stackrel{!}{=} 0; \qquad [L^z;\ ] \stackrel{!}{=} 0: \tag{4.10} $$

As a consequence, the diagonal bond variables remain unconstrained due to $[L^z;\ ] = 0$, whereas the off-diagonal parameters have to vanish, $= 0$, for Eq. (4.9) to be SO(2) invariant. Thus, the mean-field Hamiltonian reads

$$ H_{\text{mf}} = \sum_{\mathbf{k}\in BZ/2} \begin{pmatrix} c^{y}_{\mathbf{k};A}, & c^{y}_{\mathbf{k};B} \end{pmatrix} \begin{pmatrix} 0 & i(K - J\ )f(\mathbf{k}) \\ -i(K - J\ )f^{*}(\mathbf{k}) & 0 \end{pmatrix} \otimes 1_3 + \sum_{=x,y} \begin{pmatrix} 6J_{\ B} & 0 \\ 0 & 6J_{\ A} \end{pmatrix} \begin{pmatrix} c_{\mathbf{k};A} \\ c_{\mathbf{k};B} \end{pmatrix} + C(\ ;\ ); \tag{4.11} $$

with the constant part evaluating to

$$C(\ ;\ ) = -3NJ \sum_{=x;y} (\ _A\ _B - \ ^z\ ); \tag{4.12}$$

where N denotes the number of unit cells on the underlying lattice.

Self-consistency equations and ground-state energy

The approximate ground-state values of the mean-field parameters can now be obtained from a variational principle. Formally, this amounts to minimizing the expectation value of Eq. (4.11) with respect to the mean-field parameters, which then gives the self-consistency equations, defining the variational ground state for the respective set of internal parameters. However, from a practical point of view it is usually more efficient to construct the self-consistency equations by calculating the mean-field parameters explicitly, which can be shown to be equivalent [41]. For example, the magnetization on sublattice A is given by

$$\begin{aligned} _A &= \frac{1}{N} \sum_{i2A} \frac{1}{2} c_i^{|} L\ c_i\ = \frac{2}{N} \sum_{\mathbf{k}2BZ=2} \frac{1}{2} c_{\mathbf{k};A}^{|} L\ c_{\mathbf{k};A} \\ &= -\frac{2i}{N}\,'' \sum_{\mathbf{k}2BZ=2} h(c_{k;A})^y c_{k;A} i; \end{aligned} \tag{4.13}$$

and similarly,

$$_B = -\frac{2i}{N}\,'' \sum_{\mathbf{k}2BZ=2} h(c_{k;B})^y c_{k;B} i; \tag{4.14}$$

where we average over the number of unit cells N. Eq. (4.13) can be expressed in terms of single-particle eigenstates $_{\mathbf{k}} = (\ _{1;\mathbf{k}};\ldots;\ _{6;\mathbf{k}})^{|}$ of the Hamiltonian (4.11), which are defined via

$$(c_{\mathbf{k};A}; c_{\mathbf{k};B})^{|} = U_{\mathbf{k}}\ _{\mathbf{k}}; \tag{4.15}$$

where $U_{\mathbf{k}}$ denotes the eigenvector matrix of the Hamiltonian at wavevector $\mathbf{k}$. To illustrate, for the x-component of the staggered magnetization this amounts to

$$\begin{aligned} ^x &= \frac{2i}{N} \sum_{\mathbf{k}2BZ=2} \sum_{n} [(U_{\mathbf{k}})^*_{2n}(U_{\mathbf{k}})_{1n} - (U_{\mathbf{k}})^*_{1n}(U_{\mathbf{k}})_{2n}] h\ ^y_{n;\mathbf{k}}\ _{n;\mathbf{k}} i \\ &= \frac{4}{N} \sum_{\mathbf{k}2BZ=2} \sum_{n} \mathrm{Im}[(U_{\mathbf{k}})^*_{1n}(U_{\mathbf{k}})_{2n}] h\ ^y_{n;\mathbf{k}}\ _{n;\mathbf{k}} i; \end{aligned} \tag{4.16}$$

a similar expression can be derived for ^{y}. The self-consistency equations for the bond variables

are obtained analogously, giving

$$= \frac{i}{3N} \sum_{\mathbf{k}\in BZ/2} \left[f(\mathbf{k}) h(c_{k;A})^{y} c_{k;A} i - f^{*}(\mathbf{k}) h(c_{k;B})^{y} c_{k;B} i \right]; \tag{4.17}$$

where we have averaged over three bonds per unit cell. Deriving the corresponding expressions in terms of the $\mathbf{k}$ fermions is straightforward. At vanishing chemical potential $= 0$, the resulting eigenstate averages are given by the Fermi-Dirac distribution

$$h \, {}^{y}_{n;\mathbf{k}} \, {}_{m;\mathbf{k}} i = \frac{1}{e^{\ \beta \varepsilon_n(\mathbf{k})} + 1} \, {}_{mn}; \tag{4.18}$$

where $\varepsilon_n(\mathbf{k})$ denotes the n-th energy eigenvalue at wavevector $\mathbf{k}$ and $= \frac{1}{T}$ is the inverse temperature. At zero temperature $! \ 1$, this gives the step function, only averaging over modes with negative energy. With that, the ground-state energy of a particular mean-field configuration can be obtained from summation over all occupied fermionic states and the constant contribution, giving

$$E_0 = \sum_{\mathbf{k}\in BZ/2} \sum_{n} \varepsilon_n(\mathbf{k}) h \, {}^{y}_{n;\mathbf{k}} \, {}_{n;\mathbf{k}} i - 3NJ \sum_{=x;y} (\ {}_{A} \ {}_{B} - \ {}^{z} \ ); \tag{4.19}$$

which functions as a cross-check for numerical solutions of the self-consistency equations.

4.1.2 Numerical results and phase diagram

The solution to the self-consistency equations (4.13), (4.14 and (4.17) can be obtained iteratively. The iterative scheme is implemented as follows. Choosing suitable initial values, calculation of the mean-field parameter gives a new value, which is then taken as the new initial value. This procedure is repeated until the solution converges. To obtain unbiased results [21], different initial values are sampled randomly from a uniform distribution $[0; 1)$ using the Python function numpy.random.rand. Table 4.1 shows the solutions to some representative values of the antiferromagnetic coupling J. For simplicity, we assume $K = 1$ from now on, such that all obtained values are normalized with the Kitaev exchange K. Note that the number of iterations needed for convergence is not fixed, as is shown in Fig. 4.1. Away from the critical point, a few iterations are usually enough to reach convergence, whereas the iteration converges slower the closer we get to the critical point. This has to be taken into consideration when interpreting results, since the iterative approach only produces reliable results if convergence is assured.

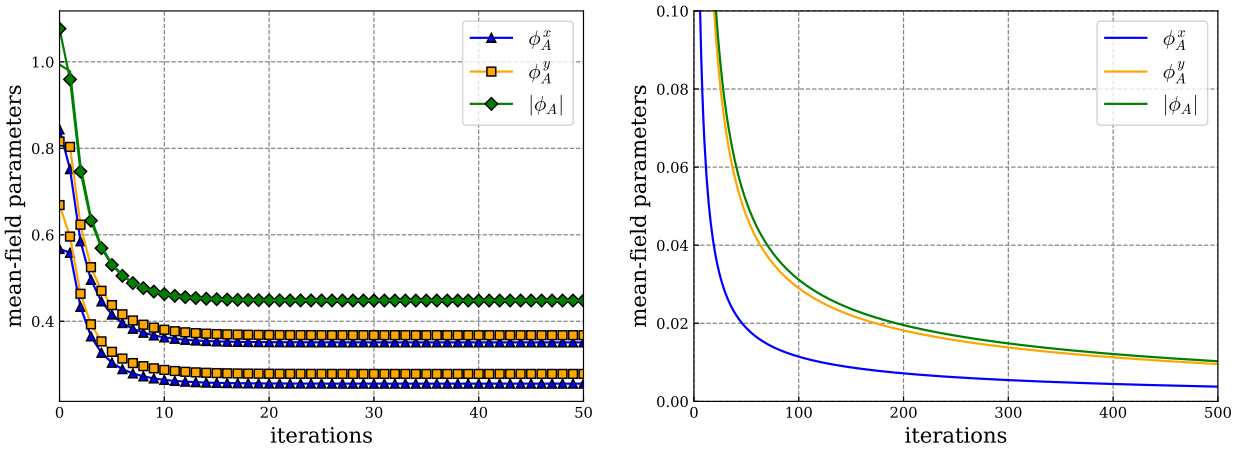

Figure 4.1: Evolution of the mean-field parameters for the magnetization for two values in the ordered phase, (a) two random initial values at $J = 0.8$ and (b) one random initial value at $J = 0.533$ ($K = 1$ assumed). In (a), which is far away from the critical point, the solutions converge quickly, whereas solutions close to the critical point converge much slower.

Paramagnetic phase

At $J = 0$, the model restores the exactly solvable limit of the Hamiltonian (4.11), with vanishing magnetization on both sublattices, describing a paramagnetic Kitaev SOL with three degenerate Dirac cones. The bond parameter acquires a characteristic value $= -0.5248$, which is exactly one third of the ground-state energy per unit cell $\frac{E_0}{N} = -1.5746$ of the Kitaev honeycomb model [8]. This is easy to understand. Since no interactions are present, the ground-state energy is solely determined by hopping of the Majorana fermions on the lattice, which is represented by . Since the Kitaev honeycomb model is represented by a single flavor of Majorana fermions and a unit cell contains three bonds, this amounts to $\frac{E_0}{N} = 3$. At small finite exchange coupling J, the ground state remains in the paramagnetic phase, also called the symmetric phase, since the ground state is invariant under U(1) spin rotations. Interestingly, bond parameters retain the same values as in the non-interacting case everywhere in the paramagnetic phase, a feature that was already described in Ref. [21], where the opposite sign stems from the antiferromagnetic Kitaev interaction assumed, and Ref. [49], where an additional factor $\frac{1}{2}$ appers due to a different normalization of the Majorana operators. Importantly, the self-consistent solutions to all parameters turn out to be independent of the initial conditions. Contrary to the SO(3)-invariant model studied in Ref. [23], the XY interaction already induces some changes in the low-energy physics in the weak coupling regime, without coupling to a finite order parameter. Due to the asymmetry in the matrix in Eq. (4.8), the bond parameters couple differently to one of the three Majorana flavors, even in the symmetric phase. This is best seen in the spectrum of the fermions, which is shown for $J = 0.5$ in Fig.

J	$\langle S^x_A \rangle$	$\langle S^y_A \rangle$	$\langle S^x_B \rangle$	$\langle S^y_B \rangle$	$\frac{\lvert \langle S_A \rangle - \langle S_B \rangle \rvert}{2}$	$\langle S^x \rangle$	$\langle S^y \rangle$	$\langle S^z \rangle$	$\langle S^x \rangle + \langle S^y \rangle$
0	0	0	0	0	0	-0.5248	-0.5248	-0.5248	-1.0496
0.5	0	0	0	0	0	-0.5248	-0.5248	-0.5248	-1.0496
0.55	0.0410	0.0519	-0.0410	-0.0519	0.0661	-0.5244	-0.5245	-0.5240	-1.0489
	0.0562	0.0348	-0.0562	-0.0348	0.0661	-0.5246	-0.5243	-0.5240	-1.0489
0.8	0.3511	0.2783	-0.3511	-0.2783	0.4480	-0.5075	-0.4973	-0.4800	-1.0048
	0.2557	0.3678	-0.2557	-0.3678	0.4480	-0.4946	-0.5102	-0.4800	-1.0048

Table 4.1: Self-consistent solutions for the mean-field parameters for typical values of the XY coupling J after 1000 iterations for an $N = 48 \times 48$ unit cell lattice. $J = 0$ corresponds to the exactly solvable case, reducing to three copies of the $S = \frac{1}{2}$ Kitaev honeycomb model. At strong couplings, the sublattice magnetizations acquire an expectation value and only SO(2) invariant quantities remain independent of the initial conditions. $K = 1$ is assumed.

4.2a, where, even though all bands stay gapless, the degeneracy is partially lifted and one of the bands acquires a different Fermi velocity to the others.

Antiferromagnetic phase

For larger exchange couplings the sublattice magnetizations $\langle S_{A;B} \rangle$ acquire a finite value, signaling the transition into a magnetically ordered phase. The phase is characterized by the antiferromagnetic Néel order parameter

$$n = \frac{\langle S_A \rangle - \langle S_B \rangle}{2}; \tag{4.20}$$

which spontaneously breaks the SO(2) flavor symmetry, corresponding to U(1) symmetry breaking in the spin-orbital model. Many of the mean-field parameters shown in Table 4.1 become dependent of the initial conditions of the iteration, which can be attributed to symmetry breaking. The random initial conditions break the symmetry along different axes in the ground-state manifold, such that different solutions are related by an SO(2) transformation and the single components of the mean-field parameters are not comparable. This can be verified by calculating the ground-state energy (4.19) for each solution, which takes the same value for all solutions at a certain coupling J. Only quantities invariant under SO(2) transformations generated by L^z are independent of the initial conditions. These quantities are given by the absolute value of the Néel order parameter, the sum $\langle S^x \rangle + \langle S^y \rangle$, which can be written as the trace of an SO(2) tensor, as well as $\langle S^z \rangle$, which is not affected by the SO(2) transformation. The appearance of a Néel order parameter could have already been anticipatied from the sublattice symmetry of the model (3.36) and the antiferromagnetic nature of the interaction J. This can also be observed from Table 4.1, which shows that, although their explicit numerical values depend strongly on the initial conditions of the iteration, the magnetization components

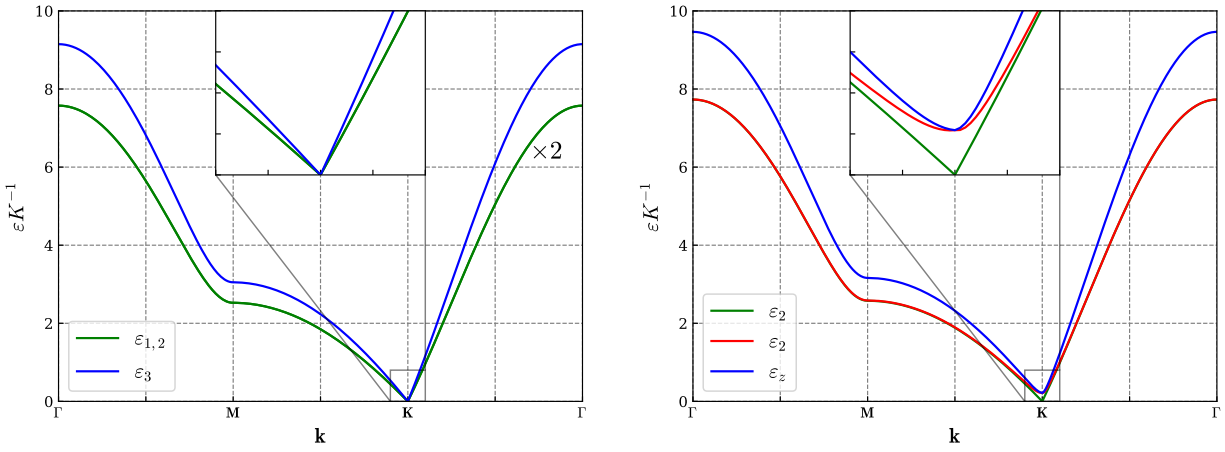

Figure 4.2: Representative spectra for the (a) symmetric phase at $J = 0.5$ and (b) the ordered phase at $J =$, obtained from the mean-field values in Table 4.1. Due to the inherent particle-hole symmetry of the Majorana spectrum [8], only states with positive energy are depicted. In the symmetric phase, all Majorana flavors remain gapless, but the interaction lifts the degeneracy for one of the three bands. In the ordered phase, two of the three Majorana flavors acquire a gap and only a single Dirac cone remains, describing a = 1 Kitaev SOL with an antiferromagnetically ordered spin sector.

always appear in pairs $_A = -_B$ with opposite signs on the respective sublattices, displaying perfect Néel order. Besides the magnetization, the ordered phase is characterized by a gradual deviation of the bond parameters from the fixed value in the symmetric phase, thus reducing the amplitude for Majorana hopping. Microscopically, this is due to the coupling of the order parameter to the fermion flavors in the mean-field Hamiltonian (4.11), which opens up a band gap for two of the three Majorana flavors, as shown in Fig. 4.2b. As a result, the bands acquire an effective mass, thereby damping the hopping amplitude. This behavior, which leaves only one of the Majorana flavors gapless, also appears in the SO(3)-invariant model [23] and characterizes a phase that is antiferromagnetically ordered in the spin-sector, but still retains gapless fractionalized degrees of freedom, describing a = 1 Kitaev SOL by the classification in Ref. [20]. However, in the low-energy limit of the present model, the two gapped bands are non-degenerate apart from the K point, where the degeneracy is protected by the algebraic structure of the SO(3) generators.

U(1) symmetry-breaking transition

An overview of our findings up to now is summarized in Fig. 4.3a, which shows the ground-state values of all relevant mean-field parameters over a wider range of couplings J 2 [0; 2]. Close to the critical point, we observe the Néel order parameter to scale linearly, giving the mean-field critical exponent for the order parameter = 1. We can extrapolate the critical

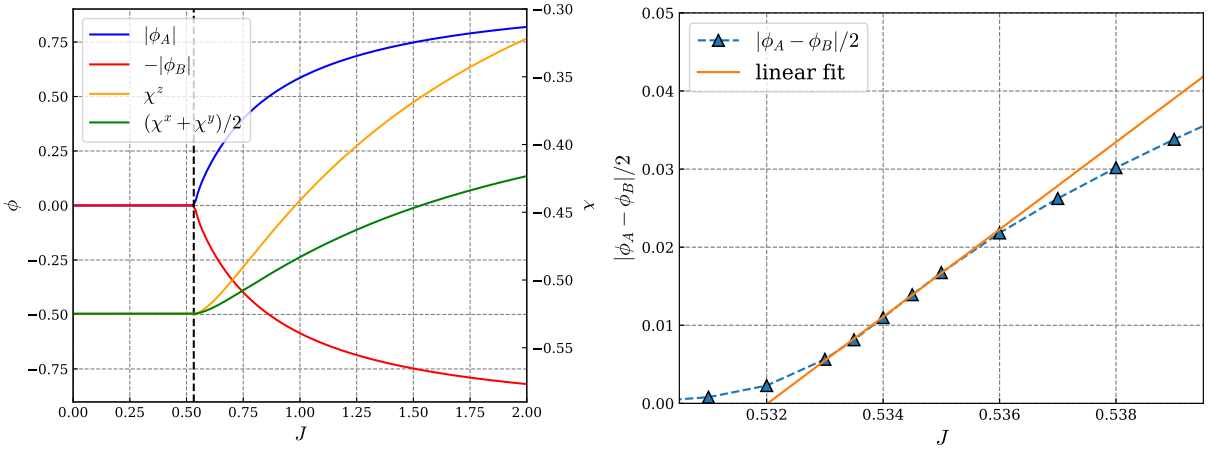

(a) (b)

Figure 4.3: (a) Ground-state values of all relevant mean-field parameters for J 2 [0; 2] for a lattice with N = 24 × 24 unit cells at 200 iterations. The dashed line marks the critical point at critical coupling J_c. At weak couplings, the the ground-state is symmetric under U(1) spin rotations, with fixed mean-field parameters. At strong couplings, the sublattice magnetizations acquire values with opposite signs, marking the transition into a Néel-ordered state. (b) Linear fit of the Néel order parameter close to the critical point at 1000 iterations for a lattice with N = 48 × 48 unit cells, giving the mean-field exponent for the order parameter = 1 and the critical coupling J_c = 0:5320. K = 1 is assumed. The data point at J = 0:5320 has been excluded from extrapolation due to its ground-state energy.

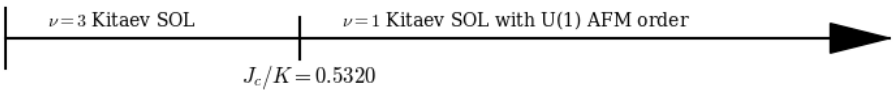

Figure 4.4: Mean-field phase diagram of the Kitaev-XY spin-orbital model.

value J from the linear scaling of the Néel order parameter close to the transition. Here, it is important to note that the numerically obtained values for the mean-field parameters have to be treated with care, since the convergence of the iterative approach takes too long to manifest right at the critical point. Only points that actually reside in the ordered phase should be included in the extrapolation. To illustrate, we consider the data point at J = 0:523. By the numerical results, the point acquires a finite magnetization, which suggests for it to reside in the ordered phase. However, comparison of the ground-state energy of this configuration with its value in the symmetric phase gives $E_0^{\text{symmetric}} < E_0^{\text{ordered}}$, such that the numerically obtained parameters do not represent the true mean-field ground state and should be omitted from the extrapolation. With that, we obtain the critical value for the antiferromagnetic XY exchange coupling J_c = 0:5320, as shown in Fig. 4.3b. The resulting mean-field phase diagram is given in Fig. 4.4.

In summary, the observations made provide convincing evidence for the emergence of a quantum critical point describing a topological phase transition with concomitant symmetry breaking between two distinct gapless Kitaev SOL phases in the Kitaev-XY spin-orbital model, featuring a similar phenomenology to the transition uncovered in Ref. [23]. However, due to a different broken symmetry, U(1) instead of SU(2), the transition is expected to belong to a different universality class, which we will continue to unravel in the following sections.

4.2 E□ective field theory

4.2.1 E□ective action from the microscopic description

While the mean-field expansion in the previous section reliably describes the stable phases that occur in the phase diagram, it only captures the right critical behavior for systems at or above the upper critical dimension. As we have already discussed shortly in Sec. 2.3, this is because collective long-wavelength fluctuations become increasingly important near the critical point for low-dimensional systems, which have been fully neglected in the mean-field approach. The first step towards a more sophisticated understanding of the critical behavior is the construction of an effective field theory, describing the low-energy limit of the Kitaev-XY spin-orbital model. We have seen in Ch. 3 that the energy dispersion of the non-interacting model given by Hamiltonian (3.22) is characterized by the appearance of three Dirac cones with the band-touching point located at the Dirac point K. At half filling, the Fermi energy lies exactly at the energy of the touching point, such that the low-energy excitations above the ground state are accurately described by spinless fermions and holes with linear energy dispersion, i. e. momentum-independent Fermi velocitiy. An effective theory can then be constructed by only considering the Fourier modes close to the Dirac point in the momentum-space Hamiltonian (3.24). Due to the formal similarities with the low-energy physics of graphene, the required gradient expansion can be carried out in analogy to the procedure laid out in Ref. [50]. For a single non-interacting Majorana flavor , this amounts to

$$H_0 = K \sum_{|\mathbf{q}|\leq\Lambda} \left((c_{\mathbf{K}+\mathbf{q};A})^{\dagger}, \; (c_{\mathbf{K}+\mathbf{q};B})^{\dagger} \right) \begin{pmatrix} 0 & i f(\mathsf{K}+\mathsf{q}) \\ -i f^{*}(\mathsf{K}+\mathsf{q}) & 0 \end{pmatrix} \begin{pmatrix} c_{\mathbf{K}+\mathbf{q};A} \\ c_{\mathbf{K}+\mathbf{q};B} \end{pmatrix}; \tag{4.21}$$

where refers to a momentum cutoff similar to the Debye frequency, in that it describes the region over which the energy dispersion may be approximated linearly. The effective Hamiltonian can be obtained from an expansion of $f(\mathsf{K}+\mathsf{q})$ about the Dirac point, which to

leading order in $\mathbf{q}$ gives

$$H_0 = v_F \sum_{|\mathbf{q}|\leq\Lambda} \psi^{\dagger}_{\alpha;\mathbf{q}} \begin{pmatrix} 0 & q_x + iq_y \\ q_x - iq_y & 0 \end{pmatrix} \psi_{\alpha;\mathbf{q}}; \tag{4.22}$$

where $\psi_{\alpha;\mathbf{q}} = (c_{\mathbf{K}+\mathbf{q};A}; c_{\mathbf{K}+\mathbf{q};B})^{\mathsf{T}}$ denotes the two-component spinor associated with the Majorana flavor α and we have introduced the Fermi velocity $v_F = K\sqrt{3}/2$, describing the slope of the energy dispersion in the vicinity of the Dirac point. In the thermodynamic limit, the momentum summation becomes a two-dimensional integral and Eq. (4.22) can be written in terms of Pauli matrices.

$$H_0 = \int_{|\mathbf{q}|\leq\Lambda} \frac{\mathrm{d}^2 q}{(2\pi)^2} \psi^{\dagger}_{\alpha}(\mathbf{q}) (q_x \sigma^x - q_y \sigma^y) \psi_{\alpha}(\mathbf{q}); \tag{4.23}$$

where the spinors have been promoted to fields in momentum space and the Fermi velocity v_F has been set to unity for simplicity. After a Fourier transformation to real space and taking into account all three Majorana flavors, the momenta in Eq. (4.23) become spatial derivatives and the full effective Hamiltonian reads

$$H_0 = \int \mathrm{d}^2 r \sum_{i=1}^{3} \psi^{\dagger}_i(\mathbf{r}) (-i\sigma^x \partial_x + i\sigma^y \partial_y) \psi_i(\mathbf{r}); \tag{4.24}$$

where the sum is over all 3 Majorana flavors and $\psi_i = (\psi_{i;A}; \psi_{i;B})^{\mathsf{T}}$ defines a two-component Dirac fermion for each flavor. Formally, Fourier transformation over a finite interval of momenta will produce a representation that is discrete in space, in accordance with the lattice on which the microscopic theory is defined. However, if we understand effective field theories to be implicitly accompanied by an intrinsic momentum cutoff Λ, we can understand the low-energy behavior of the theory in momentum space as arising from a continuum theory in real space. Loosely speaking, the appearance of the momentum cutoff "reminds" us of the fact that the microscopic degrees of freedom were integrated out and replaced by collective coarse-grained fields that vary continuously over length and time scales of the order of the inverse momentum cutoff $1/\Lambda$. Introducing a two-dimensional representation of the Clifford algebra in terms of Pauli matrices $\gamma = (\sigma^z; \sigma^y; \sigma^x)$ and defining the Dirac conjugate by $\bar{\psi}_i = \psi^{\dagger}_i \gamma^0$ as usual, by use of Eq. (2.17), the non-interacting Euclidean effective action describing the Dirac cones reads

$$S_0 = \int \mathrm{d}\tau \int \mathrm{d}^2 r\, \psi^{\dagger}_i \partial_\tau \psi_i + H_0 = \int \mathrm{d}\tau \int \mathrm{d}^2 r\, \bar{\psi}_i \gamma^\mu \partial_\mu \psi_i; \tag{4.25}$$

where summation over the flavor indices $i = 1; 2; 3$ is assumed from here on. In the single-particle limit, this recovers three copies of two-component Dirac fermions [51], thus correctly describing the low-energy physics of the model (3.16). The fermions are now represented by Grassmann-valued fields with an additional dependence on imaginary time to account for

quantum fluctuations in the functional integral. To find a continuum expression for the XY interaction, we make use of the fact that the Majorana expression for the XY interaction in Eq. (3.34) takes the form of a product of local densities $n_i = \frac{1}{2} c_i^{|} L\ c_i$. Since the densities commute, we can decompose the product

$$H_{\text{int}} = J \sum_{\hbar i j i} \sum_{=x,y} n_i n_j = \frac{J}{4} \sum_{\hbar i j i} \sum_{=x,y} [(n_i + n_j)^2 - (n_i + n_j)^2]$$
$$= \frac{J}{4} \sum_{i2A} \sum_{=x,y} [(n_{i;A} + n_{i+;B})^2 - (n_{i;A} - n_{i+;B})^2] \tag{4.26}$$

where we have used the bipartiteness of the honeycomb lattice to resolve the nearest-neighbor sum explicitly in the second line. As usual, i-summation goes over sublattice A, whereas sums over the three bonds per unit cell, connecting sublattices A and B. To leading order, we can neglect the non-local contributions arising from the crossing terms in Eq. (4.26), giving

$$H_{\text{int}} = \frac{3J}{4} \sum_{i2A} \sum_{=x,y} [(n_{i;A} + n_{i;B})^2 - (n_{i;A} - n_{i;B})^2] : \tag{4.27}$$

The continuum limit can now be obtained by expressing the local densities in terms of the field operators defined via Eq. (4.22). The continuum expressions for the local densities are, as before, derived in momentum space. Only considering Fourier modes close to the Dirac point, we obtain

$$\sum_{i2A} (n_{i;A} + n_{i;B}) \; 7! \int d^2 r \sum_{i;j=1}^{8} {}^{y}_{i} [1_2 \quad (L\ )_{ij}] \ {}_{j}; \tag{4.28}$$

$$\sum_{i2A} (n_{i;A} - n_{i;B}) \; 7! \int d^2 r \sum_{i;j=1}^{8} {}^{y}_{i} [\ {}^{z} \quad (L\ )_{ij}] \ {}_{j}; \tag{4.29}$$

from which we derive the continuum expression of the interaction Hamiltonian

$$H_{\text{int}} = h \int d^2 r \ [(\ {}^{y}_{i} [1_2 \quad (L\ )_{ij}] \ {}_{j})_2 - (\ {}^{y}_{i} [\ {}^{z} \quad (L\ )_{ij}] \ {}_{j})_2] \ ; \tag{4.30}$$

where we have absorbed all prefactors into a new four-fermion coupling $h \ / \ J$ and summation over the flavor indices $i; j = 1; 2; 3$ and $= x; y$ is assumed hereafter. The interaction now consists of two terms, which both turn out to be invariant under SO(2) flavor rotations defined via Eq. (4.2), and thus are allowed by symmetry. However, rewriting the interaction in a manifestly covariant form,

$$H_{\text{int}} = h \int d^2 r \ h(\ {}_{i} [\ {}_{0} \quad (L\ )_{ij}] \ {}_{j})_2 - (\ {}_{i} [1_2 \quad (L\ )_{ij}] \ {}_{j})_2 i \ ; \tag{4.31}$$

reveals that only the second term preserves the Lorentz invariance of the non-interacting action (4.25). The next step is a little more subtle. As we will see in Sec. 4.3, critical exponents arise from a loop expansion of the interaction. It can be shown that, due to $^{z}\,^{z} = \mathbf{1}_2$, both terms in Eq. (4.31) produce the same contributions to the critical exponents at all orders of the loop expansion such that both theories appear to belong to the same universality class [52]. Consequently, it is sufficient to keep only one of the terms for the further analysis of the critical behavior. A more thorough discussion may be found in [34]. Note that this step is only valid near the critical point. It is to be expected that the two terms produce different subleading corrections, such that their qualitative behavior will start to differ when moving away from criticality [52]. For simplicity, we keep the second term, giving the full Euclidean effective action

$$S = \int \mathrm{d}\,\mathrm{d}^2 r \Big[{}_i \;\; @ \;\; {}_i - h\big({}_i [\mathbf{1}_2 \quad (L\,)_{ij}] \;\; {}_j \big)_2 \Big] ; \tag{4.32}$$

featuring three flavors of two-component Dirac fermions coupled by a Lorentz-invariant four-fermion interaction term. The model shares formal similarities with the Gross-Neveu model[53], which was originally introduced as a toy model for chiral symmetry breaking in strongly interacting electron systems. However, instead of exhibiting just a discrete symmetry under chiral transformations of the fermions like the original Gross-Neveu model, Eq. (4.32), features a continuous symmetry. Since the third generator of SO(3) does not appear explicitly in the interaction, the model is invariant under transformations

$$ {}_i \;!\; (L^z)_{ij} \;\; {}_j ; \tag{4.33}$$

inducing SO(2) rotations in flavor space. In close analogy to the model introduced in Ref. [23], which features a continuous SO(3) flavor symmetry, we call the model (4.32) *Gross-Neveu-SO(2) model*.

4.2.2 Partial bosonization and mean-field theory

It is well known that interacting fermion systems like the one given by naturally exhibit instabilities towards strongly correlated phases, the most prominent being the Cooper instability, which facilitates the transition to a superconducting state at arbitrary attractive electron-electron interaction in metallic systems. Other examples include interacting spinless fermions, which are unstable towards a charge-density-wave state [54]. Usually, these instabilities are accompanied by the formation of a fermion condensate, whose appearance is associated with a symmetry-breaking transition for which it acts as a composite order parameter. In the literature, this is also called dynamical symmetry breaking [55]. In the symmetry-broken phase, the fermion condensate acquires a non-vanishing expectation value. Since the low-energy physics are governed by collective excitations of the fermionic degrees of freedom above the condensate, it is useful to include the order-parameter fluctuations directly into the theory.

However, the identification of the order parameter is not trivial, as four-fermion interactions allow for multiple condensation channels, describing qualitatively different physical scenarios. The identification of the physically relevant channel requires further insight [56].

Following the procedure introduced in Ref. [57], the decoupling is performed by the introduction of an auxiliary field , representing the order parameter, via a Hubbard-Stratonovich transformation. The idea is to introduce a resolution of identity in form of a Gaussian functional integral

$$1 = N \int D \exp\left[-\frac{1}{2} p \bar{r} \right]; \tag{4.34}$$

which can be multiplied with the partition function without changing the physical content of the theory. The normalization constant N does not affect any correlation functions and thus can safely be absorbed into the functional integral measure. Since the integral bounds of Eq. (4.34) approach infinity, a suitably chosen shift of the field variable allows us to cancel the four-fermion interaction in Eq. (4.32) at the cost of an additional functional integration over the order parameter field as well as the introduction of interactions between the fermions and the order parameter field. The partition function is then given by

$$Z = \int D\, D\, D \exp(-S_{HS}); \tag{4.35}$$

with the partially bosonized Hubbard-Stratonovich action $S_{HS}[\ ;\ ;\ ]$, which now explicitly depends on both the fermionic fields as well as the order parameter field. In the previous section, we have found evidence for the appearance of a quantum critical point associated with a spontaneously broken U(1) spin rotation symmetry, SO(2) flavor rotation symmetry in the fermionic formulation,, with the Néel order parameter being given by the two-component expectation value $hc_i^{\dagger} L\ c_i i$. Motivated by this result, we identify the order parameter field with the fermion bilinear

$$_i [1 \quad (L\ )_{ij}]\ _j \ : \tag{4.36}$$

For the Gross-Neveu-SO(2) model, we thus introduce a real two-component order parameter field and an appropriate shift proportional to Eq. (4.36)

$$1 = N \int D \exp\left[-\frac{1}{2} \left(p \bar{r} + p \frac{g}{\bar{r}} \right)_i [1_2 \quad (L\ )_{ij}]\ _j \right]^2 ; \tag{4.37}$$

with new couplings r and g. After multiplying Eq. (4.32) with this Gaussian factor, the four-fermion interaction precisely cancels if we impose a constraint on the newly introduced coupling constants

$$h = \frac{g^2}{2r}: \tag{4.38}$$

As such, the new couplings are not independent, which is consistent with the fact that the

physical theory from which Eq. (4.32) derives only contains a single parameter. The resulting partially bosonized action reads

$$S_{HS}[\ ;\ ;\ ] = \int \mathrm{d}\ \mathrm{d}^2x \Big({}_i\ @\ {}_i + \frac{r}{2}\ \ + g\ \ {}_i[1_2\ \ (L\ )_{ij}]\ {}_j \Big)\ ; \tag{4.39}$$

with the usual summation conventions. Thus, we have removed the four-fermion interaction at the cost of the introduction of a collective order parameter field, which the fermions couple to by an interaction of Yukawa type [53]. The SO(2) symmetry carries over from the four fermion interaction, since the bosonic fields do not transform under flavor rotations

$${}_i\ !\ (L^z)_{ij}\ {}_j ; \qquad\qquad !\ \ : \tag{4.40}$$

If the order parameter acquires a non-zero expectation value, the Yukawa interaction acts like a mass term with mass $m_F = g\sqrt{(\ \ )^2}$ for the Dirac fermions, thus dynamically generating a fermion mass in the strongly coupled regime, which corresponds to an energy gap in the condensed matter context. However, since the SO(3) generators possess a vanishing eigenvalue, only two of the three Majorana fermions acquire a gap, in accordance with the results from Sec. 4.1, see also Ref. [23].

The equivalence of Eqs. (4.39) and (4.32) becomes clear if we substitute with its classical equation of motion

$$r\ \ = -g\ \ {}_i[1_2\ \ (L\ )_{ij}]\ \ {}_j ; \tag{4.41}$$

corresponding to Gaussian integration of the order parameter field. This also explains the connection between the order parameter field and the fermion condensate. Due to the Ehrenfest theorem, we expect the classical equations of motion to hold for the quantum expectation values, justifying Eq. (4.36). Note that the Hubbard-Stratonovich transformation is exact. As such, it provides a formal justification for the mean-field decoupling of the interacting lattice Hamiltonian (4.1). In principle it is possible, and necessary, to carry out similar decouplings for the remaining channels [56]. However, since the order-parameter fluctuations dominate the other contributions in the vicinity of the critical point, it is sufficient to consider the decoupling of the order parameter to capture the relevant physics of the phase transition.

Mean-field theory

Since the fermionic degrees of freedom only appear bilinearly in the action (4.39), we can integrate them out exactly to obtain an effective theory for the order parameter field. For

that, it is necessary to rewrite the action as

$$S_{HS}[\ ;\ ;\ ] = \int \mathrm{d}\ \mathrm{d}^2x \left(\frac{r}{2} \quad + {}^{y}_{i}\left[{}^{0} \quad @ \quad {}_{ij} + {}^{0} \quad g \quad (L\ )_{ij} \right] {}_{j} \right)$$
$$= \int \mathrm{d}\ \mathrm{d}^2x \left(\frac{r}{2} \quad + {}^{y}\left[{}^{0} \quad @ \quad 1_3 + {}^{0} \quad g \quad L \quad \right] \right); \tag{4.42}$$

where we have inserted adjoint operators for the Dirac conjugate and the second line is written in a more compact matrix form. After reexponentiating the determinant resulting from the Gaussian integration of the Grassmann-valued fermion bilinear, we obtain

$$S_{eff}[\ ] = \int \mathrm{d}\ \mathrm{d}^2x \frac{r}{2} \quad - \ln\det\left[{}^{0} \quad @ \quad 1_3 + {}^{0} \quad g \quad L \quad \right]$$
$$= \int \mathrm{d}\ \mathrm{d}^2x \frac{r}{2} \quad - \mathrm{tr}\ln\left[{}^{0} \quad @ \quad 1_3 + {}^{0} \quad g \quad L \quad \right]; \tag{4.43}$$

which only depends on the and where we have used the identity $\ln\det M = \mathrm{tr}\ln M$. In principle, this allows for the exact calculation of the partition function

$$Z = \int D \quad \exp\left(-S_{eff}[\ ]\right); \tag{4.44}$$

and thus of any physical observable and the critical behavior. However, due to the appearance of derivatives in the functional trace, the $\mathrm{tr}\ln$ constitutes a highly non-local object. Additionally, the trace does not decouple in momentum space due to the presence of the order parameter field, which mediates interactions between fermions of different momenta, making an exact evaluation of the partition function impossible.

In a first approximation, we can treat the effective action as classical and approximate the partition function by its saddle-point contribution, which follows from the solutions of the saddle-point equations

$$\frac{}{(\mathrm{x};\ )} S_{eff}[\ ] \stackrel{!}{=} 0: \tag{4.45}$$

This is known as the stationary-phase approximation and is equivalent to the mean-field picture we have assumed in Sec. 4.1 [56]. It provides a microscopic justification for the Landau-Ginzburg approach, relating the phenomenological order parameter field to the microscopic fermionic degrees of freedom. If we assume a homogeneous solution for the order parameter, corresponding to Fourier components $(\mathrm{k};\ !)$ $(\mathrm{k})\ (\ !)$, the momentum integrals in the functional trace decouple and the classical solutions are given by the saddle points of the zero-momentum action

$$U(\ ) = \frac{r}{2}(\ )^2 - \int^{\wedge} \frac{\mathrm{d}\ ! \ \mathrm{d}^2k}{(2\ )^3} \mathrm{tr}\ln\left[i\ ! + (i\ {}^{z}\ {}^{y}k_x + i\ {}^{z}\ {}^{x}k_y) \quad 1_3 + {}^{z} \quad g \quad L^{1} \right]; \tag{4.46}$$

where we have rescaled the order parameter $=(2\ )^3\ !$, explicitly inserted the represen-

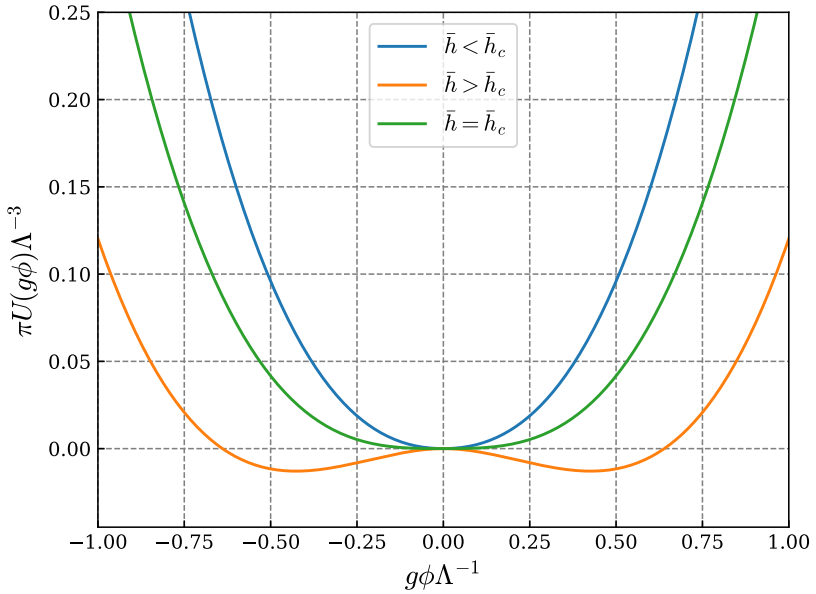

Figure 4.5: Dimensionless effective potential for various values of the dimensionless four-fermion coupling $\bar{h} = \Lambda h$. Below the critical coupling (blue line, $\bar{h} = \bar{h}_c - 1$), the minimum is pinned at the origin and the system is in the symmetric phase. Raising $\bar{h}$ above the critical point (orange line, $\bar{h} = \bar{h}_c + 5$), the U(1) symmetry is spontaneously broken as the rescaled order parameter acquires a non-zero expectation value. At the critical point the minimum stays at the origin, but the quadratic contribution to the effective potential vanishes.

tation of the and have assumed $= (\ ;0)^{\mathsf{T}}$ without loss of generality. Note that this way, we break the U(1) symmetry of the model by hand, equivalent solutions may be obtained by U(1) transformations of the chosen solution. The fate of inhomogeneous solutions to the saddle-point equations will not be discussed in this work. The homogeneous saddle-point $_0$ is then given by the minimum of the effective potential $U(\ )$

$$\begin{aligned} 0 \overset{!}{=} \frac{@}{@}U(\ )\Big|_{0} &= r_{\ 0} - 4g^2\ _0 \int^{\Lambda} \frac{\mathrm{d}!\ \mathrm{d}^2k}{(2\ )^3} \frac{1}{!^2 + k^2 + (g\ _0)^2} \\ &= r_{\ 0} - \frac{2g^2}{2}\ _0 \left[\ \ \ - g\ _0 \arctan\ \frac{\ }{g\ _0}\right] \\ &\approx r_{\ 0} - \frac{2g^2}{2}\ _0 \left(\ \ \ - gj\ _0 j\frac{\Lambda}{2}\right) ; \end{aligned} \tag{4.47}$$

where the last line holds for $gj\ _0 j$, i. e. near the phase transition, where the order parameter becomes arbitrarily small and thus the dynamically generated fermion mass $m_F = gj\ _0 j$ is small against the momentum cutoff . Besides the trivial solution $_0 = 0$, solving for m_F gives another solution

$$m_F = gj\ _0 j = \frac{2}{\Lambda}\left(\ \ - \frac{r^{\ 2}}{2g^2}\right) = \frac{2}{\Lambda}\left(\ \ - \frac{\Lambda^2}{4h}\right) ; \tag{4.48}$$

where we have inserted Eq. (4.47) to rewrite m_F in terms of the physical four-fermion coupling h. Since the fermion mass cannot be negative, Eq. (4.48) does not have a physical solution for $< {}^2/4h$. In this region, the ground state is given by the trivial solution and all three fermion flavors remain gapless. However, for $> {}^2/4h$, a finite solution is allowed. The ground state spontaneously breaks the U(1) symmetry of the action (4.39) and two of the three fermion flavors acquire an energy gap as we have explained earlier. Thus, the critical value of the four-fermion coupling in the saddle-point approximation is given by

$$h_c = \frac{^2}{4}; \tag{4.49}$$

which explicitly depends on , i. e. on the microscopic details of the lattice theory. Note that although the effective action (4.39) contains two parameters r and g, the value of the critical point is only sensitive to their ratio, corresponding to the physical parameter h. This is necessary for the description to be consistent, as the redundancy in the parameters in Eq. (4.39) was introduced artificiallythrough the Hubberd-Stratonovich transformation, and thus cannot affect any physical properties of the system. To obtain the critical exponent for the order parameter, we express in terms of the critical coupling and insert into Eq. (4.48), giving an expression that is regular at $h = h_c$ and can thus be expanded in a Taylor series. Near the critical point, this gives

$$m_F = \frac{}{2}\left(\frac{1}{h_c} - \frac{1}{h}\right) / h - h_c; \tag{4.50}$$

such that the order parameter critical exponent is given by $= 1$, in agreement with the lattice results from Sec. 4.1. To substantiate the symmetry-breaking picture, it is useful to calculate the effective potential near the transition explicitly by integrating the third line of Eq. (4.47)

$$U( ) = \int_0^{} d\, {}^0 \left[\left(r - \frac{2g^2}{^2}\right) {}^0 + \frac{g^3}{}\, j\, {}^0 j\, {}^0\right] = \frac{1}{}\left(\frac{1}{3}g^3 j\, j^3 - \frac{m_F}{2}g^2\, ^2\right); \tag{4.51}$$

where the dependence on the physical parameters h and is implicitly contained in m_F and the Yukawa coupling g can be absorbed into the definition of the order parameter. Reiterating the observations we have made up to now, we see that for $h < h_c$ the quadratic term in the effective potential is positive, stabilizing the minimum of the potential at the origin, whereas for $h > h_c$ the quadratic term becomes negative, shifting the minima to finite values of and signaling the onset of a symmetry-broken ground state. This is shown in Fig. 4.5, depicting the effective potential for various couplings.

4.3 Renormalization Group analysis

4.3.1 Gross-Neveu-SO(2) action

To go beyond the limitations of mean-field theory and systematically include fluctuations in our analysis of the critical point, we apply the Renormalization Group methods introduced in Sec. 2.2. To this end, we allow the couplings in Eq. () to flow under RG transformations. In principle, integrating out degrees of freedom in the partition function can produce any symmetry-allowed term in the effective action, even if they do not appear in the initial action. However, as we will see in Sec. 4.3.2, it turns out that close to the upper critical dimension, most symmetry-allowed are irrelevant and flow to zero near the critical point and do not affect the critical behavior, leaving only a select few relevant terms that have to be included in the analysis. Importantly, the upper critical dimension of each term can be estimated straightforwardly, such that one usually employs a semi-phenomenological approach to obtain an ansatz for the effective action. For the microscopic action defined via Eq. (4.32), we thus consider

$$S = \int d^D x \left(\quad _i \quad @ \quad _i + \frac{1}{2} \quad \left(-@^2 + r \right) \quad + g \quad _i [1 \quad (L \ )_{ij}] \quad _j + \quad (\quad)^2 \right) ; \tag{4.52}$$

where we have added dynamics for the order parameter field as well as a symmetry-allowed quartic potential with coupling > 0 that stabilizes the transition, which both vanish in the initial action. Both terms turn out to be relevant below four dimensions, which we show in the next section, such that they have to be included in the RG analysis. The form of the kinetic term of the order parameter field is chosen to preserve the relativistic invariance of the initial action, which in turn allows us to summarize the integration over d space dimensions and imaginary time into a single $D = d + 1$-dimensional Euclidean space-time integral. The order parameter is given by a real vector field and takes the form of a bosonic field in the action, thus we will from now on use the terminology interchangeably. Similarly, due to the resemblance of the control parameter r with the mass term in relativistic QFT, we will refer to r as a mass from now on. Additionally, we have generalized the action to allow for fermion fields with d components, denoted by subscript . Since a single $2n$-component fermion is equivalent to n two-component fermions [58], this enables us to generalize the problem to arbitrary number of two-component fermions, the fermion number being given by $N_F = \frac{3}{2}d$. Since we want to integrate out momentum shells it is useful to write down the momentum-space action

$$S = S_0 + S_g + S ; \tag{4.53}$$

which we have divided up into a non-interacting part S_0 and two interaction terms S_g and S ,

corresponding to Yukawa and self-interaction

$$S_0 = \int_{\wedge} (\mathrm{d}p) \left[i\, \psi_i(p)\; p\; \psi_i(p) + \frac{1}{2}\; \phi(p) \left(p^2 + r\right)\; \phi(-p) \right]; \tag{4.54}$$

$$S_g = g \int_{\wedge} (\mathrm{d}p_1)(\mathrm{d}p_2)\; (p_1 - p_2)\; \psi_i(p_1) \left[1 \; (L\;)_{ij}\right] \psi_j(p_2); \tag{4.55}$$

$$S\; = \int_{\wedge} (\mathrm{d}p_1)(\mathrm{d}p_2)(\mathrm{d}p_3)\; \phi(p_1)\; \phi(p_2)\; \phi(p_3)\; (-p_1 - p_2 - p_3); \tag{4.56}$$

where $\int (\mathrm{d}p) = \int \frac{\mathrm{d}^D p}{(2\;)^D}$ and the integrals are understood to possess a natural momentum-space cutoff as discussed in Sec. 4.2.

4.3.2 The Gaussian fixed point

We start the discussion by considering the non-interacting limit $g = \;= 0$, which is given by the action . This corresponds to a Gaussian action, such that the momentum-shell integration can be carried out exactly. Following the setup in Sec. 2.3, we split the fields into fast modes $\psi_>$ and slow modes $\psi_<$ [41] defined by

$$\psi_>(p) = \begin{cases} \psi(p) & \text{if } \;/b < p < \\ 0 & \text{otherwise} \end{cases}; \tag{4.57}$$

$$\psi_<(p) = \begin{cases} \psi(p) & \text{if } p < \;/b \\ 0 & \text{otherwise} \end{cases}; \tag{4.58}$$

with fields $\psi = \;;\;;\;$. The first step of the momentum-shell RG consists of the integration over fast modes in the partition function, leaving us with an effective action for the slow modes with momenta $p < \;/b$. Since the fields only appear quadratically in the action, there is no coupling between different momentum scales and the action can be divided into two independent parts $S_0 = S_{0<} + S_{0>}$, integrating over fast and slow modes, respectively. Thus, the partition function factorizes into contributions of slow and fast modes

$$\begin{aligned} Z &= \int D\;_< D\;_< D\;_<\, \mathrm{e}^{-S_{0<}} \int D\;_> D\;_> D\;_>\, \mathrm{e}^{-S_{0>}} \\ &= Z_{0<} Z_{0>}; \end{aligned} \tag{4.59}$$

such that integrating out high momenta does not produce any corrections in the coarse-grained theory. Since the partition function of the fast modes only contains finite momenta, it contributes to the regular part of the full partition function and can be safely absorbed into the functional integral measure of the slow modes without modifying the non-analytic behavior of the full partition function. Then, the coarse-grained effective action is given by the initial

non-interacting action for the slow modes

$$S_{0<} = \int_{\Lambda/b}^{\Lambda} (\mathrm{d}p) \left[i\, _i(p) \quad p \quad _i(p) + \frac{1}{2} \quad (p) \left(p^2 + r\right) \quad (-p) \right] ; \tag{4.60}$$

with momentum-space cutoff Λ/b. To adequately compare the effective action to its initial counterpart, it is necessary to perform the remaining steps of the momentum-shell RG, rescaling of momenta $bp \to p$ and field renormalization. As discussed in Sec. 2.3, the field renormalization is usually chosen such that the coefficients of the kinetic terms in the action are fixed under RG transformations. A peculiarity of Gaussian theories is that, due to the decoupling of momentum scales, the fields renormalize according to their canonical dimension (in momentum space), which can be obtained from naive dimensional analysis of the respective kinetic terms in the Gaussian action (4.54), giving

$$\to b^{\frac{D+2}{2}} ; \qquad \to b^{\frac{D+1}{2}} ; \tag{4.61}$$

known as *Gaussian renormalization* [48]. The renormalized effective action is then given by

$$S^{0}_{0<} = \int_{\Lambda}^{\Lambda} (\mathrm{d}p) \left[i\, _i(p) \quad p \quad _i(p) + \frac{1}{2} \quad (p) \left(p^2 + b^2 r\right) \quad (-p) \right] ; \tag{4.62}$$

from which we can read off the renormalized order parameter mass

$$r(b) = b^2 r: \tag{4.63}$$

For vanishing $r = 0$, the theory is trivially scale invariant, since there are no finite parameters in the action. Consequently, this point constitutes an RG fixed point, usually called the *Gaussian fixed point*. Since r renormalizes away from the fixed point under repeated RG iterations for any finite starting value, the fixed point is unstable against deviations of r. Notably, this is true for any space-time dimension D. Thus, in the RG sense, r is always relevant and flows away from the Gaussian fixed point under the RG flow. To assess the stability of the fixed point against the interactions given by Eqs. (4.55) and (4.56), more profound considerations are needed. Since interactions, in contrast to Gaussian terms, generically couple different momentum scales, they also couple fast and slow modes in the partition function (4.59). Consequently, the partition function does not factorize and integration over fast modes will generate corrections to the effective slow-mode action. A quantitative treatment of these corrections will be introduced in the next section. For now, we can keep the discussion on a simpler level. Since we expect the corrections to scale with some positive power of the interaction, we can, to lowest order, neglect them and compute the scaling behavior of the interactions at the Gaussian fixed point, giving

$$g(b) = b^{\frac{4-D}{2}} g; \qquad (b) = b^{4-D} : \tag{4.64}$$

In contrast to the boson mass, Gaussian scaling for both g and depends explicitly on the space-time dimension D, both having an upper critical space-time dimension $D_c = 4$. This allows for the following physical interpretation. Since r is always relevant, it acts as a control parameter for a phase transition whose critical point is given by the IR stable fixed point in the g- plane. Above the upper critical dimension, the interactions are irrelevant, which means that interactions in the microscopic theory ultimately flow towards the Gaussian limit after many RG iterations, such that the critical behavior is governed by the Gaussian fixed point. The corresponding RG flow can be derived from the recursion relation (4.63), giving

$$\frac{\mathrm{d}r}{\mathrm{d}\ln b} = 2r; \tag{4.65}$$

from which we can read off the correlation length exponent $= \frac{1}{2}$. Thus, the Gaussian fixed point describes the mean-field behavior of the corresponding O(N) Landau-Ginzburg-Wilson theory [30], in the present case with N=2. Note that this is not the mean-field behavior we have described in Sec. 4.2, due to the dependence of the integral in Eq. (4.47) on the dimension. At $D = 4$, the mean-field expansion from the previous section gives the desired result. Similarly, right at D_c the interactions become marginal, and the fixed point acquires logarithmic corrections to the mean-field scaling. [40] However, below the critical dimension, and thus for the physically interesting situation of $D = 3$, both interaction terms become relevant. The Gaussian fixed point thus has three relevant directions and cannot represent a critical point since there is only a single tunable parameter in the underlying lattice theory. As we will see in the following sections, the interactions instead flow towards a new, non-trivial fixed point located at finite interactions, which is characterized by a new set of critical exponents.

Another important point that we have already touched upon in the previous section is the fate of other symmetry-allowed terms in the full action (4.52). As already stated, we added a kinetic term and a bosonic self-interaction that were not present in the effective action derived from the microscopic model. One of the key insights of the RG theory is that the notion of relevant and irrelevant terms greatly restricts the amount of terms that have to be included in the quantitative analysis. Irrelevant terms vanish near criticality and can thus be safely ignored, whereas relevant terms become large and their corrections to the effective action will provide dominant contributions. Since we want to ultimately analyze the critical behavior below D_c, where is relevant, S has to be included. A similar argument can be made for higher-order symmetry-allowed terms, like e. g. p^2 ^{4} or ^{6}. Gaussian scaling reveals that none of these higher-order becomes relevant for $D = 3$, and can thus be safely neglected. Note that strictly speaking, the ^{6} term becomes marginal at the Gaussian fixed point for $D = 3$. However, it is believed that interaction corrections will make the term irrelevant. Interestingly, this argument also provides a rather satisfying justification for the applicability of the continuum limit to the theory of phase transitions, where we have discarded all but the

lowest contributing terms in a momentum expansion. Gaussian scaling shows that, in fact, all higher-order contributions are irrelevant and the microscopic lattice theory indeed flows towards the continuum theory given by the action (4.52) under repeated RG iterations.

4.3.3 The ε-expansion

To get a better understanding of the RG flow away from the Gaussian fixed point, we repeat the momentum-shell RG calculation with the full action (4.52). While the presence of interactions will leave the form of the action unchanged under RG, the coefficients obtain corrections from the coupling of slow and fast modes in the interaction terms. Thus, our ansatz for the effective slow-mode action reads

$$\begin{aligned} S_< = &\int^{\Lambda/b} (\mathrm{d}p) \left[Z\, i\, {}_i\, p\, {}_i + Z \frac{1}{2}p^2 + \frac{1}{2}(r + r) \right] \\ &+ \int^{\Lambda/b} (\mathrm{d}p_1)(\mathrm{d}p_2)(g + g)\, {}_i [1 \; (L)_{ij}]\, {}_j \\ &+ \int^{\Lambda/b} (\mathrm{d}p_1)(\mathrm{d}p_2)(\mathrm{d}p_3)(+) \; ; \end{aligned} \tag{4.66}$$

where the momentum dependence of the fields has been suppressed for notational convenience and r, g and refer to corrections to the couplings. Additionally, we have added wave function renormalizations Z and Z to encode corrections to the respective kinetic terms. The corrections are obtained by integrating out the momentum shell $q \in [\Lambda/b, \Lambda]$ in the partition function

$$\begin{aligned} Z &= \int D_< D_< D_< \mathrm{e}^{-S_{0<}} \int D_> D_> D_> \mathrm{e}^{-S_{0>} - S_g - S} \\ &= Z_{0>} \int D_< D_< D_< \mathrm{e}^{-S_{0<}} \left\langle e^{-S_g - S} \right\rangle_0 , \end{aligned} \tag{4.67}$$

where $Z_{0>}$ again denotes the contribution of the fast modes to the non-interacting partition function and

$$\langle A \rangle_0 = \frac{1}{Z_{0>}} \int D_> \mathrm{e}^{-S_{0>}} A \tag{4.68}$$

defines the Gaussian average over the fast modes. The most straightforward way to deal with the average over the exponential is a perturbative expansion

$$\left\langle e^{-S_g - S} \right\rangle_0 = 1 - \langle S_g + S \rangle_0 + \frac{1}{2} \left\langle (S_g + S)^2 \right\rangle_0 + \dots ; \tag{4.69}$$

which in turn reduces the problem to the evaluation of a series of Gaussian averages over field monomials. For small interactions, we can truncate the expansion at low order and expand

the resulting logarithm. After re-exponentiation, the partition function is then given by

$$Z = \int D\,\phi_< D\,\phi_< D\,\phi_< \, e^{-S_<}; \tag{4.70}$$

with the effective action

$$\begin{aligned} S_< &= S_{0<} - \ln \left\langle e^{-S_g - S} \right\rangle_0 \\ &= S_{0<} - \ln \left\langle 1 - (S_g + S) + \frac{1}{2} (S_g + S)^2 + \ldots \right\rangle_0 \\ &= S_{0<} + \langle S_g + S \rangle_0 - \frac{1}{2} \langle (S_g + S)^2 \rangle_0 + \ldots \end{aligned} \tag{4.71}$$

For the problem at hand however, there is no obvious small parameter. Specifically, the non-trivial fixed point might be located at strong couplings, which would require the evaluation of many terms of the expansion (4.17) or a non-perturbative approach. A solution to this problem is presented by the ϵ-expansion [59]. The idea is as follows. Instead of considering a fixed space-time dimension, we promote D to a continuous variable. Assuming that the critical point is located at some finite values g^*, $\ldots^*$ below the upper critical dimension, we expect both to approach zero as $D \to D_c = 4$, where the interactions become marginal and the new fixed point is expected to merge with the Gaussian fixed point. Thus, for small deviations from the upper critical dimension $\epsilon = 4 - D$, the Gaussian scalings of the interactions read

$$g(b) = b^{\epsilon/2} g; \qquad \ldots(b) = b^{\epsilon} \ldots; \tag{4.72}$$

and we expect the fixed point values to be of order

$$g_*^2; \ldots_*; r_* = O(\epsilon). \tag{4.73}$$

Consequently, close to the upper critical dimension, the fixed point values are small and a perturbative expansion in the interaction about the Gaussian fixed point is justified. To linear order in ϵ, it is then sufficient to truncate the expansion in Eq. (4.71), only keeping the leading corrections for each term in the effective action (4.66), making the necessary calculations manageable. To obtain results in the physical dimension $D = 3$, we extrapolate the results for small ϵ to $\epsilon = 1$. Obviously, we cannot expect a linear approximation to give numerically accurate results, since ϵ is not small here and we expect higher-order terms to provide significant corrections to the critical exponents. However, the topology of the RG flow generally does not [41]. Thus, while any numerical estimates from the ϵ-expansion should be treated with caution, it provides a powerful tool to classify universality classes and understand the emergence of quantitatively different critical phenomena, depending on dimensionality and symmetry of the underlying system. Additionally, systematic higher-order expansions, coupled with appropriate resummation techniques, allow for rather precise approximations of

the critical exponents [41].

Perturbative corrections and Feynman diagrams

Having established the validity of a perturbative approach, we now return to Eq. (4.71). At first order, the expansion contains two terms, S_0 and $S_g{}_0$. To get familiar with the nature of the contributions arising from the expansion, we take a detailed look at the first-order correction due to the self-interaction

$$S_0 = \int_\Lambda (dp_1)(dp_2)(dp_3) \quad {}_0. \tag{4.74}$$

Since the interaction contains fields of all momenta up to the cutoff $p \in [0, \Lambda]$, but only fast modes $p \in [\Lambda/b, \Lambda]$ are averaged over, we can rewrite the interaction in terms of slow and fast modes, giving

$$S_0 = \int_\Lambda (dp_1)(dp_2)(dp_3) \quad \langle\langle\langle\langle + \rangle\rangle\rangle\rangle_0 \\ + 2 \underbrace{\langle\langle z \rangle\rangle_0}_{I_a} + 4 \underbrace{\langle\langle z \rangle\rangle_0}_{I_b}; \tag{4.75}$$

where the equality follows from the different momentum support of fast and slow fields. We see that momentum-shell integration results in three types of terms. The first term only contains slow fields which survive the integration. This case recovers the slow part of the initial interaction S and could have been separated together with $S_{0<}$ in Eq. (4.67) from the start. Conversely, the second term encompasses only fast fields $_>$, meaning that all fields contribute to the average. Regardless of its actual value, this contribution adds a constant to the partition function. Thus, it only produces a contribution to the analytic part of the effective action, which we absorb into the functional integral measure, aligning with prior discussions. We are primarily interested in the last two terms, denoted by I_a and I_b. They both involve two fast fields, which are integrated out, and two slow fields that remain after integration, producing $O(\ )$ corrections to the bosonic part of the Gaussian action. The prefactors are the combinatorial weights of the terms, denoting in how many different ways these terms can be formed. For example, for I_a, we could have also averaged over the fields, giving two contributions. Similarly, I_b can be constructed in four different ways. Note that formally, Eq. (4.75) also contains terms with odd number of fast modes. However, Gaussian integrals over odd powers of the integration variable vanish trivially, such that we can safely ignore these contributions.

The evaluation of the interesting terms is straightforward, since they only contain two-point

averages. We start with the first term

$$I_a = 2 \int_{\Lambda=b}^{\Lambda} (dp_1)(dp_2) \quad (p_1) \quad (p_2) \int_{\Lambda=b}^{\Lambda} (dp_3)(dp_4) \quad (p_3) \quad (p_4) \quad {}_0 \; (p_1 + \cdots + p_4); \tag{4.76}$$

where we have reintroduced the momentum conservation of the self-interaction and have set the integral bounds to account for the different momentum support of fast and slow modes. The two-point average is given by the propagator of the bosonic sector of the Gaussian action

$$(p_1) \quad (p_2) \quad {}_0 = \frac{1}{p_1^2 + r} \quad (p_1 + p_2). \tag{4.77}$$

After insertion into Eq. (4.76), the momentum conservation in the propagator resolves one of the momentum-shell integrals, leaving us with a single integral over fast momenta q. The -expression for the remaining momenta is simplified, giving

$$\begin{aligned} I_a &= 2 \int_{\Lambda=b}^{\Lambda} (dp_1)(dp_2) \quad (p_1) \quad (p_2) \; (p_1 + p_2) \int_{\Lambda=b}^{\Lambda} (dq) \frac{1}{q^2 + r} \\ &= \int_{\Lambda=b}^{\Lambda} (dp) \frac{1}{2} \quad (p) \quad (-p) \int_{\Lambda=b}^{\Lambda} (dq) \frac{8}{q^2 + r}; \end{aligned} \tag{4.78}$$

where we have summed over the components $= 1; 2$ of the bosonic field. The remaining slow part is quadratic in and adds up with its corresponding term in Eq. (4.66), thus renormalizing the boson mass

$$r_{I_a} = 8 \int_{\Lambda=b}^{\Lambda} (dq) \frac{1}{q^2 + r}. \tag{4.79}$$

The expression for I_b can be similarly obtained, also producing a correction to r. Thus, to order $O( )$ the momentum-shell integration produces an effective contribution to the boson mass given by

$$r \quad = \quad r_{I_a + I_b} = 16 \int_{\Lambda=b}^{\Lambda} (dq) \frac{1}{q^2 + r}. \tag{4.80}$$

The evaluation of the integral will be discussed shortly.

The leading corrections to the other couplings can be obtained from higher-order terms in the perturbation expansion, which generally contain averages over higher-order field monomials. We have already seen in Sec. 4.1 that such averages can be resolved by application of Wick's theorem, enabling us to rewrite the n-point terms arising from the expansion as a sum over all possible permutations of products of two-point averages. Since all resulting terms are formally equivalent and produce the same contributons, this only adds additional combinatorial factors. Wick's theorem allows for a neat representation of the perturbative expansion in terms of *Feynman diagrams*. The diagrammatic conventions in this work will loosely follow

the representation in Ref. [41]. To this end, we introduce graphical representations for the self-interaction and the boson propagator

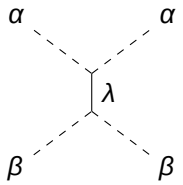

$$= \quad (p_1) \quad (p_2) \quad (p_3) \quad (p_4) \; (p_1 + p_2 + p_3 + p_4);$$

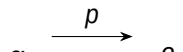

$$= \quad (p) \quad (-p) = \frac{1}{p^2 + r} \quad : \tag{4.81}$$

The interaction term S is represented by a vertex with four emanating dotted lines, which depict the bosonic fields in the interaction, commonly known as the *tree-level* vertex. Integration over the momenta of the outgoing fields is assumed. The solid line at the vertex emphasizes that the field indices $\;;\;$ appear twice and are summed over. In the Wick expansion, terms are generated by pairing up two fields each, known as a *contraction* in QFT terminology, denoted by

$$\equiv \quad _0 \tag{4.82}$$

In the diagrammatic representation, contractions are realized by connecting pairs of outgoing lines. In the corresponding integral expression, contracted fields are substituted by their Gaussian propagator. Thus, contracted lines represent fast modes $\;>$, while external lines represent slow modes $\;<$ which survive the momentum-shell integration. Similarly, we introduce the tree-level vertex for the Yukawa interaction and the fermion propagator

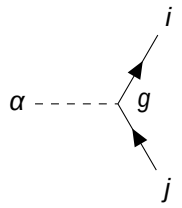

$$= \quad (p_1) \quad _i(p_2)\,[1 \quad (L \;)_{ij}] \quad _j(p_3) \; (p_1 + p_2 + p_3);$$

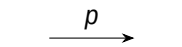

$$= \quad _i(p) \quad _j(p) = -\frac{i \quad p}{p^2} \quad _{ij}; \tag{4.83}$$

following the same guidelines as the prior definition. The fermion propagator is obtained from the fermionic sector of the Gaussian action by Gaussian integration of the Grassmann variables $\;;\;$. Since a fermionic excitation is described by two variables, the fermion propagator is directed, denoted by an arrow on the fermionic lines in the Feynman diagrams. This expresses that only combinations $h \quad i$ can be contracted, whereas $h \quad i = h \quad i = 0$, limiting the amount of contributions in the Wick expansion.

From these basic rules, so called *Feynman rules*, all terms in Eq. () can be systematically expressed as diagrams and reorganized as a *loop expansion* [48]. We have seen that renormalization corrections are produced by contributions where the fields are only partially integrated

out, corresponding to diagrams with external lines. For example, the contributions I_a and I_b arise from diagrams (a) and (b) in Fig 4.1 by contracting two of the four fields in S . To linear order in $"$, only the leading corrections contribute, corresponding to all diagrams with a single internal loop. For the action (4.52), this amounts to the remaining diagrams depicted in Fig. 4.1, loop corrections to higher-order monomials can be omitted since they are irrelevant.

4.3.4 One-loop calculations

The calculation of the Feynman diagrams is straightforward. Contractions are replaced by the appropriate propagators, carrying the momentum of the respective inner line. Due to momentum conservation at each vertex, we have to perform one momentum-shell integral per loop in the diagram. Additionally, each diagram receives a combinatorial weight that expresses in how many different ways the diagram can be realized in the Wick expansion. Since we are ultimately interested in the differential equations governing the RG flow, we will consider an infinitesimally small momentum-shell here and in the forthcoming calculations, corresponding to $\ln b \quad 1$. Since the scale parameter only appears explicitly in the integral bounds, expansion about $\ln b = 0$ gives

$$\int_{\Lambda=b}^{\Lambda} dq\, f(q) \;' \quad f(\;)\ln b; \tag{4.84}$$

which is linear in the logarithmic scale $\ln b$. This reduces the integral to the evaluation of the integrand at the cutoff, significantly easing the calculation of the momentum-shell integrals we derive from the diagrammatic representation.

Boson propagator

We begin by calculating the corrections to the boson propagator, which is given by the quadratic part of the action (4.52). This comprises three one-loop diagrams, (a)–(c) in Fig. 4.6. We have already derived and discussed the integral expressions for the first two diagrams in Eq. (4.80). Due to the rotational invariance of the integrand, we can split off the angular integration and use Eq. (4.84) to evaluate the remaining integral

$$\begin{aligned} r \quad &= 16\; \frac{S_D}{(2\;)^D} \int_{\Lambda=b}^{\Lambda} dq \frac{q^{D-1}}{q^2 + r} \\ &= 16\; \frac{S_D}{(2\;)^D} \frac{^{D-2}}{1 + \frac{r}{\Lambda^2}} \ln b; \end{aligned} \tag{4.85}$$

where S_D denotes the surface area of the D-dimensional unit sphere. Diagram (c) arises from the S_g^2 contribution of the perturbative expansion and is historically know as the *boson self-energy*. Since it is a second-order term, it enters negatively into the effective action and obtains

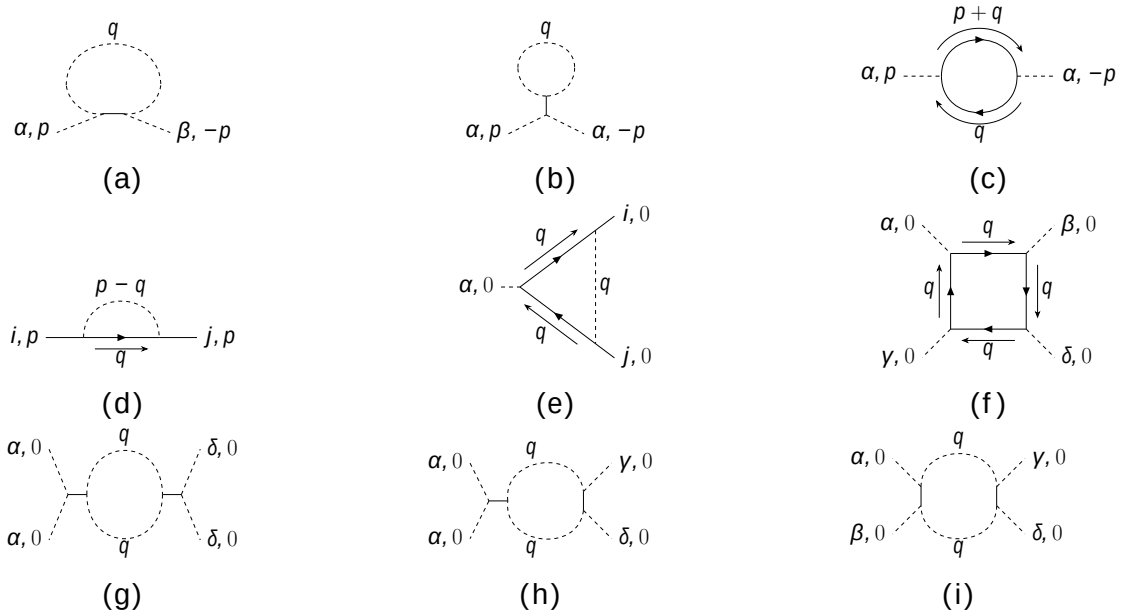

Figure 4.6: All one-loop diagrams contributing to the effective action of the Gross-Neveu-SO(2) model. Diagrams (a)–(d) denote corrections to the Gaussian part of the action, whereas (e)–(i) provide corrections to the Yukawa and self-interaction vertices.

a factor of $\frac{1}{2}$. The corresponding integral expression reads

$$I_c = -\frac{g^2}{2}\int_{\Lambda=b}^{\Lambda}(\mathrm{d}p)\int_{\Lambda=b}^{\Lambda}(\mathrm{d}q)\;\;{}_i[1\quad(L\;)_{ij}]\;{}_j\quad{}_k[1\quad(L\;)_{kl}]\;{}_l$$
$$= \frac{g^2}{2}\int_{\Lambda=b}^{\Lambda}(\mathrm{d}p)\int_{\Lambda=b}^{\Lambda}(\mathrm{d}q)\,\mathrm{tr}\,(\;[1\quad(L\;)_{ij}]\;{}_j\quad{}_k[1\quad(L\;)_{kl}]\;{}_l\quad{}_i\;); \tag{4.86}$$

where we have used $\quad = \mathrm{tr}(\quad)$ and the anticommuting properties of the fermionic fields. The next step is to replace the contractions by fermionic propagators with momenta q and $p+q$, giving

$$I_c = \frac{g^2}{2}\int_{\Lambda=b}^{\Lambda}(\mathrm{d}p)\int_{\Lambda=b}^{\Lambda}(\mathrm{d}q)\,\mathrm{tr}\,(\;[1\quad(L\;)_{ij}]\frac{i\quad q}{q^2}\;{}_{jk}[1\quad(L\;)_{kl}]\frac{i\quad(p\;+q\;)}{(p+q)^2}\;{}_{li}\;)$$
$$= -\frac{g^2}{2}\int_{\Lambda=b}^{\Lambda}(\mathrm{d}p)\;\;(L\;)_{ij}(L\;)_{ji}\int_{\Lambda=b}^{\Lambda}(\mathrm{d}q)\,\mathrm{tr}\,\Big[\frac{q\;(\;p\;+\;q\;)}{q^2(p+q)^2}\Big]$$
$$= -\frac{g^2}{2}\int_{\Lambda=b}^{\Lambda}(\mathrm{d}p)\;\;(L\;)_{ij}(L\;)_{ji}\int_{\Lambda=b}^{\Lambda}(\mathrm{d}q)\frac{p\;q\;+q^2}{q^2(p+q)^2}\,\mathrm{tr}(1\;); \tag{4.87}$$

where we have used the general properties of the Dirac matrices to resolve the expression under the trace in the last line. The remaining trace over the unit matrix is trivial, giving $\mathrm{tr}(1\;) = d$. Additionally, there is a *group-theoretical* part [60] connected to the algebra of the SO(3) generators L . From their explicit form given in Eq. (3.30), we straightforwardly

obtain $(L\ )_{ij}(L\ )_{ji} = \mathrm{tr}(L\ L\ ) = 2$, reducing Eq. (4.87) to

$$I_c = -2d\ g^2 \int_{\Lambda=b}^{\Lambda} (\mathrm{d}p)\frac{1}{2} \int_{\Lambda=b}^{\Lambda} (\mathrm{d}q)\frac{p\ q\ + q^2}{q^2(p+q)^2} \tag{4.88}$$

In contrast to the first two diagrams, this expression retains an explicit momentum-dependence after integration, making the momentum-shell integral rather difficult to solve. Here, we make use of the fact that only the terms to lowest order in the surviving momenta are relevant at the Gaussian fixed point near four dimensions. With

$$\frac{1}{(p+q)^2} = \frac{1}{q^2}\left(1 - \frac{2p\ q}{q^2} - \frac{p^2}{q^2} + \frac{4(p\ q\ )^2}{q^4} + O(p^3)\right); \tag{4.89}$$

we can expand the integrand up to order $O(p^2)$, giving

$$I_c = -2d\ g^2 \int_{\Lambda=b}^{\Lambda} (\mathrm{d}p)\frac{1}{2} \int_{\Lambda=b}^{\Lambda} (\mathrm{d}q)\left[\frac{1}{q^2} - \frac{p\ q}{q^4} - \frac{p^2}{q^4} + \frac{2(p\ q\ )^2}{q^6} + O(p^3)\right]: \tag{4.90}$$

Higher-order momentum contributions scale to zero near the critical point and can be safely ignored. The first and the third term of the integrand are rotationally invariant and can be solved similar to Eq. (4.85). The second term is odd in q and thus vanishes under momentum-shell integration. The fourth term requires additional consideration. With

$$\int (\mathrm{d}q)q\ q\ = \frac{S_D}{D}\frac{}{(2\ )^D} \int \mathrm{d}q q^{D+1}; \tag{4.91}$$

which can be proven by elementary integration in Cartesian coordinates, we can rewrite the momentum integral

$$\int_{\Lambda=b}^{\Lambda} (\mathrm{d}q)\frac{2(p\ q\ )^2}{q^6} = 2p\ p \int_{\Lambda=b}^{\Lambda} (\mathrm{d}q)\frac{q\ q}{q^6} = p^2\frac{2}{D}\frac{S_D}{(2\ )^D} \int_{\Lambda=b}^{\Lambda} \mathrm{d}q q^{D-5}: \tag{4.92}$$

With that, Eq. (4.90) simplifies to

$$\begin{aligned} I_c &= -2d\ g^2 \int_{\Lambda=b}^{\Lambda} (\mathrm{d}p)\frac{1}{2} \frac{S_D}{(2\ )^D} \int_{\Lambda=b}^{\Lambda} \mathrm{d}q \left[q^{D-3} + p^2\left(\frac{2}{D} - 1\right) q^{D-5}\right] \\ &= -2d\ g^2 \int_{\Lambda=b}^{\Lambda} (\mathrm{d}p)\frac{1}{2} \frac{S_D}{(2\ )^D} \left[{}^{D-2} - \frac{1}{2}p^2\ {}^{D-4}\right] \ln b; \end{aligned} \tag{4.93}$$

producing two distinct corrections to the effective action. The first term, similar to the first two diagrams, decouples from the remaining momenta and provides a static contribution, thereby renormalizing the boson mass

$$r_{g^2} = -2d\ g^2 \frac{S_D}{(2\ )^D}\ {}^{D-2} \ln b: \tag{4.94}$$

The second term contains a quadratic momentum-dependence and thus provides a contribution to the kinetic term, giving the wave-function renormalization

$$Z = 1 + d\, g^2 \frac{S_D}{(2\pi)^D} \Lambda^{D-4} \ln b. \tag{4.95}$$

Note that all corrections we have determined up to now contain the same prefactor $S_D/(2\pi)^D$. It is convenient to remove the prefactor and the explicit dependence on the cutoff Λ by appropriate rescaling of the parameters

$$\frac{r}{2} \to r; \qquad \frac{S_D}{(2\pi)^D} \Lambda^{D-4} \to \Lambda; \qquad \frac{S_D}{(2\pi)^D} \Lambda^{D-4} g^2 \to g^2; \tag{4.96}$$

which will also apply to all following calculations. With that, the full one-loop correction to the boson propagator is given by

$$r = \left(16 \frac{1}{1+r} - \frac{4N_F}{3} g^2 \right) \ln b; \tag{4.97}$$

$$Z = 1 + \frac{2N_F}{3} g^2 \ln b; \tag{4.98}$$

where we have substituted $N_F = \frac{3}{2}d$, as discussed, to allow for arbitrary number of fermions. Thus, the boson mass receives corrections due to both interaction, whereas changes in the wave-function renormalization are only induced by the Yukawa interaction at one-loop order.

Fermion propagator

We continue with the renormalization of the fermion propagator. At one-loop order, only a single diagram, diagram (d), the *fermion self-energy*, in Fig. 4.6, contributes an effective correction to the fermion bilinear in the action (4.54). The corresponding integral expression reads

$$\begin{aligned} I_d &= -\frac{g^2}{2} \int_{\Lambda=b}^{\Lambda} (\mathrm{d}p) \int_{\Lambda=b}^{\Lambda} (\mathrm{d}q) \; \bar{\psi}_i [1 \otimes (L_1)_{ij}] \psi_j \; \bar{\psi}_k [1 \otimes (L_1)_{kl}] \psi_l \\ &= g^2 (L_1)_{ij} (L_1)_{jl} \int (\mathrm{d}p) \int_{\Lambda=b}^{\Lambda} (\mathrm{d}q) \; \bar{\psi}_i \, i \not{q} \, \psi_l \frac{1}{q^2 [(p-q)^2 + r]}; \end{aligned} \tag{4.99}$$

where we have again substituted the contractions with the appropriate propagators. The fermionic fields can be contracted in two different ways, giving an additional factor of two. The momentum expansion of the integrand

$$\frac{q}{q^2} \frac{1}{(p-q)^2 + r} = \frac{q}{q^2(q^2+r)} + \frac{2q\, q\, p}{q^2(q^2+r)^2} + O(p^2); \tag{4.100}$$

can already be truncated at linear order, since for the fermionic fields even contributions

with quadratic momentum are irrelevant near four dimensions. The evaluation of the integral proceeds in a similar fashion to the previous one. After rescaling of all parameters, Eq. (4.99) reads

$$I_d = \frac{g^2}{2}\frac{1}{(1+r)^2}(L_\alpha)_{ij}(L_\alpha)_{jl}\int_{\Lambda/b}^{\Lambda}(\mathrm{d}p)\,\mathrm{i}\not{p}_{il}\ln b. \tag{4.101}$$

A peculiarity appears when studying the group-theoretical factor

$$(L_\alpha)_{ij}(L_\alpha)_{jl} = L_x L_x = \begin{pmatrix} 0 & 0 & 1 \\ 0 & 1 & 0 \\ 1 & 0 & 0 \end{pmatrix} \tag{4.102}$$

which turns out not to be proportional to the unit matrix for $\alpha = x, y$. This constitutes one of the main qualitative differences between the SO(2)-symmetric model considered in this work and the Gross-Neveu-SO(3) model introduced in Ref. [23]. Here, the order parameter has two components and thus only couples to two of the three SO(3) generators. Consequently, we obtain two distinct wave-function renormalizations

$$Z_{\psi,12} = 1 + \frac{g^2}{2}\frac{1}{(1+r)^2}\ln b, \tag{4.103}$$

$$Z_{\psi,3} = 1 + g^2\frac{1}{(1+r)^2}\ln b, \tag{4.104}$$

where $Z_{\psi,1}$ provides the renormalization of the kinetic term for fermion flavors ψ_1, ψ_2, whereas flavor ψ_3 is renormalized by $Z_{\psi,2}$.

Vertex corrections

Effective contributions to the interactions only arise at higher order in perturbation theory. Similar to the second-order corrections to the bosonic and fermionic propagator, the one-loop expressions depend non-trivially on momentum. However, for interaction corrections near four dimensions, only the static part produces relevant contributions and the momentum-dependent part of the vertex corrections can be fully neglected [59], meaning that external momenta are assumed to vanish. This amounts to the calculation of diagrams (e)–(i) in Fig. 4.6. Since the evaluation of the diagrams follows roughly the same steps as before, we only state the results here. The Yukawa vertex receives a single one-loop correction, given by diagram (e), arising

from contraction of S_g^3. The corresponding integral reads

$$I_e = \frac{g^3}{6} \int_{\Lambda=b} (dp_1)(dp_2) \int_{\Lambda=b}^{\Lambda} (dq) \times$$

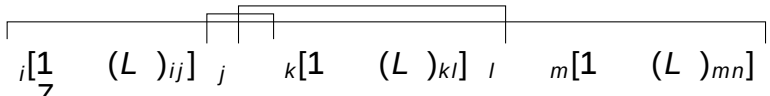

$$\times \; {}_i[1 \quad (L\ )_{ij}]\ {}_j \quad {}_k[1 \quad (L\ )_{kl}]\ {}_l \quad {}_m[1 \quad (L\ )_{mn}]\ {}_n$$

$$= -g^3 \frac{1}{1+r} \int_{\Lambda=b} (dp_1)(dp_2) \quad {}_m[1 \quad (L\ )_{ml}]\ {}_l \ln b; \tag{4.105}$$

from where we can read off the renormalization correction to the Yukawa interaction

$$g = -g^3 \frac{1}{1+r} \ln b: \tag{4.106}$$

The quartic self-interaction receives corrections from two types of diagrams. The first is given by diagram (f) arising from contraction of S_g^4, and thus only depends on the Yukawa coupling g. We get

$$I_e = -\frac{g^4}{24} \int_{\Lambda=b} (dp_1)(dp_2)(dp_3) \int_{\Lambda=b}^{\Lambda} (dq) \times$$

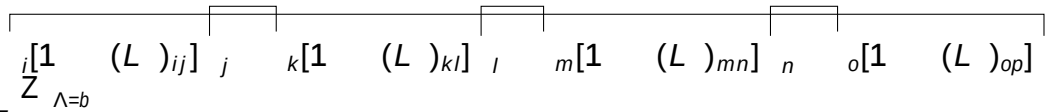

$$\times \; {}_i[1 \quad (L\ )_{ij}]\ {}_j \quad {}_k[1 \quad (L\ )_{kl}]\ {}_l \quad {}_m[1 \quad (L\ )_{mn}]\ {}_n \quad {}_o[1 \quad (L\ )_{op}]\ {}_p$$

$$= g^4 \frac{N_F}{3} \int_{\Lambda=b} (dp_1)(dp_2)(dp_3) \qquad \ln b; \tag{4.107}$$

where we have again substituted $N_F = \frac{3}{2}d$. The three remaining diagrams (g)–(i) are obtained by different contractions of S^2. The diagrams can be evaluated simultaneously

$$I_g + I_h + I_i = -\frac{\ {}^2}{2} \int_{\Lambda=b} (dp_1)(dp_2)(dp_3) \int_{\Lambda=b}^{\Lambda} (dq) \times$$

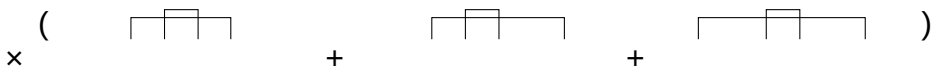

$$\times \; (\qquad + \qquad + \qquad)$$

$$= -40\ {}^2 \frac{1}{(1+r)^2} \int_{\Lambda=b} (dp_1)(dp_2)(dp_3) \qquad \ln b; \tag{4.108}$$

providing the leading correction in to the self-interaction. Together with the result from Eq. (4.107), we can read off the renormalization to the quartic coupling

$$= \left(\frac{N_F}{3} g^4 - 40\ {}^2 \frac{1}{(1+r)^2} \right) \ln b: \tag{4.109}$$

RG transformation

Having obtained all the necessary one-loop corrections for our ansatz (4.66), we now proceed with the second and third step of the RG procedure. In analogy to the procedure for the Gaussian theory in Sec. 4.3.2, we first rescale momenta $bp \to p$ to bring the cutoff of the effective action back to Λ, giving

$$\begin{aligned} S_< = & \int_\Lambda (\mathrm{d}p)\, b^{-D-1} Z_{\psi,1} \underbrace{i\bar{\psi}_i p\!\!\!/ \psi_i}_{i=1,2} + b^{-D-1} Z_{\psi,2}\, i\bar{\psi}_3 p\!\!\!/ \psi_3 \\ & + b^{-D-2} Z_\phi \frac{1}{2} p^2 \phi_- \phi_- + b^{-D} \frac{1}{2}(r + \delta r)\phi_- \phi_- \\ & + \int_\Lambda (\mathrm{d}p_1)(\mathrm{d}p_2) b^{-2D} (g + \delta g)\, \bar{\psi}_i [1 - (L_-)_{ij}]\, \psi_j \\ & + \int_\Lambda (\mathrm{d}p_1)(\mathrm{d}p_2)(\mathrm{d}p_3) b^{-3D} (\lambda + \delta\lambda)\, \ldots \end{aligned} \Big] \,. \tag{4.110}$$

As usual, the field renormalization is defined as to keep the kinetic terms constant under RG transformations. In contrast to the Gaussian theory, where the decoupling of momentum scales ensures that the fields scale with their canonical dimension, the field renormalization is modified by the appearance of non-trivial wave-function renormalizations

$$\phi \to \sqrt{\frac{1}{Z_\phi}}\, b^{\frac{D+2}{2}} \phi \,; \qquad \psi_{1,2} \to \sqrt{\frac{1}{Z_{\psi,12}}}\, b^{\frac{D+1}{2}} \psi_{1,2} \,; \qquad \psi_3 \to \sqrt{\frac{1}{Z_{\psi,3}}}\, b^{\frac{D+1}{2}} \psi_3 \,. \tag{4.111}$$

Gaussian field renormalization is recovered for $Z_\phi = 1$. For $\ln b \ll 1$ we can expand the wave-function renormalization in scaling form

$$Z_\phi = \mathrm{e}^{\ln Z_\phi} = \mathrm{e}^{\eta_\phi \ln b} = b^{\eta_\phi} \,; \tag{4.112}$$

where we have introduced the *flowing anomalous dimension* [28]

$$\eta_\phi = \frac{\mathrm{d} \ln Z_\phi}{\mathrm{d} \ln b}\bigg|_{\ln b = 0} \,; \tag{4.113}$$

by which the field renormalizations simplify to

$$\phi \to b^{\frac{D+2-\eta_\phi}{2}} \phi \,; \qquad \psi_{1,2} \to b^{\frac{D+1-\eta_{\psi,12}}{2}} \psi_{1,2} \,; \qquad \psi_3 \to b^{\frac{D+1-\eta_{\psi,3}}{2}} \psi_3 \,; \tag{4.114}$$

with the explicit values of the flowing anomalous dimensions being

$$\eta_\phi = \frac{2N_F}{3} g^2 \,; \qquad \eta_{\psi,12} = \frac{g^2}{2} \frac{1}{(1+r)^2} \,; \qquad \eta_{\psi,3} = g^2 \frac{1}{(1+r)^2} \,. \tag{4.115}$$

As the name already suggests, we can identify the fixed point value of the flowing anomalous

dimension with the critical exponent defined via Eq. (2.8). This follows from inserting the field renormalization into the homogeneity relation of the correlation function at the critical point [28]. Therefore, we refer to both as anomalous dimensions from here on. With Eq. (4.110), the renormalized effective action reads

$$\begin{aligned} S_{\text{ren}} = & \int_{\Lambda} (\mathrm{d}p) \; i_i \quad p \quad _i + \frac{1}{2}p^2 \qquad + \frac{1}{2} r(b) \\ & + g(b) \int_{\Lambda} (\mathrm{d}p_1)(\mathrm{d}p_2) \qquad _i [1 \qquad (L \;)_{ij}] \quad _j ; \\ & + \quad (b) \int_{\Lambda} (\mathrm{d}p_1)(\mathrm{d}p_2)(\mathrm{d}p_3) \qquad\qquad ; \end{aligned} \tag{4.116}$$

taking the same form as the initial momentum-space action (4.53). Collecting all one-loop corrections and inserting $\varepsilon = 4 - D$, we finally obtain the renormalized couplings

$$r(b) = b^{2-} \quad r + \quad 16 \quad \left(\frac{1}{1+r} - \frac{4N_F}{3} g^2 \right) \quad \ln b \quad ; \tag{4.117}$$

$$g(b) = b^{\frac{1}{2}(\varepsilon - \quad - \quad ;12 - \quad ;3)} \quad g - g^3 \frac{1}{1+r} \ln b \quad ; \tag{4.118}$$

$$(b) = b^{\varepsilon - 2} \quad + \quad \left(\frac{N_F}{3} g^4 - 40 \quad ^2 \frac{1}{(1+r)^2} \right) \quad \ln b \quad : \tag{4.119}$$

4.3.5 RG flow and critical exponents

The differential recursion relations governing the RG flow can now be obtained by differentiating the renormalized couplings (4.117)–(4.119) with respect to the logarithmic scale parameter $\ln b$. At one-loop order, the flow equations of the squared Yukawa coupling g^2 and the self-interaction of the order parameter read

$$\frac{\mathrm{d}g^2}{\mathrm{d}\ln b} = g^2(\varepsilon - \quad - \quad ;1 - \quad ;2) - 2g^4 \frac{1}{1+r} ; \tag{4.120}$$

$$\frac{\mathrm{d}}{\mathrm{d}\ln b} = \quad (\varepsilon - 2 \quad) + \frac{N_F}{3} g^4 - 40 \quad ^2 \frac{1}{(1+r)^2} ; \tag{4.121}$$

where , $_{;12}$ and $_{;3}$ again refer to the anomalous dimensions defined in Eq. (4.115). Equally, the flow of the order parameter mass r is given by

$$\frac{\mathrm{d}r}{\mathrm{d}\ln b} = r(2 - \quad) - \frac{4N_F}{3} g^2 + 16 \quad \frac{1}{1+r} : \tag{4.122}$$

Since the microscopic theory only has a single tunable parameter, the RG fixed point describing the phase transition has one relevant direction. In the context of the ε-expansion, all parameters are considered small and we can expand the non-linearities appearing in the flow equations and anomalous dimensions. For small ε, we can expand the flow equations (4.120)–(4.122) to

leading order in ε. Since the expansion of the non-linear factors only produces r-dependent contributions at subleading order, this effectively fixes $r_* = 0$ to leading order in ε. Within this approximation, we obtain the beta functions for the couplings g^2 and at criticality

$$_{g^2} = g^2(\varepsilon - \quad - \quad _{;1} - \quad _{;2}) - 2g^4; \tag{4.123}$$

$$= \quad (\varepsilon - 2 \quad) + \frac{N_F}{3} g^4 - 40 \quad ^2: \tag{4.124}$$

Since r decouples from both beta functions (4.123) and (4.124), it turns out to be a relevant direction for all fixed points at $O(\varepsilon)$. Consequently, the critical manifold is fixed at $r = 0$ and the fixed point associated with the transition is given by the fully stable IR fixed point of the beta functions. The inverse of the correlation length exponent $y = \frac{1}{}$ can then be computed by linearizing the flow of the order parameter mass r, given by Eq. (4.122), near the fixed point

$$y = \frac{1}{} = \frac{@}{@r} \frac{\mathrm{d}r}{\mathrm{d}\ln b} \quad _* = 2 - 2g_*^2 - 16 \quad _*; \tag{4.125}$$

where we again have set $r_* = 0$ to leading order in ε. This is a recurring pattern in the ε-expansion and one of the reasons why we are able to do analytical calculations based on the momentum-shell RG. In principle, we could have assumed $r_* = 0$ from the start, severely simplifying the discussion. We make use of this feature in the following chapter to study a more complicated model, whose critical behavior would be inaccessible without this simplification. However, beyond the leading order, we expect the fixed point to acquire a finite value r_*, such that the critical manifold is generally curved.

As illustrated in Fig. 4.7, the flow of the couplings g^2 and in the critical manifold features several fixed points. Linearizing the RG flow in the vicinity of the fixed points gives

$$\frac{\mathrm{d}}{\mathrm{d}\ln b} \begin{pmatrix} g^2 \\ \end{pmatrix} = \begin{pmatrix} \varepsilon - 11g_*^2 & 0 \\ 2g_*^2 - 4 \quad _* & \varepsilon - 4g_*^2 - 80 \quad _* \end{pmatrix} \begin{pmatrix} g^2 \\ \end{pmatrix} + O(g^4; \quad ^2); \tag{4.126}$$

where the coefficients are given by the Jacobian of the beta functions for g^2 and , evaluated at the fixed point. The eigenvectors of the linearized RG flow determine relevant and irrelevant directions of the fixed point, given by positive and negative eigenvalues, respectively. For $g^2 = 0$, two fixed points are found, corresponding to the Gaussian fixed point at $(g_*^2; \quad _*) = (0; 0)$, which is fully unstable and the O(2) Wilson-Fisher fixed point at $(g_*^2; \quad _*) = (0; \frac{\varepsilon}{40}) + O(\varepsilon^2)$, which is stable in the direction, but unstable against small Yukawa couplings g^2. The appearance of the Wilson-Fisher fixed point is no surprise, as setting $g = 0$ in the action (4.52) decouples the fermionic degrees of freedom from the order parameter field and reduces to the Landau-Ginzburg-Wilson action of a two-component order parameter field, whose criticality is described by the O(2) Wilson-Fisher fixed point. Thus, we expect the fixed point to be characterized by the same critical exponents as well as a vanishing fermionic anomalous dimensions

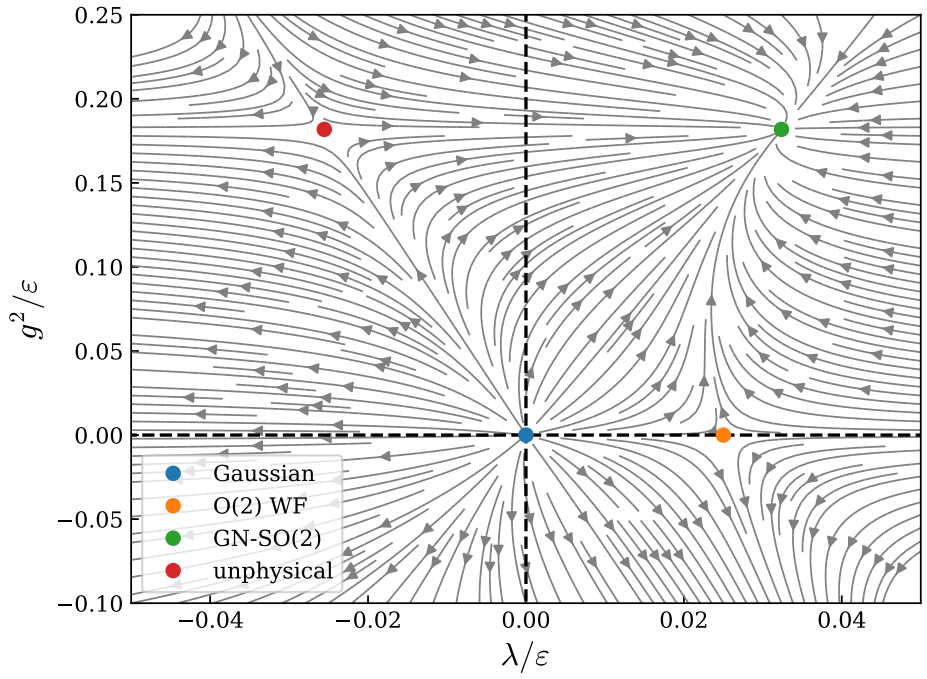

Figure 4.7: RG flow in the critical surface of the Gross-Neveu-SO(2) model. The Gaussian and O(2)-Wilson-Fisher fixed points both turn out to be unstable against Yukawa interactions. The critical fixed point is located at finite interactions $(g_*^2;\ _*) = (\frac{2}{11}\varepsilon;\ \frac{3+\sqrt{649}}{880}\varepsilon)$, giving the critical exponents $\frac{1}{}$ = 2 − 0:881″ and = $\frac{2}{11}\varepsilon$. A fourth fixed point is located at unphysical negative self-interactions and can be safely ignored, as discussed in the main text.

$_{;12}$ and $_{;3}$ to all orders in ″, whose appearance can be fully attributed to the Yukawa coupling. Evaluation of Eq. (4.125) and calculation of the boson anomalous dimension given in Eq. (4.115) gives

$$\begin{aligned} y = \frac{1}{} &= 2 - 0{:}4\varepsilon + O(\varepsilon^2); \\ &= 0; \end{aligned} \tag{4.127}$$

which precisely agrees with the one-loop results at linear order in ″ for the O(2) Wilson-Fisher universality class [30]. Thus, the inclusion of the Yukawa interaction in the action may be seen as the addition of an extra relevant coupling that drives the criticality away from Wilson-Fisher type to a new universality class.

Additionally, the RG flow admits a fixed point at finite Yukawa couplings g^2, which is fully IR stable and thus describes the critical point of the action (4.52). To leading order in ″, the

Figure 4.8: RG flow of the Gross-Neveu-SO(2) model away from the critical surface for the order parameter mass r. All couplings flow towards the fixed point after only a few RG iterations. Systems far away from the fixed point only stay in its vicinity for a few iterations, whereas systems close to criticality stay for a many iterations, thus providing a microscopic explanation for universal behavior.

fixed point values of the couplings are

$$(g^2;\ ) = \frac{6}{4N_F + 21}; \frac{4N_F + \sqrt{16N_F^2 + 1752N_F + 441} + 21}{80(4N_F + 21)}\ \Big)\ " + O("^2): \tag{4.128}$$

The critical exponents for the relevant case of $N_F = 3$ fermions, which describes criticality in the Kitaev-XY spin-orbital model, are then given by

$$\frac{1}{} = 2\ \ 0{:}881" + O("^2); \tag{4.129}$$

$$= \frac{4}{11}" + O("^2); \tag{4.130}$$

$$_{;1} = \frac{1}{11}" + O("^2); \tag{4.131}$$

$$_{;2} = \frac{2}{11}" + O("^2): \tag{4.132}$$

Thus, two numerical estimates for the correlation length exponent can be found. First, a direct calculation from Eq. (4.125) gives

$$= \frac{1}{y} = \frac{1}{2\ \ 0{:}881"}: \tag{4.133}$$

A second, possibly more rigorous estimate is given by an expansion of the correlation length exponent to linear order in ε

$$= \frac{1}{y} = \frac{1}{2} + 0{:}220\varepsilon + O(\varepsilon^2); \tag{4.134}$$

which is consistent with the preceding discussion where we have neglected all but the leading order terms in ε. Extrapolating to $\varepsilon = 1$, the values of the above critical exponents for the physically relevant case of a (2+1)-dimensional space-time can be obtained. With the hyperscaling relations given by Eqs. (2.12) and (2.13), the universal critical exponents ; and of the U(1) symmetry-breaking transition can be derived. Numerical estimates for the critical exponents can be read off from Table 4.2. Interestingly, the critical exponent, describing the critical isotherm, here giving the magnetization curve at the critical coupling J_c, evaluates to = 10 in both approximations. For completeness, let us note that there is a fourth fixed point, located at negative quartic interaction . Since the effective potential for the order parameter becomes unbound from below for < 0, such a fixed point is deemed unphysical. Moreover, Fig. 4.7 shows that no physical theories flow into the unphysical sector, so that this fixed point can be safely ignored.

Away from the critical manifold, i. e. for finite renormalized mass r, the renormalization group flow can be integrated numerically for suitable initial conditions for the couplings g_0, $_0$ and r_0, which represent the non-universal couplings of a specific microscopic theory. To understand the behavior of theories near criticality, it is instructive to consider the RG trajectory of a theory near the critical manifold but away from the stable fixed point. For the flow relevant to the spin-orbital model, i. e. $N_F = 3$ and $\varepsilon = 1$, the evolution of r and g^2 under repeated iterations of the renormalization group for such initial parameters is depicted in Fig. 4.8. We observe that the flow of the boson mass divides into two sectors, corresponding to aprroaching positive or negative infinity, respectively. Here, the sector which flows towards $r \to 1$ corresponds to the symmetric phase, while the sector with $r \to 1$ describes the symmetry-broken phase. Another important observation is given by the rate of evolution under repeated RG transformations in dependence of its distance to the critical point. While large deviations from the critical value r_c approach infinity after only a few renormalization group iterations, initial values close to r_c, stay near the critical point for many iterations. This also justifies the identification of the fixed point criticality with the physical behavior close to the phase transition and provides a microscopic explanation for the phenomenon of universality. Theories in the vicinity of the critical point will need infinite renormalization group iterations to approach infinity, and thus, their behavior at all length scales is governed by the linearized flow of the IR stable fixed point in the critical manifold.

Note that in the spin-orbital model, the fermionic excitations are fractionalized. The main consequence is that single-fermion excitations are not gauge invariant and thus forbidden in the spectrum. Thus, in principle, the fermion anomalous dimensions are not measurable. This

" = 1			; 12	; 3				
(a)	0.894	4/11	1/11	2/11	0.212	0.162	1.463	10
(b)	0.720	4/11	1/11	2/11	0.560	0.131	1.178	10

Table 4.2: Critical exponents of the Gross-Neveu-SO(2)* universality calss for $N_F = 3$ in $D = 3$ space-time dimensions. (a) refers to the value obtained from the direct calculation in Eq. 4.133, whereas (b) stems from the proper $O(")$ approximation given by Eq. 4.134. Surprisingly, the exponent for the critical isotherm $= 10$ agrees for both approximations. The fermion anomalous dimensions are listed for completeness and are not measurable in the fractionalized theory.

de nes a new type of fractionalized universality class, coined Gross-Neveu-SO(2)*. Due to gauge invariance of the order parameter and its excitations, both the correlation length exponent and the boson anomalous dimension agree with the values for the non-fractionalized universality class. Consequently, the hyperscaling relations imply that the macroscopic critical exponents also agree. This is in stark contrast to their bosonic O(n)* counterparts, where the absence of a gauge-invariant local order parameter gives rise to highly nontrivial critical behavior [25]. Still, due to a mapping of the scaling dimensions of a conformal eld theory to its nite-size spectrum on a torus, it is still possible to physically di erentiate between the fractionalized GN-SO(2)* and its trivial counterpart. Within this approach, fractionalized universality classes are characterized by missing energy levels in their trus spectrum, corresponding to the scaling dimensions of operator that are not gauge-invariant. Additionally, the spectrum of the conformal eld theory is expected to feature a topological ground-state degeneracy, emphasizing the topolgical nature of the critical point [25].

5 Anisotropic Kitaev spin-orbital model

Having developed the necessary methods in detail in the previous chapter, the stage is now set to take a closer look at a far more interesting model, which is the anisotropic Kitaev spin-orbital model de ned via Eq. (3.36), where an independent Ising interaction along the z-axis in the spin sector is introduced in addition the XY term we have discussed extensively. As we have already seen in Sec. 3.2, The model encompasses both the model discussed in the previous chapter, as well as the SU(2)-symmetric model introduced in Ref. [23] as limiting cases and allows for the continuous deformation of one into the other by introducing an easy-plane anisotropy. Since both of these models have been shown to support paramagnetic phases that are adiabatically connected to the exact solution of the SU(2)-symmetric model given in Eq. (3.16) at weak perturbations, we expect the same to happen for the region between the two theories in the extended parameter space of the anisotropic model. This suggests the appearance of a line of symmetry-breaking transitions at strong couplings with nite anisotropy and the question naturally arises as to which universality class describes the critical behavior at this transition line. For the study of critical phenomena, the anisotropic model is particularly interesting due to the presence of two tunable parameters in the theory. As such, RG xed points with two relevant directions become physically accessible, facilitating the appearance of multicritical behavior in the phase diagram.

The discussion of the critical behavior will proceed in a similar manner to the one in the previous chapter. First we uncover the mean- eld phase diagram on the lattice and characterize all appearing phases in Sec. 5.1, before proceeding with the RG analysis of the low-energy e ective eld theory in Sec. 5.2 to obtain the equations governing the RG ow, which is shown to exhibit various critical regimes and supports multiple critical points with di erent associated exponents.

5.1 Majorana mean- eld theory

5.1.1 Mean- eld Hamiltonian

In the lattice formulation, an approriate mean- eld description of the anisotropic Kitaev spin-orbital model (3.36) can again be derived from the Majorana representation. Assuming that the ground-state is located in the ux-free sector $u_{ij} = +1$ of the spin-orbital Hamiltonian (3.36), we get

$$H_K^{\text{ext}} = K \sum_{\langle ij \rangle_\gamma} \mathrm{i} c_i c_j + J_{xy} \sum_{\langle ij \rangle_\gamma} \sum_{\gamma = x,y} \left(\tfrac{1}{2} c_i \right) L^\gamma \left(\tfrac{1}{2} c_j \right) L^\gamma + J_z \sum_{\langle ij \rangle_\gamma} \left(\tfrac{1}{2} c_i \right) L^z \left(\tfrac{1}{2} c_j \right) L^z ; \tag{5.1}$$

where all conventions carry over from Secs. 3.2 and 4.1. The $U(1)_Z \times Z_2$ symmetry in the spin-orbital formulation maps onto $SO(2)_Z \times Z_2$ in avor space. Due to the structural similarity of Eqs. (4.1) and (5.1), we can again decouple the interaction into on-site and bond parameters

$$\alpha_i = \left(\tfrac{1}{2} c_i \right) L^\alpha c_i ; \qquad \chi_{ij} = \mathrm{i} \langle c_i c_j \rangle ; \tag{5.2}$$

where we have summarized the diagonal and o -diagonal decouplings in Eq. () into a single tensor χ_{ij} . The o -diagonal components again vanish when enforcing the $SO(2)_Z \times Z_2$ symmetry. Assuming translational invariance, $\chi_{i,j} = \chi_{A,B}$ and $\chi_{ij} =$ with $i(j)$ belonging to sublattices $A(B)$. We have seen in Sec. 4.1 that the sublattice symmetry ensures $\alpha_A = \alpha_B$, such that we obtain the mean- eld Hamiltonian

$$H_{\text{mf}} = \sum_{k \in BZ/2} \begin{pmatrix} c^\dagger_{k,A} , & c^\dagger_{k,B} \end{pmatrix} \begin{pmatrix} 0 & \mathrm{i}(K + \chi_J) f(k) \\ \mathrm{i}(K + \chi_J) f(k) & 0 \end{pmatrix} \otimes 1_3 + 6 J_{xy} \sum_{\gamma = x,y} \begin{pmatrix} 0 & \alpha_A \\ \alpha_A & 0 \end{pmatrix} \otimes L^\gamma + 6 J_z \begin{pmatrix} 0 & \alpha_A \\ \alpha_A & 0 \end{pmatrix} \otimes L^z \begin{pmatrix} c_{k,A} \\ c_{k,B} \end{pmatrix} + C(\alpha, \chi); \tag{5.3}$$

where the matrix reads

$$\chi_J = \begin{pmatrix} 0 & J_{xy} \chi_z + J_z \chi_y & 0 \\ J_{xy} \chi_z + J_z \chi_x & 0 & 0 \\ 0 & 0 & J_{xy} (\chi^x_{ij} + \chi^y_{ij}) \end{pmatrix} . \tag{5.4}$$

The constant contribution to the mean- eld Hamiltonian now depends on both exchange

$(J_{xy}; J_z)$	^x_A	^y_A	$^z_A = n_z$	$\lvert n_{xy}\rvert$	^{x}	^{y}	^{z}	$^x + {}^y$
(0.5, 0.5)	0	0	0	0	-0.5248	-0.5248	-0.5248	-1.0496
(0.5, 0.2)	0	0	0	0	-0.5248	-0.5248	-0.5248	-1.0496
(0.2, 0.5)	0	0	0	0	-0.5248	-0.5248	-0.5248	-1.0496
(0.6, 0.2)	0.0727	0.0898	0	0.1155	-0.5233	-0.5238	-0.5222	-1.0471
	0.0819	0.0815	0	0.1155	-0.5236	-0.5236	-0.5222	-1.0471
(0.2, 0.6)	0	0	0.2405	0	-0.5132	-0.5132	-0.5248	-1.0264
	0	0	0.2405	0	-0.5132	-0.5132	-0.5248	-1.0264
(0, 0.5)	0	0	0.1278	0	-0.5217	-0.5217	-0.5248	-1.0434
	0	0	0.1278	0	-0.5217	-0.5217	-0.5248	-1.0434

Table 5.1: Self-consistent solutions for the mean- eld parameters for typical values of the exchange couplings J_{xy} and J_z after 1000 iterations for an $N = 48 \quad 48$ unit cell lattice, where $\lvert n_{xy}\rvert^2 = (^x_A)^2 + (^y_A)^2$ is the XY Néel order parameter. The rst three points reside in the symmetric phase, characterized by vanishing sublattice magnetization and the characteristic value for the bond variables. At larger couplings, two distinct symmetry-broken phases stabilize, characterized by nite XY and Ising-type Néel order parameters, whereas the opposite order parameter vanishes.

couplings J_{xy} and J_z, as well as all symmetry-allowed mean- eld parameters, giving

$$C(; \quad) = \quad 3NJ_{xy} \sum_{=x;y} (\quad _A \quad _B \quad ^z \quad) \quad 3NJ_z(^z_A \ ^z_B \quad ^x \ ^y); \tag{5.5}$$

which reduces to the constant expression (4.12) in the limit $J_z = 0$. The self-consistency equations again take the form of Eqs. (4.12), (4.13) and (4.16), which we will repeat for availability

$$_x = \frac{2i}{N} \sum_{k2BZ=2} h(c_{k;x})^y c_{k;x}; i \qquad (x = A; B); \tag{5.6}$$

$$= \frac{i}{3N} \sum_{k2BZ=2} f(k)h(c_{k;A})^y c_{k;A}i \quad f \ (k)h(c_{k;B})^y c_{k;B}i \ : \tag{5.7}$$

The ground-state energy for a particular set of mean- eld parameters is given by

$$E_0 = \sum_{k2BZ=2} \sum_n "_n(k)h \ ^y_{n;k} \ _{n;k}i + C(; \quad): \tag{5.8}$$

5.1.2 Numerical results and phase diagram

The self-consistency equations (5.5) and (5.6) are again solved iteratively with random initial values for the iteration procedure. Since we are already familiar with the approach, we will

Figure 5.1: Mean-field phase diagram of the anisotropic Kitaev spin-orbital model. At small interactions J_{xy} and J_z, the model supports a paramgnetic Kitaev SOL phase with three gapless itinerant Majorana fermions. The phase is adiabatically connected to the ground state of the exactly solvable model at vanishing interaction. At stronger couplings, the model transitions into a Kitaev SOL phase with a single remaining gapless Majorana fermion, with concomitant Z_2 or U(1) symmetry-breaking in spin-space, depending on the anisotropy. They are separated by a symmetry-enhanced first-order transition, where both phases become unstable against the formation of order breaking both symmetries.

proceed directly to the numerical results. The model supports four distinct stable phases, which we will discuss briefly, as well as phase transitions between those phases. The phase diagram is shown in Fig. 5.1. Typical values of the mean-field parameters, characterizing the respective phase, are given in Table 5.1. The symmetric phase, describing a $\mathbb{Z}_2$ Kitaev SOL characterized by vanishing sublattice symmetry and the characteristic value of the bond parameters, extends into the region where both J_{xy} and J_z are finite, provided they are small. At strong couplings, the system transitions into a symmetry-broken phase with antiferromagnetic long-range order, whose nature depends on the type of anisotropy present in the system. In contrast to the model studied in Ch. 4, the additional Ising term in Eq. (5.1 introduces competition between two ordering channels. To characterize the emerging phases, we introduce two Néel order parameters

$$n_{xy} = \frac{\langle A \rangle - \langle B \rangle}{2} = \langle A \rangle \qquad (\ = x, y); \tag{5.9}$$

which acquires a finite value under spontaneous breaking of the U(1) sector of the Hamiltonian (3.36), whereas

$$n_z = \frac{\langle \tau^z_A \rangle - \langle \tau^z_B \rangle}{2} = \langle \tau^z_A \rangle; \tag{5.10}$$

describing spontaneous symmetry breaking in the $\mathbb{Z}_2$ sector. In both definitions, the second

Figure 5.2: Representative spectra for (a) the U(1) SSB phase at $(J_{xy}; J_z) = (0.6; 0.2)$ and (b) the Z_2 SSB phase at $(J_{xy}; J_z) = (0.2; 0.6)$. Spectrum (a), which is adiabatically connected to the ordered phase of the Kitaev-XY spin-orbital model and thus shares the same qualitative features as the dispersion in Fig. 4.2b. Spectrum (b) features two degenerate gapped with one remaining Dirac cone, a defining feature of the Z_2 symmetry-broken phase.

equality is due to the sublattice symmetry and the antiferromagnetic nature of the interactions, as discussed before. We again consider $K = 1$ for simplicity.

U(1) symmetry-breaking transition

Sec. 4.1 shows that in the limit of vanishing Ising exchange coupling, $J_z = 0$, the model exhibits a U(1) symmetry under spin rotations along the z-axis, which is spontaneously broken at strong couplings, transitioning into an magnetically ordered phase where the XY order parameter, defined via Eq. (5.9), acquires a finite value. At the level of the mean-field expansion, the critical value is given by $J_{xy}^c(J_z = 0) = 0.5320$. For finite $J_z < J_{xy}$, the easy-plane anisotropy is preserved, such that the system still favors XY order at strong couplings. Since the Z_2 symmetry is fully preserved, which follows from the vanishing of the Ising order parameter, n_z, the ordered phase in the easy-plane regime is adiabatically connected to the ordered phase at $J_z = 0$, sharing all features. We call this phase U(1) SSB. The equivalence between the ordered phases with vanishing and finite J_z also becomes clear from Fig. 5.2, which depicts a representative spectrum in the XY-ordered phase. Apart from small numerical differences, the spectrum is equal to the one shown in Fig 4.2b). Especially in the low-energy limit both spectra share the same qualitative features, describing two non-degenerate gapped modes that only coincide at the K point and a remaining Dirac cone. The transition is now described by an extended line in parameter space, whose position can be obtained as before by extrapolation of the XY order parameter n_{xy} close to criticality. Due to the competition of the two symmetry-breaking channels, the critical line is shifted towards stronger couplings J_{xy} for growing J_z.

(a) (b)

Figure 5.3: Extrapolation of the order parameter to obtain the critical value at 1000 iterations for $N = 48 \quad 48$ unit cells for (a) the U(1) symmetry-breaking transition described by the XY order parameter n_{xy} at $J_z = 0{:}2$, giving $J_{xy}^c(J_z = 0{:}2) = 0{:}5600$, and (b) the Z_2 symmetry-breaking transition at $J_{xy} = 0{:}2$, which gives $J_z^c(J_{xy} = 0{:}2) = 0{:}5159$, arising from a linear fit of the Ising order parameter $n_z = \frac{z}{A}$.

To illustrate this, we consider the transition at $J_z = 0{:}2$, for which the XY order parameter close to the transition and the extrapolation are depicted in Fig. 5.3b, giving the critical value $J_{xy}^c(J_z = 0{:}2) = 0{:}5600$. Other points may be obtained similarly.

Z_2 symmetry-breaking transition

Conversely, in the opposite limit $J_{xy} = 0$, the exactly solvable model (3.24) is perturbed by a pure Ising interaction, featuring a Z_2 spin-flip symmetry along the z-axis, which has not been discussed before. The corresponding spin-orbital interaction is given by (c) in Table 3.2. Due to the absence of the XY interaction in this limit, only a single symmetry-breaking channel remains and the system undergoes a transition into an ordered state, characterized by a finite Ising order parameter n_z and a spontaneously broken Z_2 symmetry. Similar to the previous case, the ordered phase remains stable in the region of finite J_{xy} under the assumption that J_z sufficiently large and that the system is in the easy-axis regime, $J_{xy} < J_z$ and the SO(2) symmetry is preserved in the ordered phase due to $n_{xy} = 0$. Thus, we call this phase Z_2 SSB. The last two lines in Table 5.1 reveal that the ordered phase exhibits several interesting features that we did not find with the U(1) SSB phase. First, we observe that the ground-state value of the bond parameter ^{z} assumes the characteristic value associated with the symmetric phase even in the ordered phase. To understand this, we consider how the mean-field Hamiltonian (5.3) changes at the phase transition. We have seen in Sec. 4.1 that the ground-state values for the bond parameters in the ordered phase deviate from the characteristic value due to the coupling of the Majorana fermions to the order parameter. However, in the Z_2 SSB phase, only the Ising order parameter n_z acquires a finite value, which

(a) (b)

Figure 5.4: (a) Extrapolation of the composite order parameter $n_{SO(3)}$ close to the SO(3) symmetry-breaking transition at 1000 iterations for $N = 48 \quad 48$ unit cells, giving the critical coupling $J_H = J_{xy} = J_z = 0{:}6185$. (b) Mean-field values of the XY and Ising order parameters close to the first-order transition. At the transition, the adjacent phases become unstable against a state breaking both symmetries. The finite values close to the transition are numerical artifacts, as discussed in the main text.

couples to only two of the three Majorana flavors due to the specific form of the generator L^z. Consequently, the single remaining flavor remains effectively non-interacting even after breaking the Z_2 symmetry and thus retains the bond parameter associated with the non-interacting limit $J_{xy} = J_z = 0$. Similarly, the ground-state values of the bond parameters ^{x} and ^{y} turn out to be equal and independent of the random initial conditions. This is because only the Z_2 sector of the full symmetry was broken at the transition, such that the SO(2) symmetry is still intact. Consequently, the results must be invariant under SO(2), leading to the observed values. The high symmetry of the mean-field solutions in the Z_2 SSB phase, and thus of the mean-field Hamiltonian (5.3) also leaves traces in the spectrum. Due to the SO(2) symmetry, the interaction affects the two gapped Majorana flavors equivalently, leading to a full degeneracy of the two gapped bands, as shown in Fig. 5.2b. However, the phenomenology of the remaining Dirac cone matches the observations made in the U(1) SSB phase, such that the Z_2 SSB phase also describes a = 1 Kitaev SOL, but associated with a different broken symmetry. To obtain the location of the transition line, we thus have to extrapolate the values of the Ising order parameter n_z close to the transition at fixed J_{xy}. This is illustrated exemplary in Fig. 5.3b for the transition at $J_{xy} = 0{:}2$, giving $J_z^c(J_{xy} = 0{:}2) = 0{:}5159$.

Symmetric limit and symmetry-enhanced first-order transition

In the symmetric limit $J_{xy} = J_z$, no anisotropy is present and the interaction in the spin-orbital model (3.36) simplifies to a Heisenberg interaction. The symmetry of the Hamiltonian (5.1) is enhanced to SO(3), corresponding to the low-energy (flux-free) description of the SU(2)-

symmetric spin-orbital model (3.32). As discussed in Sec. 3.2.2, a Majorana mean- eld analysis has of this model has already been performed in Ref. [23]. We recover their results, predicting a phase transition to a Néel-ordered phase with a spontaneously broken SU(2) symmetry in the spin sector upon variation of the Heisenberg coupling J_H. In Majorana avor space, the transition is described by a composite SO(3) order parameter

$$n_{SO(3)} = (n_{xy}; n_z)^{|}; \tag{5.11}$$

originating from the enhanced symmetry on the symmetric line. Within our implementation, we obtain a critcal value of $J_H^c = 0{:}6185$, see Fig. 5.4a, which is close to the value from Ref. [23]. The critical point acts as an endpoint for the neighboring SO(2) and Z_2 transition lines. This raises the question of the nature of the transition between the two anisotropic ordered phases. Since both phases break di erent symmetries of the general model, we naturally expect the appearance of a rst-order transition, which is con rmed by our mean- eld calculations. This is shown in Fig. 5.4b for couplings J_{xy} and J_z close to the symmetric line. Starting out in the U(1) SSB phase, the XY order parameter has a nite value, whereas the Ising order parameter vanishes. Upon tuning J_H through the symmetric line the order parameters jump, and the system transitions into the Z_2 SSB phase. However, instead of showing the usual phase coexistence at the transition, where the ground-state energy is minimized for just the two adjacent phases, both phases become unstable against the formation of a state that breaks both symmetries due to the enhanced SO(3) symmetry of the system at the transition point. This is a typical feature of a symmetry-enhanced rst-order transition [61], whose origin will be discussed later.

A small remark is to be made concerning the numerical data of points close to the transition, which, ithin the iterative scheme, acquire a nite value for both order parameters. This is an artifact of the numerical approach, which can be explained by the large ground-state degeneracy at the transition point. Close to the transition, the converges to a local minimum close to the actual ground-state energy. This can be remedied by comparing with the ground-state energy of the respective ordered phases, which turn out to be the global minima.

5.2 RG analysis

5.2.1 E ective eld theory

We have seen in the previous section that the introduction of anisotropy facilitates the appearance of a bicritical point. A bicritical point arises naturally in the presence of two independent order parameters connected to the breaking of di erent symmetries and describes the point where both order parameters change non-analytically. Most generally, its emergence is de-

scribed by the Landau free energy [41]

$$f = \frac{1}{2} r_1 |\ _1|^2 + \frac{1}{2} r_2 |\ _2|^2 + \ _1 |\ _1|^4 + \ _2 |\ _2|^4 + 2\ _{cr} |\ _1|^2 |\ _2|^2; \tag{5.12}$$

where $(r\ ;\ > 0)$ denote pairs of parameters for the individual e ective potentials of the two order parameters $_1$ and $_2$ and $_{cr} > 0$ is an additional independent parameter $_{cr}$ describing the interaction between the order parameters. At $_{cr} = 0$, Eq. (5.12) describes two independent symmetry breaking transitions at $r_1 = 0$ and $r_2 = 0$, corresponding to either $_1$ or $_2$ acquiring a nite expectation value. Thus, the phase diagram features four qualitatively di erent regimes. Besides the symmetric regime for $r_1; r_2 > 0$ and the regimes where one of the two order parameters becomes nite, there is a regime with $r_1; r_2 < 0$, where both $_1$ and $_2$ acquire nite values, spontaneously breaking their associated symmetry group. Finite $_{cr}$ introduce an energy penalty for con gurations with both nite $_1$ and $_2$, e ectively narrowing the region where both symmetries are broken. In this case, four continuous transitions meet at the at $r_1 = r_2 = 0$, describing a tetracritical point. For $^2_{cr}\ \ _1\ _2$, the phase with fully broken symmetry vanishes completely and is replaced by a rst-order transition between the phases associated with partial symmetry breaking. Thus, $r_1 = r_2 = 0$ now connects two distinct continuous transition lines and equally marks the end point of a line of rst-order transition. Such a scenario de nes a bicritical point.

For the speci c case of the Hamiltonian (5.1) the symmetry group is given by $U(1) \times Z_2$. Thus, Eq. (5.12) accurately describes the phenomenology of the phase diagram obtained in the previous section if we choose $_1 = (\ ^x;\ ^y)^|$ as an XY order parameter associated with the U(1) spin rotation symmetry in the x-y plane, and $_2 = \ ^z$, corresponding to an Ising order parameter which spontaneously breaks the Z_2 spin- ip symmetry along the z-axis. Following the considerations from Sec. 4.2, we can construct a partially bosonized e ective eld theory for the Hamiltonian (5.1) near criticality by including dynamics in space and imaginary time and by coupling the itinerant Majorana fermions to both order parameters via Yukawa couplings g_{xy} and g_z. With the dynamical critical exponent $z = 1$ for both elds, the corresponding action is Lorentz invariant and can be written as an integral over $D = d + 1$-dimensional space-time if generalized to arbitrary spatial dimension d, giving

$$\begin{aligned} S = \int d^D x \Big[& \ _i\ @\ _i + \frac{1}{2}\ (\ @^2 + r_{xy})\ \ + \frac{1}{2}\ ^z (\ @^2 + r_z)\ \ ^z \\ & + g_{xy}\ \ _i\ 1_d\ \ (L\ )_{ij}\ \ _j + g_z\ \ ^z\ _i\ 1_d\ \ (L^z)_{ij}\ \ _j \\ & + \ _{xy}\ \ \ ^2 + \ _z (\ ^z)^4 + 2\ _{cr} (\ ^z)^2 \Big]; \end{aligned} \tag{5.13}$$

which describes three massless fermion avors, representing the Majorana fermions, coupled to two real bosonic elds and ^{z} with masses r_{xy} and r_z, representing the two order param-

Figure 5.5: Possible critical scenarios in the anisotropic Gross-Neveu-SO(3) model. The realized scenario depends on the strength of the quartic interactions, based on the minimization of the e ective action. (a) For $^2_{cr} < _{xy} _z$, the model features a tetracritical point, acting as an endpoint for four continuous transitions. (b) For $^2_{cr} > _1 _2$, the phase where both symmetries break is suppressed to a line of rst-order transitions, denoted by the double line. Note that the exact values and the shape of the phase boundaries are expected to change under RG transformations. Fro the RG ow, the nature of the multicritical behavior can be deduced from the xed point values of the quartic interactions.

eters. The elds are assumed to be space-time dependent to include quantum uctuations and $d = \frac{2}{3}N_F$ again denotes the number of components of the fermionic elds, generalized to arbitrary number of Majorana avors. Summation over $i; j = 1; 2; 3$, referring to the three fermion avors, and $= x; y$, denoting the components of the U(1) order parameter, is assumed. The conventions for the Dirac matrices and the Dirac conjugate spinor $_i = ^y_i \, ^0$ carry over from the discussion in Sec. 4.3 as well. In accordance with Eq. (5.12), we have also added local self-interactions $_{xy}; _z$ for each order parameter, as well as a crossing term parameterized by $_{cr}$, describing local interactions between the di erent order parameter elds, which is unconstrained due to the absence of symmetry relations between the two order parameters. The two possible critical scenarios of the model are shown in Fig. 5.5, following the earlier arguments. In momentum space, we again divide the action into three contributions

$$S = S_0 + S_g + S \; ; \tag{5.14}$$

which consists of a non-interacting part S_0 as well as interaction terms S_g, containing the two Yukawa interactions, and S , which encompasses the quartic interactions of the bosonic elds,

giving

$$S_0 = \int (dp)\ i\ _i\ \ p\ \ _i + \frac{1}{2}\ \ p^2 + r_{xy}\ \ \ + \frac{1}{2}\ ^z\ p^2 + r_z\ \ ^z\ ; \tag{5.15}$$

$$S_g = \int (dp_1)(dp_2)\ g_{xy}\ \ _i [1\ \ (L\ )_{ij}\ ]\ _j + g_z\ ^z\ _i [1\ \ (L^z)_{ij}\ ]\ _j\ ; \tag{5.16}$$

$$S\ = \int (dp_1)(dp_2)(dp_3)\ \ _{xy}\ \ \ \ + \ _z(\ ^z)^4 + 2\ _{cr}\ \ \ (\ ^z)^2\ ; \tag{5.17}$$

where the momentum-dependence of the elds has been suppressed and takes the same form as in Eqs. (4.54) (4.56). Thus, the action contains seven independent parameters, which we will assume to be scale-dependent in the ensuing RG analysis. It is straightforward to show that all interactions included in have the upper critical dimension $D_c = 4$ at the Gaussian xed point, such that the critical behavior of the model is accessible in $D = 4\ \ "$ space-time dimensions.

5.2.2 Momentum-shell RG

The momentum-shell transformation proceeds in similar fashion to the procedure presented in Sec. 4.3. We start by splitting the elds into fast and slow Fourier modes. After integrating out the fast modes in the partition function, the e ective action for the slow modes takes the form

$$\begin{aligned} S_< = & \int_{\ b}^{} (dp)\ (1 + \ \ )i\ _i\ \ p\ \ _i + (1 + \ _{;xy})\frac{1}{2}p^2\ \ \ + (1 + \ _{;z})\frac{1}{2}p^2(\ ^z)^2 \\ & + \frac{1}{2}(r_{xy} + \ r_{xy})\ \ \ + \frac{1}{2}(r_z + \ r_z)(\ ^z)^2 \\ & + \int_{\ b}^{} (dp_1)(dp_2)\ \Big(g_{xy} + \ g_{xy})\ \ _i [1\ \ (L\ )_{ij}\ ]\ _j + (g_z + \ g_z\ ^z\ _i [1\ \ (L^z)_{ij}\ ]\ _j \Big) \\ & + \int_{\ b}^{} (dp_1)(dp_2)(dp_3)\ \Big(\ _{xy} + \ _{xy})\ \ \ \ + (\ _z + \ _z)(\ ^z)^4; \\ & \qquad + 2(\ _{cr} + \ _{cr})\ \ \ (\ ^z)^2 \end{aligned} \tag{5.18}$$

where we have introduced corrections to all couplings and anomalous dimensions to the kinetic terms of the fermionic sector and the two order parameters via Eqs. (4.12) and (4.113). Since the order parameter masses r_{xy} and r_z can be tuned independently, the corresponding Gaussian propagators read

$$(p)\ \ (\ p)\ _0 = \frac{1}{p^2 + r_{xy}}\ \ \ ; \tag{5.19}$$

$$^z(p)\ \ ^z(\ p)\ _0 = \frac{1}{p^2 + r_z}; ; \tag{5.20}$$

(a) (b) (c)

(d) (e) (f)

Figure 5.6: All diagrams contributing to the renormalization of the quartic boson-boson interaction $_{cr}$. After careful evaluation of the combinatorial factors, the diagrams are evaluated following the scheme in Sec. 4.3.4.

the fermion propagator is unchanged. In the -expansion, we only keep the leading contributions to the e ective action, which are obtained from all one-loop Feynman diagrams in the diagrammatic expansion introduced in Sec. 4.3. Formally, the appearance of additional interaction terms requires the de nition of corresponding interaction vertices in the diagrammatic representation. However, due to the structural similarity to the terms appearing in the action (4.52), the topology of the new vertices does not change. Thus, we can reuse the same vertices, di erentiating between the interaction terms in (5.13) with the coupling constants and eld indices of outgoing lines. To obtain all contributing diagrams, we now have to consider all combinations of the new interaction vertices for each diagram in Fig. 4.6. Besides the diagrams considered in Sec. 4.3 and the equivalent contributions from the new interactions, which are calculated analogously, this procedure introduces diagrams that contract two di erent vertices. To illustrate this, we consider all diagrams contributing to the fermion propagator

$$= \quad + \quad + \quad : \qquad (5.21)$$

The rst diagram has already been evaluated in Eq. 4.101 and the value for second, corresponding to the Ising contribution, contains the same loop integral and is obtained analogously. The third diagram contains both Yukawa couplings linearly and is therefore a rst order term in the perturbative expansion. Evaluation of the diagram gives

$$= \int_{=b} (dp) \int_{=b} (dq) \langle \{z\} \rangle_{=0}^{z} \; {}_i[1 \quad (L \;)_{ij}] \; {}_j \; {}_k[1 \quad (L^z)_{kl}] \; {}_l = 0 \,; \qquad (5.22)$$

where the contraction of the two order parameter vanishes due to the diagonal form of the boson propagators (5.19) and (5.20). As before, we thus obtain two distinct fermion anomalous

dimensions

$$\eta_{;12} = \frac{g_{xy}^2}{2}\frac{1}{(1+r_{xy})^2} + \frac{g_z^2}{2}\frac{1}{(1+r_z)^2}; \tag{5.23}$$

$$\eta_{;3} = \frac{g_{xy}^2}{(1+r_{xy})^2}: \tag{5.24}$$

The boson propagator receives no crossing terms because the external legs of the corresponding diagram are fixed, giving the anomalous dimensions

$$\eta_{;xy} = \frac{2}{3}N_F g_{xy}^2; \tag{5.25}$$

$$\eta_{;z} = \frac{2}{3}N_F g_z^2: \tag{5.26}$$

Similarly, most terms in the action (5.14) receive no corrections from crossing terms. Their contribution to the effective action can be calculated following Sec. 4.3.4. Only the vertex corrections to the quartic boson-boson coupling$_{cr}$ has to be treated with special care, the contributing diagrams are depicted in Fig. 5.5. Collecting all contributions, we rescale momenta and renormalize the fields as in Sec. 4.3.4 and obtain the renormalized boson masses

$$r_{xy}(b) = b^2\left[\eta_{;xy}\, r_{xy} + \frac{16\,\eta_{xy}}{1+r_{xy}} + \frac{4\,\eta_{cr}}{1+r_z} - \frac{4N_F}{3}g_{xy}^2\right]\ln b\ ; \tag{5.27}$$

$$r_z(b) = b^2\left[\eta_{;z}\, r_z + \frac{12\,\eta_z}{1+r_z} + \frac{8\,\eta_{cr}}{1+r_{xy}} - \frac{4N_F}{3}g_z^2\right]\ln b\ ; \tag{5.28}$$

and the renormalized interactions

$$g_{xy}(b) = b^{\frac{1}{2}(\epsilon - \eta_{;xy} - \eta_{;12} - \eta_{;3})}\left[g_{xy} - \frac{g_{xy}^3}{1+r_{xy}}\right]\ ; \tag{5.29}$$

$$g_z(b) = b^{\frac{1}{2}(\epsilon - \eta_{;xy} - 2\eta_{;12})}\left[g_z - \frac{g_z^3}{1+r_{xy}}\right]\ ; \tag{5.30}$$

$$\lambda_{xy}(b) = b^{\epsilon - 2\eta_{;xy}}\left[\lambda_{xy} + \frac{N_F}{3}g_{xy}^4 - \frac{40\,\lambda_{xy}^2}{(1+r_{xy})^2} - \frac{4\,\lambda_{cr}^2}{(1+r_z)^2}\right]\ ; \tag{5.31}$$

$$\lambda_z(b) = b^{\epsilon - 2\eta_{;z}}\left[\lambda_z + \frac{N_F}{3}g_z^4 - \frac{36\,\lambda_{xy}^2}{(1+r_z)^2} - \frac{8\,\lambda_{cr}^2}{(1+r_{xy})^2}\right]\ ; \tag{5.32}$$

$$\begin{aligned}\lambda_{cr}(b) = b^{\epsilon - \eta_{;xy} - \eta_{;z}}\Big[&\lambda_{cr} + \frac{N_F}{3}g_{xy}^2 g_z^2 - \frac{16\,\lambda_{xy}\,\lambda_{cr}}{(1+r_{xy})^2} \\ &- \frac{12\,\lambda_z\,\lambda_{cr}}{(1+r_z)^2} - \frac{16\,\lambda_{cr}^2}{(1+r_{xy})(1+r_z)}\Big]\ :\end{aligned} \tag{5.33}$$

5.2.3 Renormalization Group flow and critical exponents

Next, we differentiate the renormalized couplings (5.27) (5.33) with respect to the logarithmic scale parameter $\ln b$, giving the flow equations for the masses

$$\frac{dr_{xy}}{d\ln b} = (2 - \eta_{;xy})r_{xy} - 2d\, g_{xy}^2 + \frac{16\,\eta_{xy}}{1+r_{xy}} + \frac{4\,\eta_{cr}}{1+r_z}; \tag{5.34}$$

$$\frac{dr_z}{d\ln b} = (2 - \eta_{;z})r_z - 2d\, g_z^2 + \frac{12\,\eta_z}{1+r_z} + \frac{8\,\eta_{cr}}{1+r_{xy}}; \tag{5.35}$$

and the interactions

$$\frac{dg_{xy}^2}{d\ln b} = (\varepsilon - \eta_{;xy} - \eta_{;12} - \eta_{;3})g_{xy}^2 - \frac{2g_{xy}^4}{1+r_{xy}}; \tag{5.36}$$

$$\frac{dg_z^2}{d\ln b} = (\varepsilon - \eta_{;z} - 2\eta_{;12})g_z^2 - \frac{2g_z^4}{1+r_z}; \tag{5.37}$$

$$\frac{d\,\eta_{xy}}{d\ln b} = (\varepsilon - 2\eta_{;xy})\,\eta_{xy} + \frac{N_F}{3}g_{xy}^4 - \frac{40\,\eta_{xy}^2}{(1+r_{xy})^2} - \frac{4\,\eta_{cr}^2}{(1+r_z)^2}; \tag{5.38}$$

$$\frac{d\,\eta_z}{d\ln b} = (\varepsilon - 2\eta_{;z})\,\eta_z + \frac{N_F}{3}g_z^4 - \frac{36\,\eta_{xy}^2}{(1+r_z)^2} - \frac{8\,\eta_{cr}^2}{(1+r_{xy})^2}; \tag{5.39}$$

$$\frac{d\,\eta_{cr}}{d\ln b} = (\varepsilon - \eta_{;z} - \eta_{;xy})\,\eta_{cr} + \frac{N_F}{3}g_{xy}^2 g_z^2 - \frac{16\,\eta_{xy}\,\eta_{cr}}{(1+r_{xy})^2} - \frac{12\,\eta_z\,\eta_{cr}}{(1+r_z)^2} - \frac{16\,\eta_{cr}^2}{(1+r_{xy})(1+r_z)}. \tag{5.40}$$

Following the arguments in Sec. 4.3.5, the critical manifold in the ε-expansion is located at vanishing boson mass. Since we have two order parameters, whose masses can be tuned independently, this presents us with three critical regimes. The $r_{xy} = r_z = 0$ regime corresponds to tuning both physical parameters to their critical value, describing the multicritical regime. The multicritical behavior is governed the corresponding IR stable fixed point in the five-dimensional interaction subspace. The critical lines between the symmetric phase and the partially symmetry-broken phases are given by $r_{xy} = 0, r_z > 0$, describing the SO(2) symmetry-breaking transition and $r_{xy} > 0, r_z = 0$, describing the Z_2 symmetry-breaking transition, as shown in Fig 5.5. The critical behavior at the line is governed by the respective IR fixed point. Since the flow of the boson masses is relevant near the multicritical point, they flow towards infinity under repeated RG transformations. This reveals two more critical regimes: The critical behavior of the SO(2) line is described by the IR fixed point in the $r_{xy} = 0, r_z \to \infty$ regime, whereas the fixed point governing the Z_2 line resides in the $r_{xy} \to \infty, r_z = 0$ regime.

Multicritical point

We first discuss the multicritical regime. A similar analysis has been carried out for a Gross-Neveu-Yukawa theory in the context of competing order in graphene-like materials, but with

Figure 5.7: RG flow of the anisotropic Gross-Neveu-SO(3) model in the bicritical manifold. The IR stable fixed point is GN-(SO(2)+I)*, featuring an emergent SO(3) symmetry. The quantum critical points GN-SO(2)* and GN-Ising* are retained in the XY and Ising limit, respectively.

an SO(3) Z_2 composite order parameter [62] and an even amount of fermion flavors. The procedure followed here is based on their work. For vanishing boson masses, the flow equations for the interactions (5.36) (5.40) simplify, giving the multicritical beta functions for the Yukawa couplings

$$\beta_{g_{xy}} = (\epsilon - \gamma_{\phi_{xy}} - \tfrac{1}{2}\gamma_{\phi_z} - \tfrac{3}{2})g_{xy}^2 - 2g_{xy}^4, \tag{5.41}$$

$$\beta_{g_z} = (\epsilon - \gamma_{\phi_z} - 2\gamma_{\phi_{xy}} - \tfrac{1}{2})g_z^2 - 2g_z^4, \tag{5.42}$$

and the flow of the quartic couplings

$$\beta_{\lambda_{xy}} = (\epsilon - 2\gamma_{\phi_{xy}})\lambda_{xy} + \frac{N_F}{3}g_{xy}^4 - 40\lambda_{xy}^2 - 4\lambda_{cr}^2, \tag{5.43}$$

$$\beta_{\lambda_z} = (\epsilon - 2\gamma_{\phi_z})\lambda_z + \frac{N_F}{3}g_z^4 - 36\lambda_{xy}^2 - 8\lambda_{cr}^2, \tag{5.44}$$

$$\beta_{\lambda_{cr}} = (\epsilon - \gamma_{\phi_z} - \gamma_{\phi_{xy}})\lambda_{cr} + \frac{N_F}{3}g_{xy}^2 g_z^2 - 16\lambda_{xy}\lambda_{cr} - 12\lambda_z\lambda_{cr} - 16\lambda_{cr}^2. \tag{5.45}$$

where the anomalous dimensions have also been evaluated at $r_{xy} = r_z = 0$. The flow of the Yukawa couplings decouples from the bosonic sector, such that the fixed point values of the Yukawa couplings and their stability are independent of the quartic couplings and can be obtained analytically in the g_{xy}^2 – g_z^2 subspace. The fixed point values for the quartic couplings

are then obtained from the RG flow bosonic subspace, at the respective Yukawa fixed point. In the Yukawa subspace, we find four fixed points, which are displayed in Fig. 5.7. Apart from the Gaussian fixed point at the origin, we find a fixed point

$$(g_{xy}^2 ; g_z^2) = \frac{6\varepsilon}{4N_F + 21}; 0 + O(\varepsilon^2); \tag{5.46}$$

which recovers the GN-SO(2) fixed point discussed in the previous Chapter, corresponding to the limit $g_z = {}_z = {}_{cr} = 0$. Another fixed point is located at

$$(g_{xy}^2 ; g_z^2) = 0; \frac{3\varepsilon}{2N_F + 9} + O(\varepsilon^2); \tag{5.47}$$

which turns out to describe yet another fractionalized universality class, corresponding to the limit $g_{xy} = {}_{xy} = {}_{cr} = 0$, at which the anisotropic model reduces to a Z_2-symmetric model describing the low-energy physics of the Kitaev spin-orbital Hamiltonian (3.16) with an Ising interaction. The details will be worked out shortly. The fourth fixed point is given by

$$(g_{xy}^2 ; g_z^2) = \frac{3\varepsilon}{2N_F + 12}; \frac{3\varepsilon}{2N_F + 12} + O(\varepsilon^2); \tag{5.48}$$

displaying SO(3) symmetry. The stability of the fixed points is determined by the linearized flow close to the fixed point

$$\frac{d}{d\ln b}\begin{pmatrix} g_{xy}^2 \\ g_z^2 \end{pmatrix} = \begin{pmatrix} -\varepsilon + (\frac{4N_F}{3} + 7) g_{xy}^2 - \frac{1}{2} g_z^2 & \frac{1}{2} g_{xy}^2 \\ g_z^2 & -\varepsilon + (\frac{4N_F}{3} + 1) g_{xy}^2 - 6 g_z^2 \end{pmatrix} \begin{pmatrix} g_{xy}^2 \\ g_z^2 \end{pmatrix} + O(g_{xy}^4; g_z^4); \tag{5.49}$$

revealing the SO(3)-symmetric fixed point (5.48) to be IR stable, describing the fractionalized bicritical Gross-Neveu-(SO(2)+I)* universality class. Both the SO(2) and the Z_2 fixed point have one relevant and one irrelevant eigenvalue each, realizing quantum critical points in their respective limits. For the fixed-point values of the Yukawa couplings, the bosonic flow admits two symmetric fixed points with opposite sign, of which the positive fixed point is stable, giving the fixed point value

$${}_{xy} = {}_z = {}_{cr} = \frac{6 \quad N_F + \sqrt{N_F^2 + 120N_F + 36}}{88(N_F + 6)}; \tag{5.50}$$

such that the fixed point retains its SO(3) symmetry. This allows for two conclusions. The fixed point values for the quartic couplings provide information about the nature of the multicritcal behavior. Due to the symmetry, ${}^2_{cr} = {}_{xy}\,{}_z$. As discussed earlier, this explains the appearance of a bicritical point and the symmetry-enhanced first-order transition in the microscopic model. However, it might be interesting to investigate if additional interactions might change the nature of the transition due to the proximity of the fixed point to the tetracritical regime.

Additionally, the fixed point possesses an emergent SO(3) symmetry. For the microscopic model, this is trivial, since the bicritcal point is inherently SO(3) symmetric. However, since all theories on the critical manifold define critical theories, more complicted systems realizing this bicritcal point might not feature this inherent symmetry. The critical behavior of the fixed point is characterized by two relevant with associated correlation length exponents. They are obtained from diagonalizing the linearized flow of the boson masses

$$\frac{d}{d\ln b}\begin{pmatrix} r_{xy} \\ r_z \end{pmatrix} = \begin{pmatrix} 2 - \frac{2N_F}{3}g_{xy}^2 - 16\,\Delta_{xy}^2 & -8\,\Delta_{cr}^2 \\ -4\,\Delta_{cr}^2 & 2 - \frac{2N_F}{3}g_z^2 - 12\,\Delta_z^2 \end{pmatrix}\begin{pmatrix} r_{xy} \\ r_z \end{pmatrix} + O(r_{xy}^2; r_z^2); \quad (5.51)$$

giving the two critical exponents for the physically relevant case $N_F = 3$

$$y_1 = \frac{1}{\nu_1} = 2 - 0.567\varepsilon + O(\varepsilon^2); \quad (5.52)$$

$$y_2 = \frac{1}{\nu_2} = 2 - 0.917\varepsilon + O(\varepsilon^2); \quad (5.53)$$

The leading divergence of the correlation length is given by the larger correlation length exponent ν_2, the corresponding eigenvector is parallel to the symmetric line $r_{xy} = r_z$ and the fixed point anomalous dimensions read

$$\eta_{\Delta,xy} = \eta_{\Delta,z} = \frac{\varepsilon}{3} + O(\varepsilon^2); \qquad \eta_{\Delta,12} = \eta_{\Delta,3} = \frac{\varepsilon}{6} + O(\varepsilon^2); \quad (5.54)$$

recovering the critical behavior of the GN-SO(3)* universality class. Before we proceed with the discussion, a small remark regarding the relevance of the fixed point (5.48) is necessary. In the Ising limit, the RG flow equations reduce to the two-dimensional subspace

$$\beta_{g_z} = (\varepsilon - \frac{2N_F}{3}g_z^2)g_z^2 - 3g_z^4; \quad (5.55)$$

$$\beta_{\Delta_z} = (\varepsilon - \frac{2N_F}{3}g_z^2)\,\Delta_z + \frac{N_F}{3}g_z^4 - 36\,\Delta_{xy}^2. \quad (5.56)$$

The flow supports a non-trivial stable fixed point, which, for $N_F = 3$ is given by

$$(g_z^2\,;\,\Delta_z) = (\frac{1}{5}\varepsilon;\, \frac{1+\sqrt{145}}{360}\varepsilon) + O(\varepsilon^2); \quad (5.57)$$

with the fixed point anomalous dimensions

$$\eta_{\Delta,z} = \frac{6\varepsilon}{15} + O(\varepsilon^2); \qquad \eta_{\Delta,12} = \frac{\varepsilon}{10} + O(\varepsilon^2); \qquad \eta_{\Delta,3} = 0; \quad (5.58)$$

and the inverse correlation length exponent

$$y = \frac{1}{\nu} = 2 - 0.835\varepsilon + O(\varepsilon^2). \quad (5.59)$$

Figure 5.8: RG flow in the critcal regime $r_{xy} = 0; r_z \to 1$, describing the U(1) symmetry-breaking transition line in the mean-field phase diagram. The IR stable fixed point recovers the exponents recovers the exponents of the GN-SO(2)* universality class.

This defines the Gross-Neveu-Z_2 universality class, which presents another instance of a fractionalized fermionic quantum critical point. Remarkably, the fixed point anomalous dimension η_3 vanishes at one-loop order. This is in accordance with our findings in the lattice calculations of the Ising limit, where one of the three Majorana flavors did not participate in the interaction. Since its correlation function scales according to dimensional analysis at the critical point, it effectively decouples from the interaction. It is not clear whether the the anomalous dimension acquires a finite value at higher orders of the expansion, similar to the situation of the O(N) universality class [30].

SO(2) transition line

We continue with the analysis of the SO(2) transition line in the mean-field phase diagram. As discussed, the critical behavior is governed by the stable fixed point in the regime $r_{xy} = 0; r_z \to 1$. There, the non-linear contributions arising from Ising order parameter are suppressed and r_{xy} remains as the only relevant direction. The beta functions in the Yukawa sector read

$$\beta_{g_{xy}} = (\epsilon - \eta_{\phi,xy} - \eta_{12} - \eta_3) g_{xy}^2 - 2 g_{xy}^4, \tag{5.60}$$

$$\beta_{g_z} = (\epsilon - \eta_{\phi,z} - 2\eta_{12}) g_z^2 - 2 g_z^4; \tag{5.61}$$

Figure 5.9: RG flow describing the Z_2 symmetry-breaking transition line in the mean-field phase diagram. The IR stable fixed point recovers the exponents recovers the exponents of the GN-Ising* universality class.

The RG flow is depicted in Fig. 5.8. The IR stable fixed point is given by

$$(g_{xy}^2 ; g_z^2) = \frac{2}{4N_F + 7}\varepsilon ; \frac{4N_F + 5}{2N_F(4N_F + 7)}\varepsilon + O(\varepsilon^2); \tag{5.62}$$

and the corresponding fixed point values in the bosonic sector for $N_F = 3$ read

$$_{xy} = \frac{3 + \sqrt{649}}{880}\varepsilon + O(\varepsilon^2); \tag{5.63}$$

$$_{z} = \frac{4212 \sqrt{649} \quad 85860}{177408}\varepsilon + O(\varepsilon^2); \tag{5.64}$$

$$_{cr} = \frac{3 \sqrt{649} \quad 39}{352}\varepsilon + O(\varepsilon^2): \tag{5.65}$$

We can tune through the transition line by varying the only relevant parameter r_{xy}, giving the critical exponent

$$y = \frac{1}{\nu} = \frac{@}{@r_{xy}}\frac{dr}{d\ln b} = 2 \quad _{;xy} \quad 16 \, _{xy} ; \tag{5.66}$$

which takes the same form as as the critical exponent in Eq. (4.125). Interestingly, the fixed point values g_{xy} and $_{xy}$ take the same values as the fixed point in Eq. (4.128). This can be understood from the redundancy introduced via Hubbard-Stratonovich transformation. The physical coupling is $h / \frac{g^2}{2r}$. Thus, the limits $g = 0$ and $r \to 1$ describe the same physical system and the fixed point (5.63) describes the same quantum critical point as the transition

" = 1	$1/\nu_1$	$1/\nu_2$	η_{xy}	η_z	η_{12}	η_3	universality class
bicritical	1.083	1.433	1/3	1/3	1/6	1/6	GN-(SO(2)+I)*
SO(2) line	1.119	-	4/11	0	1/11	2/11	GN-SO(2)*
Z_2 line	1.165	-	0	6/15	1/10	0	GN-Ising*

Table 5.2: Critical regimes in the anisotropic Kitaev spin-orbital model. The bicritical point is governed by the GN-(SO(2)+I)* universality class. The divergence at the bicritical point is dominated by its largest correlation length exponent, recovering the exponent of the GN-SO(3)* universality class. Moving away from the bicritical point, the IR limit of the SO(2) (Z_2) critical line is located at $r_z(r_{xy}) \to 1$, recovering GN-SO(2)* (GN-Ising*) criticality, both possessing only a single correlation length exponent. Remarkably, the xed point anomalous dimension for one of the fermion avors vanishes at one-loop order for GN-Ising*, acquiring Gaussian scaling at criticality, e ectively decoupling from the interaction. The fermion anomalous dimensions are listed for completeness and are not measurable in the fractionalized theory.

discussed in Ch. 4. We conclude that the critical behavior of the SO(2) transition line in the mean- eld phase diagram is described by the exponents as the transition in the extreme limit $J_z = 0$ in the lattice model and thus also belongs to the GN-SO(2)* universality class.

Z_2 transition line

In the regime$r_{xy} \to 1$; $r_z = 0$, describing the IR limit of the Z_2 transition line in the mean- eld phase diagram, the RG ow in the Yukawa couplings reduces to

$$g_{xy} = (" - \eta_{xy} - \eta_{12} - \eta_3) g_{xy}^2 - 2g_{xy}^4 ; \tag{5.67}$$

$$g_z = (" - \eta_z - 2\eta_{12}) g_z^2 - 2g_z^4 ; : \tag{5.68}$$

The corresponding RG ow is depicted in Fig. (5.9). Since the calculation proceeds analogous to the previous one, we will just state the results. As before, the IR limit of the critical line describes a known xed point, recovering the exponents of the GN-SO(2)* universality class. Thus, the phenomenology of the critical behavior is the same as before. Close to the Z_2 transition line, the critical exponents are the same as those associated with the Ising limit in the lattice model. Extrapolating our to " = 1, we summarize the ndings of this section in Table (5.2) for the physical dimension$D = 3$, correspondung to two space dimensions.

6 Summary and outlook

In this work, we have studied the behavior of exactly solvable Kitaev spin-orbital models with additional antiferromagnetic nearest-neighbor interactions. We have started out by investigating the ground state and low-energy excitations of various Kugel-Khomskii type models with Kitaev interactions in the orbital sector in Ch. 3. The models were exactly solved with the Majorana representation introduced in Ref. [20], displaying $= 3$ Kitaev SOL ground states whose Z_2 gauge excitations are fully gapped and provide a static background for three avors of itinerant fractionalized Majorana fermions in the ux-free sector. Besides the SU(2)-symmetric Kitaev spin-orbital model, which form the basis of the larger part of this thesis, we studied models of lower symmetry, whose Majorana spectra feature interesting characteristics, such as at bands and or inequivalent Fermi velocities between the Majorana avors.

Motivated by the ndings of Ref. [23], we have studied the critical behavior of the Kitaev-XY spin-orbital model, which comprises the SU(2)-symmetric exactly solvable model perturbed with a spin-only XY interaction in Ch. 4. An approximate phase diagram was obtained using a Majorana mean- eld expansion, predicting a transition from into a Néel-ordered phase at strong XY couplings, spontaneously breaking the U(1) spin rotation symmetry of the model. In Majorana avor space, this corresponds to SO(2) symmetry breaking. At the transition, only two of the three Majorana avors couple to the order parameter. One avor remains gapless, such that the ordered phase describes a $= 1$ Kitaev SOL, with additional magnetic order in the spin sector, displaying a similar phenomenology as the model studied in Ref. [23]. This behavior is typical for the transitions considered in this thesis, owing to the properties of the SO(3) generators used to construct the interaction.

The quantum critical point is described by a partially bosonized Gross-Neveu-SO(2) model, which we have shown to describe the continuum limit of the microscopic model. We have obtained estimates for the critical exponents associated with the phase transition by performing a momentum-shell RG transformation to leading order in an $"$-expansion about the upper critical space-time dimension $D_c = 4$. The xed-point structure of the RG ow predicts the transition in the lattice model to be described by a new fractionalized fermionic universality class, which we have called GN-SO(2)*, whose critical exponents are the same as those of the non-fractionalized version of the theory. Numerical estimates for the critical exponents relevant to the U(1) symmetry-breaking transition in the Kitaev-XY spin-orbital model, corresponding to $" = 1$ and $N_F = 3$, are shown in Table 4.2.

Furthermore, we have constructed a model with anisotropic spin interactions in Ch. 5 by adding both XY and Ising terms to the SU(2)-symmetric Kitaev spin-orbital model, reducing the symmetry of the model to U(1) Z_2. Majorana mean- eld theory predicts a rich phase diagram, shown in Fig. 5.1, which supports several symmetry-breaking phases. In the easy-plane regime, the phase diagram shows a line of transitions to a= 1 Kitaev SOL phase breaking the U(1) sector of the full symmetry, while the easy-axis regime supports a transition to an Ising-ordered phase, such that the phase diagram is characterized by two order parameters associated with the two symmetry-breaking channels. In the isotropic limit, the model exhibits full SU(2) symmetry and, in agreement with the results of ref. [23], a transition to an SU(2) symmetry breaking phase. The enhanced symmetry of the model at the transition between the two phases with partially broken symmetry facilitates the appearance of a symmetry-enhanced rst-order transition, where both neighbouring phases become unstable with respect to the SU(2) symmetry-breaking phase and both order parameters acquire a nite value. The transition point on the isotropic line describes a bicritical point where two continuous transitions and a rst-order transition meet.

To study the critical behavior of the anisotropic model, we have constructed an e ective eld theory for two order parameter elds, coupled to the gapless Majorana fermions. The RG ow resides in a seven-dimensional theory space and describes three critical regimes, corresponding to the continuous transitions in the mean- eld phase diagram. The U(1) symmetry-breaking line was shown to be governed by the GN-SO(2) universality class. The bicritical point is described by a xed point with two relevant eigenvalues, featuring an emergent SO(3) symmetry at the xed point, de ning the fractionalized bicritical GN-(SO(2)+I)* universality class. The scaling behavior of the correlation length is dominated by the largest exponent, which recovers the critical behavior of the GN-SO(3)* universality class. Studying the critical regime, we have uncovered yet another fractionalized universality class, GN-Ising*, describing the Z_2 symmetry-breaking transition in the easy-axis regime, as well as in the limit of vanishing XY interaction. Remarkably, the anomalous dimension of one of the Majorana avors vanishes at the Z_2 transition, such that it stays decoupled at the transition. The critical exponents for the anisotropic Kitaev spin-orbital model are listed in Table 5.2.

An obvious direction for further research would be to solidify the results we have obtained in this thesis by comparison with other RG schemes, such as the $\frac{1}{N}$ expansion or the FRG. For the Gross-Neveu-SO(3) model, such calculations have been carried out [47], providing even more precise estimates for the critical exponents. Since no other estimates on the critical exponents besides our results are available right now, it is di cult to estimate the reliability of our approach, especially in the anisotropic model. The close proximity of the bicritical point to the tetracritical regime naturally leads to the question, whether the rst-order transition, which we were able to con rm to leading order in', survives at higher orders or in non-perturbative approaches.

Another possible avenue is to consider some of the more exotic spin-orbital models introduced in Ch. 2 and study their behavior in the presence of interactions. An example would be the model (3.26), which introduces independent Fermi velocities for each Majorana flavor. A similar analysis with anisotropic velocities at nematic quantum phase transitions has been carried out in Ref. [63], predicting non-trivial behavior. From a more general point of view, it is remarkable that we have observed the appearance of a bicritical point describing a topological phase transition under such similar circumstances as in a conventional magnetic system. It might be possible to construct other interactions in the spin sector, describing topological analogs to similar well-known transitions in conventional materials. To this end, it would be important to clarify under which conditions Lieb's theorem is applicable for interacting systems.

7 Bibliography

[1] J. Knolle and R. Moessner. A Field Guide to Spin Liquids . In: Annual Review of Condensed Matter Physics 10.1 (2019), pp. 451 472.

[2] Yi Zhou, Kazushi Kanoda, and Tai-Kai Ng. Quantum spin liquid states . In: Rev. Mod. Phys. 89 (2 2017), p. 025003.

[3] Matthias Vojta. Frustration and quantum criticality . In: Reports on Progress in Physics 81.6 (2018), p. 064501.

[4] J. S. Helton et al. Spin Dynamics of the Spin-1=2 Kagome Lattice Antiferromagnet $ZnCu_3(OH)_6Cl_2$. In: Phys. Rev. Lett. 98 (10 2007), p. 107204.

[5] M. R. Norman. Colloquium: Herbertsmithite and the search for the quantum spin liquid . In: Rev. Mod. Phys. 88 (4 2016), p. 041002.

[6] P.W. Anderson. Resonating valence bonds: A new kind of insulator? In: Materials Research Bulletin 8.2 (1973), pp. 153 160.

[7] Lucile Savary and Leon Balents. Quantum spin liquids: a review . In: Reports on Progress in Physics 80.1 (2016), p. 016502.

[8] Alexei Kitaev. Anyons in an exactly solved model and beyond . In: Annals of Physics 321.1 (2006), pp. 2 111.

[9] G. Jackeli and G. Khaliullin. Mott Insulators in the Strong Spin-Orbit Coupling Limit: From Heisenberg to a Quantum Compass and Kitaev Models . In: Physical Review Letters 102.1 (2009), p. 017205.

[10] Y. Kasahara et al. Majorana quantization and half-integer thermal quantum Hall e ect in a Kitaev spin liquid . In: Nature 559.7713 (2018), pp. 227 231.

[11] J. a. N. Bruin et al. Robustness of the thermal Hall e ect close to half-quantization in a-RuCl3 . In: Nature Physics 18.4 (2022), pp. 401 405.

[12] Lukas Janssen and Matthias Vojta. Heisenberg Kitaev physics in magnetic elds . In: Journal of Physics: Condensed Matter 31.42 (2019), p. 423002.

[13] Simon Trebst and Ciarán Hickey. Kitaev materials . In: Physics Reports Kitaev materials 950 (2022).

[14] Jeffrey G. Rau, Eric Kin-Ho Lee, and Hae-Young Kee. Generic Spin Model for the Honeycomb Iridates beyond the Kitaev Limit. In: Physical Review Letters 112.7 (2014), p. 077204.

[15] Hong Yao, Shou-Cheng Zhang, and Steven A. Kivelson. Algebraic Spin Liquid in an Exactly Solvable Spin Model. In: Phys. Rev. Lett. 102 (21 2009), p. 217202.

[16] R. Nakai, S. Ryu, and A. Furusaki. Time-reversal symmetric Kitaev model and topological superconductor in two dimensions. In: Phys. Rev. B 85 (15 2012), p. 155119.

[17] Hong Yao and Dung-Hai Lee. Fermionic Magnons, Non-Abelian Spinons, and the Spin Quantum Hall Effect from an Exactly Solvable Spin-1/2 Kitaev Model with SU(2) Symmetry. In: Phys. Rev. Lett. 107 (8 2011), p. 087205.

[18] Kliment I Kugel' and D I Khomskii. The Jahn-Teller effect and magnetism: transition metal compounds. In: Soviet Physics Uspekhi 25.4 (1982), p. 231.

[19] Zohar Nussinov and Jeroen van den Brink. Compass models: Theory and physical motivations. In: Rev. Mod. Phys. 87 (1 2015), pp. 1–59.

[20] Sreejith Chulliparambil et al. Microscopic models for Kitaev's sixteenfold way of anyon theories. In: Phys. Rev. B 102 (20 2020), p. 201111.

[21] Hui-Ke Jin et al. Unveiling the S=3/2 Kitaev honeycomb spin liquids. In: Nature Communications 13.1 (2022), p. 3813. issn: 2041-1723.

[22] W. M. H. Natori, Hui-Ke Jin, and J. Knolle. Quantum liquids of the $S = \frac{3}{2}$ Kitaev honeycomb and related Kugel-Khomskii models. In: Phys. Rev. B 108 (7 2023), p. 075111.

[23] Urban F. P. Seifert et al. Fractionalized Fermionic Quantum Criticality in Spin-Orbital Mott Insulators. In: Phys. Rev. Lett. 125 (25 2020), p. 257202.

[24] Willian M. H. Natori and Johannes Knolle. Dynamics of a Two-Dimensional Quantum Spin-Orbital Liquid: Spectroscopic Signatures of Fermionic Magnons. In: Phys. Rev. Lett. 125 (6 2020), p. 067201.

[25] Michael Schuler et al. Universal Signatures of Quantum Critical Points from Finite-Size Torus Spectra: A Window into the Operator Content of Higher-Dimensional Conformal Field Theories. In: Phys. Rev. Lett. 117 (21 2016), p. 210401.

[26] T. Senthil. Deconfined quantum critical points: a review. 2023. arXiv: 2306.12638 [cond-mat.str-el].

[27] John Cardy. Scaling and Renormalization in Statistical Physics. Cambridge Lecture Notes in Physics. Cambridge: Cambridge University Press, 1996.

[28] Peter Kopietz, Lorenz Bartosch, and Florian Schütz. Introduction to the Functional Renormalization Group. Vol. 798. Lecture Notes in Physics. Berlin, Heidelberg: Springer, 2010.

[29] B. Widom. Equation of State in the Neighborhood of the Critical Point . In: The Journal of Chemical Physics 43.11 (1965), pp. 3898 3905.

[30] Igor Herbut. A Modern Approach to Critical Phenomena. 1st ed. Cambridge University Press, 2007.

[31] Subir Sachdev. Quantum Phase Transitions. 2nd ed. Cambridge: Cambridge University Press, 2011.

[32] Matthias Vojta. Quantum phase transitions . In: Reports on Progress in Physics 66.12 (2003), pp. 2069 2110.

[33] John W. Negele and Henri Orland. Quantum many-particle systems. Addison-Wesley, 1988.

[34] Igor F. Herbut, Vladimir Juricic, and Bitan Roy. Theory of interacting electrons on the honeycomb lattice . In: Phys. Rev. B 79 (8 2009), p. 085116.

[35] Leo P. Kadano . Scaling laws for ising models near ${T}_{c}$. In: Physics Physique Fizika 2.6 (June 1, 1966), pp. 263 272.

[36] Kenneth G. Wilson. Renormalization Group and Critical Phenomena. I. Renormalization Group and the Kadano Scaling Picture . In: Physical Review B 4.9 (1971), pp. 3174 3183.

[37] Kenneth G. Wilson. Renormalization Group and Critical Phenomena. II. Phase-Space Cell Analysis of Critical Behavior . In: Physical Review B 4.9 (Nov. 1, 1971), pp. 3184 3205.

[38] G. Morandi, F. Napoli, and E. Ercolessi. Statistical Mechanics. An Intermediate Course. 2nd Edition. World Scienti c, 2001.

[39] Kenneth G. Wilson. The renormalization group and critical phenomena . In: Reviews of Modern Physics 55.3 (1983), pp. 583 600.

[40] Nigel Goldenfeld. Lectures On Phase Transitions And The Renormalization Group. Boca Raton: Addison-Wesley, 1992.

[41] P. M. Chaikin and T. C. Lubensky. Principles of Condensed Matter Physics. Cambridge University Press, 1995.

[42] M. Hermanns, I. Kimchi, and J. Knolle. Physics of the Kitaev Model: Fractionalization, Dynamic Correlations, and Material Connections . In: Annual Review of Condensed Matter Physics 9.1 (2018), pp. 17 33.

[43] Kevin O'Brien. Three-dimensional Kitaev Spin Liquids . PhD thesis. Universität zu Köln, 2019.

[44] G. Baskaran, Saptarshi Mandal, and R. Shankar. Exact Results for Spin Dynamics and Fractionalization in the Kitaev Model . In: Physical Review Letters 98.24 (2007), p. 247201.

[45] Elliott H. Lieb. Flux Phase of the Half-Filled Band . In: Phys. Rev. Lett. 73 (16 1994), pp. 2158 2161.

[46] Hidenori Takagi et al. Concept and realization of Kitaev quantum spin liquids . In: Nature Reviews Physics 1.4 (2019), pp. 264 280.

[47] Shouryya Ray et al. Fractionalized quantum criticality in spin-orbital liquids from eld theory beyond the leading order . In: Physical Review B 103.15 (2021), p. 155160.

[48] J. Zinn-Justin. Quantum Field Theory and Critical Phenomena: Fifth Edition. International Series of Monographs on Physics. OUP Oxford, 2021.

[49] Yi-Zhuang You, Itamar Kimchi, and Ashvin Vishwanath. Doping a spin-orbit Mott insulator: Topological superconductivity from the Kitaev-Heisenberg model and possible application to $Na_2Li_2IrO_3$. In: Physical Review B 86.8 (2012), p. 085145.

[50] Igor F. Herbut. Interactions and Phase Transitions on Graphene's Honeycomb Lattice . In: Phys. Rev. Lett. 97 (14 2006), p. 146401.

[51] A. H. Castro Neto et al. The electronic properties of graphene . In: Rev. Mod. Phys. 81 (1 2009), pp. 109 162.

[52] Bernhard Ihrig et al. Decon ned criticality from the QED_3-Gross-Neveu model at three loops . In: Phys. Rev. B 98 (11 2018), p. 115163.

[53] David J. Gross and André Neveu. Dynamical symmetry breaking in asymptotically free eld theories . In: Physical Review D 10.10 (1974), pp. 3235 3253.

[54] R. Shankar. Renormalization-group approach to interacting fermions . In: Rev. Mod. Phys. 66 (1 1994), pp. 129 192.

[55] Kiyoshi Higashijima. Theory of Dynamical Symmetry Breaking . In: Progress of Theoretical Physics Supplement 104 (1991), pp. 1 69.

[56] Alexander Altland and Ben D. Simons. Condensed Matter Field Theory. 2nd ed. Cambridge University Press, 2010.

[57] Jens Braun, Holger Gies, and Daniel D. Scherer. Asymptotic safety: A simple example . In: Phys. Rev. D 83 (8 2011), p. 085012.

[58] Laura Classen et al. Competition of density waves and quantum multicritical behavior in Dirac materials from functional renormalization . In: Phys. Rev. B 93 (12 2016), p. 125119.

[59] Kenneth G. Wilson and J. Kogut. The renormalization group and the expansion . In: Physics Reports 12.2 (1974), pp. 75 199.

[60] Bernhard Ihrig. “Deconfined Quantum Critical Behavior of Dirac materials”. PhD thesis. Universität zu Köln, 2021.

[61] Charlotte Beneke and Matthias Vojta. “Divergence of the Grüneisen ratio at symmetry-enhanced first-order quantum phase transitions”. In: *Phys. Rev. B* 103 (17 2021), p. 174420.

[62] Laura Classen et al. “Mott multicriticality of Dirac electrons in graphene”. In: *Phys. Rev. B* 92 (3 2015), p. 035429.

[63] Jonas Schwab et al. “Nematic Quantum Criticality in Dirac Systems”. In: *Phys. Rev. Lett.* 128 (15 2022), p. 157203.

Erklärung

Hiermit erkläre ich, dass ich diese Arbeit im Rahmen der Betreuung am Institut für Theoretische Physik ohne unzulässige Hilfe Dritter verfasst und alle Quellen als solche gekennzeichnet habe.

Max Fornoville
Dresden, Dezember 2023